

**EFFECT OF AGING ELECTROLYTE AND  
ORGANIC COATING TYPE ON THE CORROSION  
MECHANISM OF TINPLATE**

**A Thesis Submitted to  
the Graduate School of Engineering and Sciences of  
İzmir Institute of Technology  
in Partial Fulfillment of the Requirements for the Degree of  
MASTER OF SCIENCE  
in Chemical Engineering**

**by  
Koray YILDIRIM**

**December 2019  
İZMİR**

We approve the thesis of **Koray YILDIRIM**

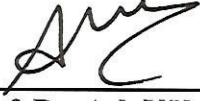
**Examining Committee Members:**



**Assist. Prof. Dr. Ali Can KIZILKAYA**  
Department of Chemical Engineering, İzmir Institute of Technology



**Assist. Prof. Dr. Nilay GİZLİ**  
Department of Chemical Engineering, Ege University



**Assoc. Prof. Dr. Aslı Yüksel ÖZŞEN**  
Department of Chemical Engineering, İzmir Institute of Technology

**18 December 2019**



**Assist. Prof. Dr. Ali Can KIZILKAYA**  
Supervisor, Department of Chemical  
Engineering, İzmir Institute of  
Technology



**Assist. Prof. Dr. Başar ÇAĞLAR**  
Co-supervisor, Department of Energy  
Systems Engineering, Yaşar University



**Prof. Dr. Erol ŞEKER**  
Head of the Department of Chemical  
Engineering



**Prof. Dr. Mehtap EANES**  
Dean of the Graduate School of  
Engineering and Science

## ACKNOWLEDGEMENTS

First, I would like to express my appreciation and gratitude to my supervisor Assist. Prof. Dr. Ali Can KIZILKAYA for guiding me on every subject in this study. I could not complete my master's degree without his guidance, patience and knowledge during this project.

I am profoundly grateful to my manager Sara Bilge ÖZCAN. My research would have been impossible without her endorsement. I would like to thank my company Toyoink for the spared research period and funding of the consumables.

I really appreciate my co-supervisor Assist. Prof. Dr. Başar ÇAĞLAR for the technical support and very helpful discussions about the electrochemical experiments which were carried out in chemistry laboratory of Yaşar University.

I'd like to recognize the help that I received from Mine BAHÇECI, Adem YAVUZ, Duygu OĞUZ KILIÇ, Mutlu Devran YAMAN, Zehra Sinem YILMAZ and Burcu AKDAĞ ÇAĞLAR about the spectroscopic measurements and discussions about material characterization in Center for Materials Research of IZTECH.

Finally, I would like to thank my family for inspiring me to pursue a graduate degree and my fiancée for her great support.

## ABSTRACT

### EFFECT OF AGING ELECTROLYTE AND ORGANIC COATING TYPE ON THE CORROSION MECHANISM OF TINPLATE

Market share of the can coating industry was 2 billion dollars in 2018 globally. A large portion of this market is focused on protecting valuable goods such as foods and cosmetics. Recent bans on the Bisphenol A(BPA) created a BPA-free coating demand due to the high portion of BPA based coatings in the industry such as epoxy. A conventional epoxy based (EP) can coating was compared with a new design of BPA-free polyester coating(PE). Atomic Force Microscopy(AFM), Scanning Electron Microscopy(SEM), Electron Dispersive Spectroscopy(EDX), Electrochemical Impedance Spectroscopy(EIS), Direct Current(DC) Polarization were used to investigate degradation. Industrial and model tinplate samples are compared with surface investigation methods. AFM results indicate the surface composition difference. To investigate bare tinplate corrosion, a mixture of acidic electrolyte was prepared and compared with other conventional aging electrolytes, containing mono acids. The electrolyte prepared from mixed acids was found to have the highest detinning abilities. Therefore, coated samples were aged with this mixed acid solution electrolyte. EIS results indicated that the type of electrolyte alters the corrosion mechanism, indicated by the observance of different time constants at different time scales. During immersion tests, EP based coatings showed better corrosion resistance as shown by higher impedance at low frequency, higher coating resistance and lower capacitance values. However, after sterilization, polyester coated samples showed better corrosion protective abilities (indicated by lower amount of corrosion products and higher impedance values) compared to the epoxy sample even though AFM measurements indicated that it had larger pore sizes after aging compared to epoxy sample. These results are attributed to the larger electrochemical area and higher diffusion properties of EP coatings, obtained after modelling of EIS data.

## ÖZET

### YAŞLANDIRMA SOLÜSYONU VE ORGANİK KAPLAMA TİPİNİN KALAY KAPLI ÇELİK KOROZYONU ÜSTÜNE ETKİSİ

Dünya genelinde metal ambalaj kaplamalarının pazar payı, 2018 yılında 2 milyar olarak raporlanmıştır. Bu pazarın büyük bir kısmı gıda ve kozmetik gibi değerli ürünlerin korunmasına odaklanmaktadır. Kullanılan kaplamaların büyük bir kısmı Bisfenol A (BPA) ile üretilen epoksi bazlı reçineler içermektedir. BPA ile ilgili geçtiğimiz yıllarda getirilen yasal kısıtlamalar, BPA içermeyen kaplamalara yönelik yeni bir talep yaratmıştır. Bu tezde, epoksi (EP) ve polyester bazlı (PE) reçinelerle üretilen iki farklı kaplama karşılaştırılmıştır. Atomik Kuvvet Mikroskobu (AFM), Taramalı Elektron Mikroskobu (SEM), Elektron Dispersif Spektroskopisi (EDX), Elektrokimyasal Empedans Spektroskopisi (EIS) ve DC Polarizasyon testleri, kaplamaların bozunma düzeyini incelemek için kullanılmıştır. Endüstriyel ve model kalay kaplı çelik(tinplate) numuneleri, yapılan yüzey analizleri ile karşılaştırılmıştır. Alınan AFM sonuçları, yüzey kompozisyonunda farklılıklar olduğunu göstermektedir. Kaplanmamış tinplate korozyonu incelemek için, asidik bir elektrolit, endüstride sık kullanılan mono asit çözeltileri ile karşılaştırılmıştır. En yüksek kalay çözme hızı, karışık asitlerden hazırlanan elektrolit ile gözlemlenmiştir. Bu nedenle, kaplanmış yüzeyler bu karışık asit çözeltisi ile yaşlandırılmıştır. EIS sonuçları, elektrolit tipinin, korozyon mekanizmasını etkilediğini göstermektedir. Elektrolitte bekletme sırasında, EP numunelerinde, düşük frekansta daha yüksek empedans, daha yüksek kaplama direnci ve düşük kapasitans değerleri gözlemlenmiştir. Sterilizasyondan sonra gerçekleştirilen AFM ölçümleri, PE'in yüzeyinde EP'ye göre daha büyük porlar oluştuğunu göstermektedir. Buna rağmen EP'ye kıyasla daha iyi korozyon koruyucu özellikler (daha düşük korozyon ürünleri ve daha yüksek empedans değerleri) gözlemlenmiştir. EIS verilerinin modellenmesinden sonra elde edilen bu sonuçlar EP sisteminin, daha geniş elektrokimyasal aktif alana ve düşük difüzyon direncine atfedilmiştir.

# TABLE OF CONTENTS

LIST OF FIGURES .....	ix
LIST OF TABLES .....	xiii
LIST OF EQUATIONS .....	xiv
CHAPTER 1. INTRODUCTION .....	1
1.1. Can Coating Industry .....	1
1.1.1. Can Coating Market .....	1
1.1.2. Substrates and Can Production .....	2
1.1.3. Can Coating Types .....	7
1.1.4. Production and Quality Control Parameters of the Can Coatings .....	8
1.2. Electrochemical Corrosion .....	10
1.2.1. Thermodynamic Aspects of Corrosion .....	11
1.2.2. Kinetic Aspects of Corrosion .....	14
1.2.3. Corrosion Types .....	15
1.2.4. Corrosion of Tinfoil .....	17
1.3. General Insights of Organic Coating Degradation .....	18
1.3.1. Permeability Properties of the Coatings .....	18
1.3.2. Cathodic Delamination .....	19
1.4. Investigation of Organic Coating Degradation with EIS .....	19
1.4.1. Basics of EIS .....	20
1.4.2. Significance of the Passive Elements .....	24
1.4.3. Common Equivalent Electrical Circuit Models .....	27
1.4.4. Commonly Accepted EIS Parameters for Better Understanding of Coating Degradation .....	29
1.4.5. Statistical Confidence of EIS Data .....	31
1.4.6. Weathering of Coatings .....	32

CHAPTER 2. LITERATURE SURVEY.....	33
2.1. Investigations and Reported Problems of Can Coating Industry .....	33
2.1.1. Electrochemical Impedance Measurements of Real Cans and Simulations.....	34
2.2. Surface Structure and Electrochemical Properties of Tinplate.....	43
2.2.1. Nano Characterization of Coating Degradation .....	50
2.3. Aim of the Study .....	52
 CHAPTER 3. EXPERIMENTAL.....	 54
3.1. Aging Electrolytes .....	54
3.2. Aging Bare Tinplates.....	55
3.3. Aging Coated Tinplates.....	56
3.4. Electrochemical Measurements.....	56
3.5. SEM and EDX Measurements.....	57
3.6. AFM Measurements .....	58
 CHAPTER 4. RESULTS.....	 61
4.1. Packaging Steel in the Industry .....	61
4.2. Corrosion of Bare Tinplate on Different Electrolytes .....	65
4.2.1. 1% Citric Acid 3% NaCl Solution .....	66
4.2.2. 3% Acetic Acid 1% NaCl Solution .....	70
4.2.3. 0.1M NaCl 0.1M Acetic Acid 0.01M Citric Acid Solution .....	74
4.3. Corrosion of Lacquered Tinplates .....	78
 CHAPTER 5. DISCUSSION.....	 86
5.1. Packaging Steel in the Industry .....	86
5.2. Corrosion of Bare Tinplate on Different Electrolytes .....	86
5.3. Corrosion of Coated Tinplate on Different Coating Formulations .....	90
 CHAPTER 6. CONCLUSION .....	 94
 REFERENCES .....	 95

APPENDICES

APPENDIX A. AFTER PULL-OFF SEM IMAGES OF COATED SAMPLES..... 100  
APPENDIX B. MAGNITUDES OF FITTED PHYSICAL ELEMENTS ..... 102  
APPENDIX C. FITTING PROCEDURE AND CALCULATION OF  
STANDARD ERRORS..... 105





## LIST OF FIGURES

<u>Figure</u>	<u>Page</u>
Figure 1.1. Production of tinplate. <sup>7</sup> .....	3
Figure 1.2. Cross-section during tinplating. ....	4
Figure 1.3. Schematic representation of ideal electrolytic tinplate cross-section. <sup>4</sup> .....	5
Figure 1.4. Roller coating and thermal curing of tinplate sheets.....	6
Figure 1.5. Electrochemical corrosion cell.....	11
Figure 1.6. Equilibrium state of anodic reaction. ....	11
Figure 1.7. Tafel curve. ....	15
Figure 1.8. Corrosion types. ....	16
Figure 1.9. Tin as anode(left) and cathode(right) for the representation of different corrosion reactions on tinplate in different oxygen containing media. <sup>14,18</sup> .....	17
Figure 1.10. Sinusoidal current response to the potential perturbation. ....	21
Figure 1.11. Different plotting techniques of EIS data a) Nyquist plot, b) Impedance magnitude of Bode plot, c) Phase shift of Bode plot. ....	22
Figure 1.12. Sum of impedance elements as a) series b) parallel.....	24
Figure 1.13. Nyquist plot of different diffusion elements. <sup>28</sup> .....	26
Figure 1.14. Common equivalent electrical circuit models for coating degradation I) pure capacitive behavior II) single time constant III) two time constant IV) single time constant with diffusion. ....	28
Figure 1.15. Nyquist spectra of common electrical circuits. <sup>13</sup> .....	28
Figure 1.16. Equivalent electrical circuit with 3-time constant.....	29
Figure 1.17. Water uptake trend for a polyester coated galvanized steel before and after 100h of UV radiation. <sup>27</sup> .....	30
Figure 1.18. EIS measurements of non-corroding epoxy coated tin plate. <sup>30</sup> .....	32
Figure 2.1. An example of tin discontinuity in a food can. <sup>33</sup> .....	34
Figure 2.2. Calculation of ideal percentage behavior of a degraded coating with bode plot. <sup>41</sup> .....	36
Figure 2.3. Pore resistance values with respect to immersion time. <sup>39</sup> .....	37
Figure 2.4. A complex equivalent electrical circuit model <sup>37</sup> .....	38

<b><u>Figure</u></b>	<b><u>Page</u></b>
Figure 2.5. Nyquist plot of epoxy-phenolic lacquered energy drink, corrosion stage III. <sup>46</sup> .....	40
Figure 2.6. Nyquist plots of beverage cans with different storage time: a)1 month, b)3 months, c) 12 months, d)12 months with defect. <sup>47</sup> .....	40
Figure 2.7. Pore resistance of epoxy-phenolic lacquered ECCS immersed in 1% NaCl solution with respect to time. <sup>48</sup> .....	41
Figure 2.8. Reduction of rust to magnetite. <sup>48</sup> .....	41
Figure 2.9. Evaluation of the coating surface as blister formation. <sup>48</sup> .....	42
Figure 2.10. Before(a) and after(b) immersion of 0.1 M Citric acid of epoxy-phenolic lacquered ECCS plates. <sup>48</sup> .....	42
Figure 2.11. Polarization curves of different passivation on tinplate. <sup>38</sup> .....	43
Figure 2.12. Structure model of the tinplate surface and interface. <sup>49</sup> .....	44
Figure 2.13. Schematic diagram of structure models of the tinplate treated with (a) reflowing before passivation; (b,c) chemical passivation for 3 s and 6 s, respectively; and (d,e) electrolytic passivation for 3 s and 6 s respectively. <sup>49</sup> .....	45
Figure 2.14. Nyquist plots for lacquered tinplates after 7 days of immersion in citric acid solution a) titanium passivated b) chromium passivated. <sup>11</sup> .....	46
Figure 2.15. XPS Surface composition by weight of scratched and unscratched coated tinplate. <sup>50</sup> .....	47
Figure 2.16. Model of the tinplate proposed by Caiazzo et. al. <sup>51</sup> .....	48
Figure 2.17. Atomic concentration of the elements on the sputtered tinplate. <sup>54</sup> .....	49
Figure 2.18. Electrochemical potential of galvanically oxidized tin plate. <sup>55</sup> .....	50
Figure 2.19. Dissolution of tin. <sup>55</sup> .....	50
Figure 2.20. AFM Spectra of the degradation of epoxy-phenolic can coating applied on polished steel applied on polished steel <sup>57</sup> a)unaged, b) after 7 days immersion in 5% w/w NaCl, (c) after 21 days immersion in 5% w/w NaCl electrolyte; (d) after 7 days immersion in deionized water and (e) after 21 days immersion in deionized water. ....	51
Figure 3.1. Experimental procedure of the thesis.....	54
Figure 3.2. Experimental setup for electrochemical measurements.....	57
Figure 3.3. Electron sample interactions. <sup>59</sup> .....	58
Figure 3.4. AFM working principle and modes. <sup>60</sup> .....	59

<b><u>Figure</u></b>	<b><u>Page</u></b>
Figure 3.5. Phase angle change according to the hardness of the surface in tapping mode.....	60
Figure 4.1. SEM(BSED) images of different tinplate samples. I, II, III from Toyoink customers, IV from QLAB.....	61
Figure 4.2. EDX mapping of the sample I.....	62
Figure 4.3. AFM phase images of different tinplates.....	64
Figure 4.4. Polarization curves of tinplate in different aggressive media.....	65
Figure 4.5. SEM images of Citric acid immersion of tinplate with BSE detector (left) and SE detector(right).....	68
Figure 4.6. Tinplate corrosion in citric acid solution for I) 1h, II) 5h, III) 12h, IV) 24h immersion, bar 5 microns.....	69
Figure 4.7. EIS data of corroding tinplate in 3% NaCl 1% Citric acid as aging electrolyte.....	70
Figure 4.8. SEM images of acetic acid aged tinplates I) for 12h II) for 24h.....	71
Figure 4.9. SEM images of acetic acid immersed QLAB tinplate.....	72
Figure 4.10. EIS data of corroding tinplate in 1% NaCl 3% acetic acid as aging electrolyte.....	73
Figure 4.11. AFM phase images of QLAB tinplates immersed in I) Citric acid II) Acetic acid for 1h.....	74
Figure 4.12. 12h aged tinplate in 0.1M NaCl 0.1M Acetic acid 0.01M Citric acid I)1000x II)10000x III) 25000x magnification.....	75
Figure 4.13. Open circuit potential evolution with respect to immersion time of different aging solutions.....	76
Figure 4.14. Low frequency impedance evolution with respect to immersion time.....	76
Figure 4.15. EIS data of corroding tinplate in 0.1M NaCl 0.1M acetic acid 0.01M citric acid as aging electrolyte.....	77
Figure 4.16. Evolution of the OCP and low frequency impedance for coated samples, with standard errors.....	80
Figure 4.17. Bode plot of fitted models for coated samples.....	80
Figure 4.18. Nyquist plot of EIS data for coated samples with fits.....	81
Figure 4.19. AFM images of Epoxy phenolic(left) and Polyester coated(right) tinplates immersed in acidic electrolyte.....	82

<b><u>Figure</u></b>	<b><u>Page</u></b>
Figure 4.20. AFM images of Epoxy phenolic(left) and Polyester coated(right) tinplates sterilized in acidic electrolyte.....	84
Figure 4.21. Corrosion products on the EP surface, bottom optical microscopy images. ....	85
Figure 5.1 Fitted equivalent electrical circuit models for bare tinplate aging.....	87
Figure 5.2. Evolution of circuit elements with respect to aging with fitting errors for bare tinplates.....	88
Figure 5.3. Evolution of circuit elements with respect to aging with fitting errors for coated tinplates. ....	91
Figure 5.4. Fitted equivalent electrical circuit models for coated tinplate aging. ....	92
Figure 5.5. Evolution of bound diffusion elements before corrosion products were observed. ....	93
Figure A.1. SEM images of pulled-off epoxy coated tinplates.....	100
Figure A.2. SEM images of pulled-off polyester coated tinplate.....	101

## LIST OF TABLES

<b><u>Table</u></b>		<b><u>Page</u></b>
Table 1.1.	Standard electrode potentials of different metals. <sup>14</sup> .....	12
Table 1.2.	Electrical impedance elements. <sup>13</sup> .....	23
Table 2.1.	Common equivalent circuit elements and typical values. <sup>37</sup> .....	38
Table 2.2.	Chemical composition of a tinplate surface. <sup>49</sup> .....	44
Table 2.3.	Free Tin and Alloyed tin calculated results via equation.....	48
Table 4.1.	Bulk EDX analysis of IV and III samples.....	62
Table 4.2.	Roughness values of different virgin tinplates.....	63
Table 4.3.	Corrosion current and potential of tinplate in different aggressive media.....	66
Table 4.4.	EDX Data of citric acid immersed bare Qpanel tinplate surfaces. ....	67
Table 4.5.	EDX Data of acetic acid immersed bare QLAB tinplate surfaces.....	71
Table 4.6.	EDX analysis of the pulled-off lacquered surfaces.....	78
Table 4.7.	Low frequency impedance values of tested coatings.....	79
Table 4.8.	Roughness analysis of EP coated plates. ....	83
Table 4.9.	Roughness analysis of PE coated plates. ....	83
Table B.1.	Equivalent electrical circuit fitted elements for bare samples. ....	102
Table B.2.	Equivalent electrical circuit fitted elements for Epoxy coated samples ..	103
Table B.3.	Equivalent electrical circuit fitted elements for Polyester coated samples.....	103

## LIST OF EQUATIONS

<u>Equation</u>	<u>Page</u>
Equation 1.1. Anodic and cathodic reactions. ....	10
Equation 1.2. Relationship between standard potential and gibbs free energy change.....	13
Equation 1.3. Nernst equation. ....	13
Equation 1.4. Relation between over potentials and Tafel constants. <sup>16</sup> .....	14
Equation 1.5. Butler-Volmer equation.....	14
Equation 1.6. Stern-Geary equation.....	15
Equation 1.7. Ohm's Law. ....	20
Equation 1.8. AC perturbation and measured current at a time t. ....	21
Equation 1.9. Impedance representation as complex number. ....	21
Equation 1.10. Coating capacitance.....	25
Equation 1.11. Brasher-Kingsbury equation, used for the calculation of $\phi$ , the ratio of water penetrated with respect to free pore volume of the coating. <sup>27</sup> .....	25
Equation 1.12. Calculation of electrochemically active area. <sup>13</sup> .....	27
Equation 1.13. Relation of Breakpoint frequency and delaminated area. ....	30
Equation 1.14. Calculation of delaminated are with double layer capacitance. <sup>27</sup> .....	31

# CHAPTER 1

## INTRODUCTION

In this chapter, background information about can coating industry, corrosion and electrochemical impedance spectroscopy is provided as a basis for the understanding of the results and discussion presented in the thesis.

### 1.1. Can Coating Industry

Can coating industry is focused mainly on corrosion protection and metal packaging decoration. The demand for corrosion protection has been on the rise since the development of high technology can manufacturing since 1940's.<sup>1</sup>

Although performance demands may change due to the application, in general, an ideal coating should;<sup>2</sup>

- be flexible enough to withstand formation of the can,
- resist a wide temperature range, because food may be processed in the cans at high temperatures and under pressure,
- not transfer constituents to food in quantities that endanger human health,
- withstand the chemistry of aggressive food types (e.g. acidic foods) and protect the metal of the can from corrosion,
- preserve the flavor and appearance of food and maintain its organoleptic properties,
- be stable over several years.

#### 1.1.1. Can Coating Market

Global can coating market share was measured as \$ 2.05 billion in 2018.<sup>3</sup> More than 30% of the share belongs to coatings for beverage cans and most of the share belongs to food contact compliant coatings, i.e. interior coatings.

Innovations in the can coating industry mainly focus on producing faster, cheaper and healthier cans. The market trend of the interior can coatings are highly dependent of the local and global regulations. As an example, a recent ban of BPA in France lead to a demand of BPA-NI (BPA non intent, meaning BPA is not an intentionally added substance in the coating) coatings in Europe.

More than 80% of the cost of a can is metal. Therefore, there is a continuous improvement of reducing the metal thickness. As an example, enabling a can manufacturer to use a lower grade steel due to a lacquer would be a successful innovation.

PPG Industries, Akzo Nobel, ALTANA, Toyochem, International Packaging Coatings, TIGER Coatings, Valspar, KANSAI PAINT, VPL Coatings, Covestro AG, Henkel AG & Co are leading can coating manufacturers present.

### **1.1.2. Substrates and Can Production**

Packaging steel, aluminum and their alloys are most used substrates for metal packaging. Both have their capabilities and disadvantages which lead to usage in different applications. Aluminum is relatively lighter and ductile; however it is weaker, more expensive, harder to solder compared to steel. Aluminum is commonly used in beverage cans, collapsible tubes and monoblock aerosol cans.

Tin and metallic chromium are the mostly used metals that are electrolytically coated to packaging steel<sup>4</sup>. Tin coated packaging steel is known as tinplate and chromium coated packaging steel is known as electrolytic chromium coated steel(ECCS) or tin-free steel. While ECCS has better adhesion abilities in general, matt surface, welding complexities, regulations and environmental impact, usage in tinplate in the metal packaging industry is more common<sup>5</sup>. The measurements in this thesis are performed on tinplate. Although aluminum and ECCS substrates are also of interest, their effects on the corrosion mechanism of can coatings are out of the scope of this thesis.

#### **1.1.2.1. Tinplate**

Production of the tinplate includes following steps<sup>6</sup> as schemed in Figure 1.1;

- I. Producing pig iron
- II. Producing low carbon steel from pig iron



- III. Casting steel into solid slabs, roughly 250mm
- IV. Hot rolling thick slabs to thin coils, typically 1.5-3.5 mm
- V. Pickling, a cleaning process to remove impurities
- VI. Cold rolling to reduce thickness
- VII. Continuous or batch annealing to recrystallize steel
- VIII. Temper rolling to adjust final thickness, mechanical properties and surface roughness
- IX. Tinplating

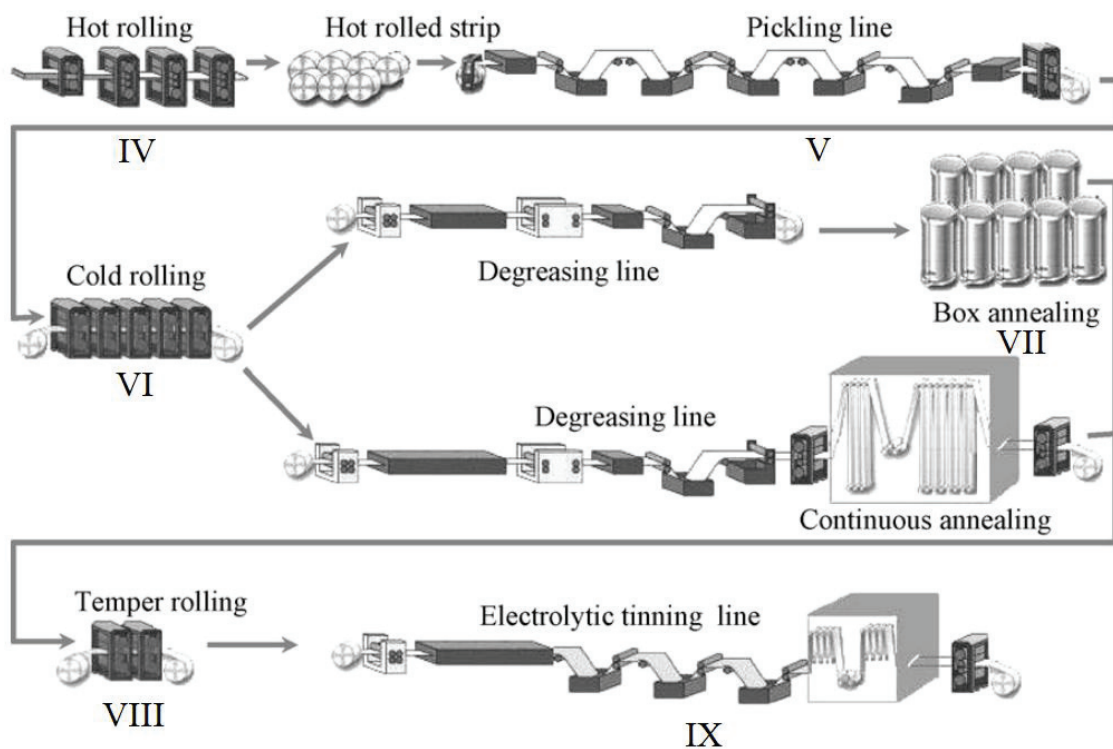


Figure 1.1. Production of tinplate.<sup>7</sup>

Tinplate processing steps I to VIII may affect surface roughness and finish, which is expected to have an influence on lacquer adhesion. Good coating adhesion is seen as a prerequisite for the anticorrosive properties of coatings. Therefore, assessing the coating adhesion is important both for academia and industry.

Tinplating process step IX usually includes three sub-processes;

- I. Electrotinning

## II. Tin reflowing

### III. Passivation

After tin is plated on the metal, it has a dull and matt appearance. Tin reflowing is heating the steel to above the melting temperature of the tin. After this process, surface gains a brighter appearance. In addition, there is a formation of a new iron-tin alloy layer which is nobler than the tin and iron. The thickness of this layer depends on the reflow temperature and duration. The thickness of coated tin, steel base and pickling process do not affect the layer thickness.<sup>8</sup> There is a formation of tin oxides on the surface during reflowing process.

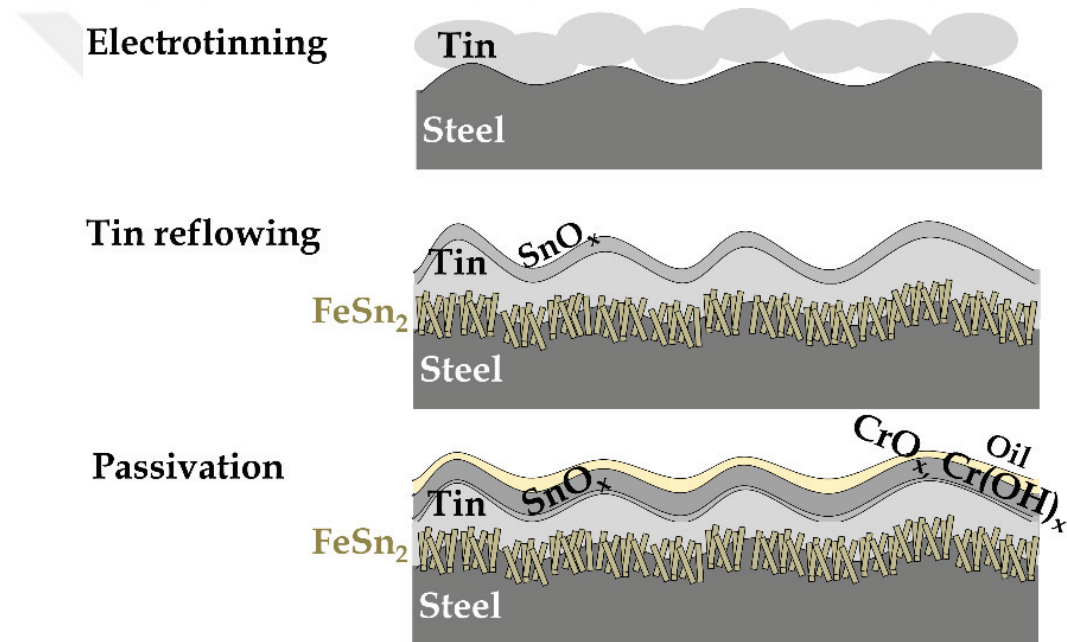


Figure 1.2. Cross-section during tinplating.

After reflowing, a passivation treatment is a common application among the packaging steel. 311 type pretreatment, which is cathodic sodium dichromate coating on the surface is one of the most common passivation methods. There are different passivation methods and studies due to the environmental impact of chromium. The studied samples in this thesis are 311 type passivated.

After passivation treatment, a food grade oil is usually applied on top of the surface due to protect the steel and to prevent the growth of oxides before it is used, such

as transport and storage duration as shown in Figure 1.2. Most used oils are dioctyl sebacate, butyl stearate and acetyl tributyl citrate. Uneven distribution of these oils may result as a pinhole problem during curing of the organic coating.

Typical thicknesses of the layers are shown in Figure 1.3. Free tin thickness depends on applied tin. There are different coating weights available in the market however, packaging steel must be coated with a minimum of 2.3 g/m<sup>2</sup> tin to be able to be used for food contact in local regulations.<sup>9</sup>

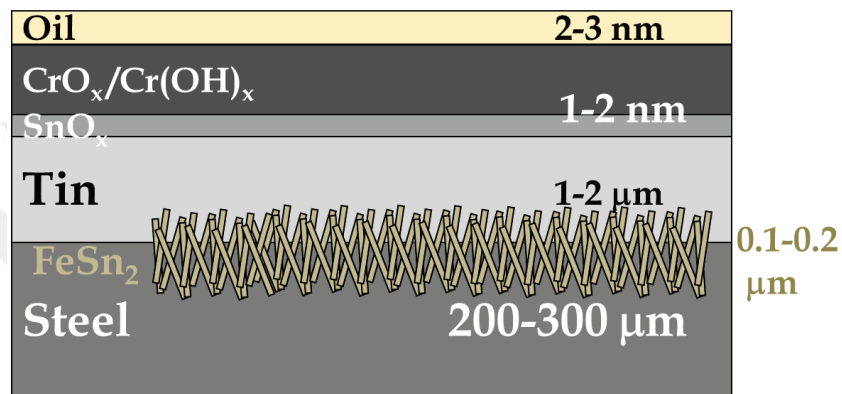


Figure 1.3. Schematic representation of ideal electrolytic tinplate cross-section.<sup>4</sup>

### 1.1.2.2. Coating Application and Production of Cans

Depending on the type of the can and the curing mechanism of the applied coating, application of the coating and production of the can may include multiple different steps. Printed sheets may be subjected to mechanical deformation however in this thesis only non-deformed coated tinplates are investigated as a simulation of general line production.

After the desired sizing of the tinplate coils, they are coated by roller coaters with interior coatings i.e. food contact lacquers and exterior coatings i.e. base coats, inks and overprint varnishes until the desired food contact properties and the looks are reached. Protective effects of exterior coatings are out of the scope of this thesis.

A common curing method for interior coatings is oven curing. Sheet metal curing is acquired with a special designed oven, wicket ovens. In wicket ovens, roller coated sheets are picked up with metal straps and cured in moving trays as shown in Figure 1.4.

The aim is to evaporate the solvent completely and achieve the desired curing level on the substrate.

The dry coating thickness of both internal and external coatings vary from 5 to 15 microns. As a lower standard,  $6\pm 0.5$  micron coated sheets are used in this thesis.

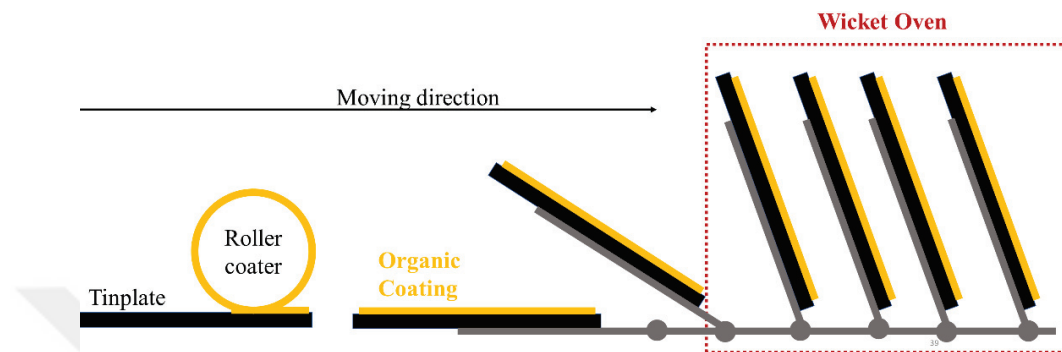


Figure 1.4. Roller coating and thermal curing of tinplate sheets.

### 1.1.2.3. Post-Production of The Cans

Cans are shipped to the food manufacturer i.e. filler after the production. A good advantage of a can compared to other types of packaging is that it allows the filler for thermal process of the food that is packed. A food can be cooked after the filling. Most canned foods are thermally treated to prevent bacterial growth inside the can. Pasteurization ( $70^{\circ}\text{C}$  for 30 min) or sterilization ( $121\text{-}130^{\circ}\text{C}$  for 30-90 minutes) are common thermal treatments. However, these thermal processes have some drawbacks such as increasing migration risk or increased water uptake due to relaxation of polymer.

Another critical parameter of filling is the oxygen content of the food. Oxygen is used in the cathodic reactions of tin corrosion. Therefore, filling temperature, oxygen content and/or low head space in the can is critical for successful filling.

Therefore, the scope of this thesis is  $121^{\circ}\text{C}$  60 minutes sterilized acidic food cans.

### 1.1.3. Can Coating Types

Can coatings can be divided into 3 categories as; protective internal coatings, pigmented external coatings, clear external coatings.<sup>4</sup> External coatings are used to protect the metal from atmospheric corrosion and create a desired look. Metal printing inks usually have adhesion issues when applied directly to metal. To fix this issue, a desired colored (usually white) basecoat is applied and cured. After that the ink and varnish are applied and cured. Applied coatings can be thermal or beam curing. According to applied coating, proper curing treatment is applied. Most of the available food contact lacquers are thermally cured. In this thesis, is protective internal coatings for 3-piece cans are investigated.

Basically, a coating includes following types of raw materials;

- I. Pigments and fillers
- II. Solvents
- III. Base resins
- IV. Reactive resins and cross-linkers
- V. Catalysts
- VI. Other additives

Pigments and fillers are used to color the surface, but they have also other functions such as hiding the stains, leaching sacrificial ions, altering water diffusion pathways, etc. The systems investigated in this thesis are pigment-free, Base resin usually forms more than %40 of the dry weight of the coating. Crosslinking degree of a coating is determined by crosslinker, catalyst and curing conditions. Main objective of a coating catalyst is to reduce the curing temperature and/or increase the speed of the cross-linking reaction. Other additives are used for modifying rheology, surface levelling, surface slip, scratch resistance etc.

Different coating systems may have superiorities compared to each other on different application such as different foodstuffs, type of can, type of metal etc. Following resin types are commonly used in can coating industry;<sup>2</sup>

- I. Epoxy
- II. Oleoresin
- III. Vinyl
- IV. Phenolic

V. Acrylic

VI. Polyester

VII. Polyolefins

It must be mentioned that a properly formulated coating may satisfy all quality standards. There are various studies for different resin alternatives,<sup>2</sup> which will be discussed in more detail in Literature Survey, and two different formulations sharing the same base resin may show different performance results.

Among the above-mentioned resins, Epoxy is the most commonly used resin type in can-coating industry.<sup>2</sup> Main reason for the usage of epoxy-based coatings is applicability to wide range of applications due to its flexibility, corrosion resistance, chemical resistance and heat resistance. However due to the restrictions of BPA,<sup>10</sup> now EU market are switching to non-BPA based coatings.. Therefore, epoxy alternatives are more seriously considered for the last decade.<sup>2</sup> A promising alternative of the epoxy resins are polyester resins. An epoxy based and a polyester based can coating formulation are used to investigate corrosion performance.

#### **1.1.4. Production and Quality Control Parameters of the Can Coatings**

Performance tests of the lacquers should ensure;

- I. Proper coating application
- II. Packaging formation
- III. Final pack performance

Coating manufacturer should ensure the coating can be applied trouble-free. To ensure that, a suitable rheology is essential. These tests can be executed on the wet form of the coating. Viscosity, solid mater, drying performance are examples of these tests. For solvent based food contact lacquers, it is common to measure the flow cup measurement standard DIN 53211. Viscosity between 70-120 seconds measured with DIN 4 cup is common in the industry(kinematic viscosity of 200-600 cSt).

As a requirement, a coated sheet should withstand the processes of can making. These processes may require the sheet to be scratch resistant, flexible and not to stich with each other when piled together. Each of the following properties are controlled in the design or quality control stages. Scratch testers, adhesion tests, wedge band tests, blocking resistance, solvent rubs are some of the common applications. It is also common

to execute tape adhesion and scratch resistance tests after the aging process. Scratch resistance test is executed according to EN 13523-12 standard. Scratch resistance of a 1kg to penetrate coating with a tungsten carbide tip is an industry minimum. Solvent rub test is executed according to ASTM D4752 standard which is rubbing coated sample until the substrate is visually exposed. Common solvents are MEK and Acetone. Minimum of 100 double rubs are desired for food contact side of the plate.

To test the final performance, there are variety of methods available however at the end the filler asks a real pack test to the packager to be sure that the specific packaging is suitable for the specific food. A pack test is a real simulation of food filling to a packaging. The filled packages are kept at the storage conditions and periodically opened to check if there are any changes can be observed visually or organoleptically. The minimum of a two-year pack resistance is an industry standard. As a result of this, commercialization of an interior protective coating is minimum of two years.

Except the pack test, there are numerous shorter methods. To be able to make the tests shorter, increasing chemical aggressiveness, increasing sterilization temperature and duration are common applications. Following chemicals are commonly used in the industry with a concentration range of 0.5% to 5%;<sup>4,11,12</sup>

- I. Acetic acid
- II. Citric acid
- III. Lactic acid
- IV. NaCl
- V. L-cysteine
- VI. Ammonia(solution)
- VII. NaOH

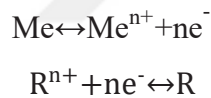
Citric acid and lactic acid have a potential to produce complexes with tin i.e. complexing acids. These acids reduce the pH of the electrolytes and may also disturb the chemical structure of the coatings i.e. hydrolysis. L-cysteine is used to simulate as sulfur containing proteins. Ammonia and NaOH are used to test alkaline resistance of the system.

The coated metal test panel can be immersed in electrolyte, thermally processed in electrolyte i.e. pasteurization or sterilization or electrochemically polarized in the electrolyte i.e. DC corrosion. The purpose of these tests is to visually observe the aging defects and predict the performance. Matting due to the coating degradation, darkening due to the corrosion products, color change of the electrolyte are such observed effects

however it could be hard to distinguish the nuance between the compared samples and predict the eventual performance.<sup>4</sup> As a result, more advanced methods are needed to evaluate coating degradation. Electrochemical impedance spectroscopy are suggested by many scientist for investigating coating degradation for various type of coatings.<sup>4,13</sup> Therefore, electrochemical impedance spectroscopy is used to investigate coating degradation in this thesis.

## 1.2. Electrochemical Corrosion

Corrosion is oxidation of a metal surface which dissolution and oxidation of the metal occurs simultaneously in the metal-electrolyte interphase. Dissolution reaction of a metal is called anodic reaction which gives electron to the system, i.e. oxidation. Electrons released to the system are used up in cathodic reaction , i.e. reduction. In other words, oxidation is loss of electrons and reduction is pick-up of electrons as shown in Equation 1.1.



Equation 1.1. Anodic and cathodic reactions.

Corrosion processes depend primarily on two factors;<sup>14</sup>

- I. Potential factor i.e. thermodynamic aspects
- II. Facility factor i.e. kinetic aspects

Thermodynamic favorability is not enough for a corrosion process to continue. If the corrosion rate is very low, it is hard to observe corrosion.

An electrochemical corrosion cell consists of the following elements, electrode, electrolyte and conducting wire as shown in Figure 1.5.



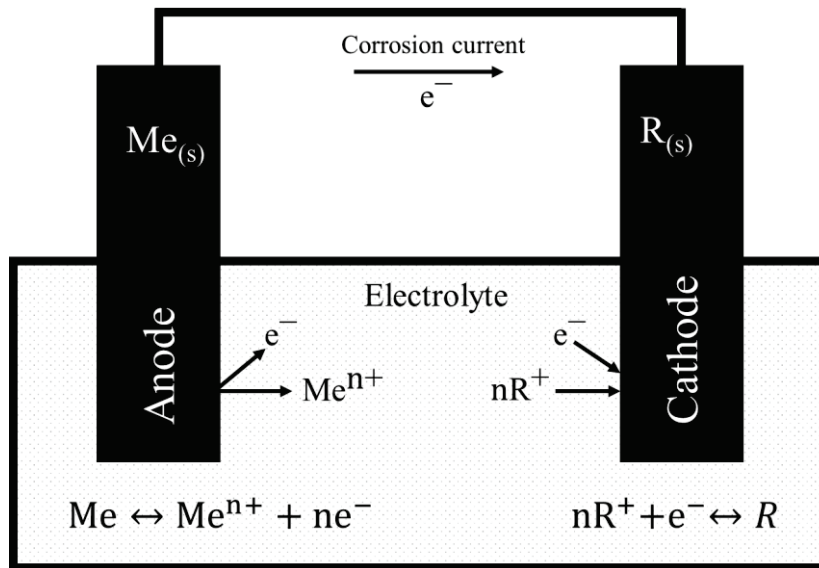


Figure 1.5. Electrochemical corrosion cell.

### 1.2.1. Thermodynamic Aspects of Corrosion

The thermodynamic tendency of a metal to give electrons in a redox reaction as Equation 1.1 can be expressed as standard reduction potential ( $E^\circ_{\text{cell}}$ ).<sup>14</sup> Due to anodic reactions, metal ions diffuse to the electrolyte, until the equilibrium is reached i.e. equal negative and positive charges occur at the electrode as shown in Figure 1.6. An electrical double layer is formed this way. An example of a thickness of a double layer is  $1\text{nm}^{14}$

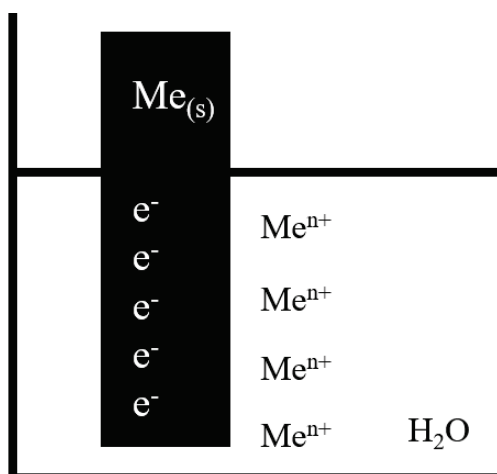


Figure 1.6. Equilibrium state of anodic reaction.

It should be noted that, negative charged electrodes compared to the electrolyte is a result of negative value of their “electrode potential” i.e.  $E_{ox}$ . There are many metals that have positive electrode potential such as silver, gold, etc. The electrode potentials of different reactions compared to standard hydrogen electrode are given at Table 1.1.

Table 1.1. Standard electrode potentials of different metals.<sup>14</sup>

Unit activity	E vs SHE (V)	Unit activity	E vs SHE (V)
Li/Li <sup>+</sup>	-3.045	V/V <sup>+++</sup>	-0.876
Rb/Rb <sup>+</sup>	-2.925	Zn/Zn <sup>++</sup>	-0.762
K/K <sup>+</sup>	-2.925	Cr/Cr <sup>+++</sup>	-0.740
Cs/Cs <sup>+</sup>	-2.923	Ga/Ga <sup>++</sup>	-0.530
Ra/Ra <sup>+</sup>	-2.920	Fe/Fe <sup>++</sup>	-0.440
Ba/Ba <sup>++</sup>	-2.900	Cd/Cd <sup>++</sup>	-0.402
Sr/Sr <sup>++</sup>	-2.890	In/In <sup>++</sup>	-0.342
Ca/Ca <sup>++</sup>	-2.870	Tl/Tl <sup>+</sup>	-0.336
Na/Na <sup>+</sup>	-2.714	Mn/Mn <sup>+++</sup>	-0.283
La/La <sup>+++</sup>	-2.520	Co/Co <sup>++</sup>	-0.277
Mg/Mg <sup>++</sup>	-2.370	Ni/Ni <sup>++</sup>	-0.250
Am/Am <sup>+++</sup>	-2.320	Mo/Mo <sup>+++</sup>	-0.200
Pu/Pu <sup>+++</sup>	-2.070	Ge/Ge <sup>++++</sup>	-0.150
Th/Th <sup>++++</sup>	-1.900	Sn/Sn <sup>++</sup>	-0.136
Np/Np <sup>+++</sup>	-1.860	Pb/Pb <sup>++</sup>	-0.126
Be/Be <sup>++</sup>	-1.850	Fe/Fe <sup>+++</sup>	-0.036
U/U <sup>+++</sup>	-1.800	H <sub>2</sub> /H <sup>+</sup>	0.000
Hf/Hf <sup>++++</sup>	-1.700	Cu/Cu <sup>++</sup>	+ 0.337
Al/Al <sup>+++</sup>	-1.660	Cu/Cu <sup>+</sup>	+ 0.521
Ti/Ti <sup>++</sup>	-1.630	Hg/Hg <sup>++</sup>	+ 0.789
Zr/Zr <sup>++++</sup>	-1.530	Ag/Ag <sup>+</sup>	+ 0.799
U/U <sup>++++</sup>	-1.50	Rh/Rh <sup>+++</sup>	+ 0.800
Np/Np <sup>++++</sup>	-1.354	Hg/Hg <sup>++</sup>	+ 0.857
Pu/Pu <sup>++++</sup>	-1.280	Pd/Pd <sup>++</sup>	+ 0.987
Ti/Ti <sup>+++</sup>	-1.210	Ir/Ir <sup>+++</sup>	+ 1.000
V/V <sup>++</sup>	-1.180	Pt/Pt <sup>++</sup>	+ 1.190
Mn/Mn <sup>++</sup>	-1.180	Au/Au <sup>+++</sup>	+ 1.500
Nb/Nb <sup>+++</sup>	-1.100	Au/Au <sup>+</sup>	+ 1.680
Cr/Cr <sup>++</sup>	-0.913		

In corrosion process, cathodic and anodic reactions have their different reversible electrode potentials. For a spontaneous corrosion process, reversible electrode potentials of cathodic reactions must be greater than anodic reactions i.e  $E_{red} > E_{ox}$  so that electromotive force (EMF,  $E_{cell} = E_{red} - E_{ox}$ ) is positive. A more negative Gibbs free energy change ( $\Delta G^\circ$ ) of the reaction represents the tendency to occur spontaneously. The relationship between  $\Delta G^\circ$  and  $E^\circ_{cell}$  is expressed in Equation 1.2 where  $n$  is the valance number of the metal and  $F$  is the Faraday's constant. Therefore, more negative electrode potential represents its willing to give electrons.

$$\Delta G^\circ = -nFE^\circ_{cell}$$

Equation 1.2. Relationship between standard potential and gibbs free energy change.

Equilibrium potential of a cell ( $E_{eq}$ ,  $E_{rev}$ ) at a different concentration than 1M can be obtained via Nernst equation, Equation 1.3 in which  $R$  is ideal gas constant,  $T$  is absolute temperature,  $F$  is Faraday's constant,  $n$  is valance electrons and  $Q$  (reaction activity quotient, 1 means the activity of right hand side and left hand side of the reaction is equal, ox/red) is molar ionic concentration of the metal.<sup>15</sup> When  $Q$  is 1,  $E_{cell}$  is equal to the standard potential of the cell ( $E^\circ_{cell}$ ).

$$E_{cell} = E^\circ_{cell} - \frac{RT}{nF} \ln(Q)$$

Equation 1.3. Nernst equation.

$E_{ox}$  and  $E_{red}$  are electrode potentials at the equilibrium and the corrosion potential (of the redox reaction),  $E_{corr}$  is the equilibrium potential between them. It is also commonly referred as open-circuit potential  $E_{oc}$ .

## 1.2.2. Kinetic Aspects of Corrosion

Nernst equation does not give information about the kinetic properties of the corrosion process. In equilibrium conditions of redox reactions, the current generated by reduction ( $i_{\text{red}}$ ) and oxidation ( $i_{\text{ox}}$ ) is equal. When there is not a net transfer of charge, current at this condition is called exchange current density,  $i_0$ . Corrosion current is a direct measure of corrosion rate. The change of the potential from the equilibrium due is defined as overpotential or polarization,  $\eta$ . When the difference is positive, it is anodic overpotential  $\eta_a$ , when it is negative it is cathodic overpotential  $\eta_c$  as shown in Equation 1.4.

$$\eta_a = E - E_{\text{corr}} = \beta_a \log \frac{i_a}{i_0}$$
$$\eta_c = E_{\text{corr}} - E = \beta_c \log \frac{i_c}{i_0}$$

Equation 1.4. Relation between over potentials and Tafel constants.<sup>16</sup>

A way of measuring corrosion current is potentiodynamic polarization curves i.e. Tafel curves as shown Figure 1.7. The intersection of anodic and cathodic lines gives the corrosion current and potential. The slope of the anodic and cathodic lines gives Tafel constants  $\beta_a$  and  $\beta_c$  respectively. From the derivation of Equation 1.4, Butler-Volmer equation can be obtained in which  $\alpha_a$  and  $\alpha_c$  is transfer coefficient<sup>15</sup> and sum of them is unity. In the literature, they are also mentioned as symmetry coefficient and charge transfer coefficient.<sup>16</sup>

$$i = i_{\text{corr}} \left( e^{\frac{\alpha_a n F \eta_a}{RT}} - e^{-\frac{\alpha_c n F \eta_c}{RT}} \right)$$

Equation 1.5. Butler-Volmer equation.

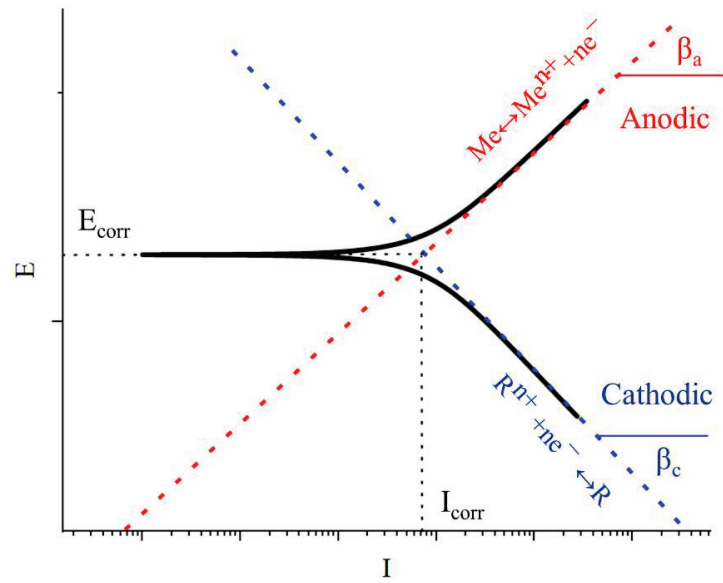


Figure 1.7. Tafel curve.

Potentials near  $E_{\text{corr}}$ , potential-current curves approximate to a straight line. The slope of this line has a unit of resistance and called polarization resistance,  $R_p$ . From the simplification of Equation 1.5, one form of Stern-Geary function can be obtained as Equation 1.6.

$$i_{\text{corr}} = \frac{1}{R_p} \frac{\beta_a \beta_c}{2.303(\beta_a + \beta_c)}$$

Equation 1.6. Stern-Geary equation.

### 1.2.3. Corrosion Types

Internal corrosion of the food media is an interest of this thesis, therefore types of aqueous corrosion is explained briefly.

### 1.2.3.1. Uniform Corrosion

Uniform corrosion is a common corrosion type where the metal is corroding uniformly.<sup>17</sup> It is easy to investigate. Corrosion of pure iron in sea salt is an example of uniform corrosion. With this type of corrosion, corrosion rate is commonly referred as thickness per year as the metal degradation is homogeneous in the entire surface.

### 1.2.3.2. Galvanic Corrosion

Galvanic corrosion occurs when a less noble metal is in electrical contact with a more noble metal in the electrolyte.<sup>17</sup> Protecting the metal as a sacrificial anode is an example of galvanic corrosion(cathodic protection). Electrochemical cell shown in Figure 1.5 is an example of galvanic corrosion.

### 1.2.3.3. Pitting and Filiform Corrosion

Pitting corrosion is a commonly seen localized corrosion form as a result of a breakdown of the passivated film.<sup>17</sup> Corrosion occurs rapidly at the defect. This result as a formation of a pit as shown in Figure 1.8.

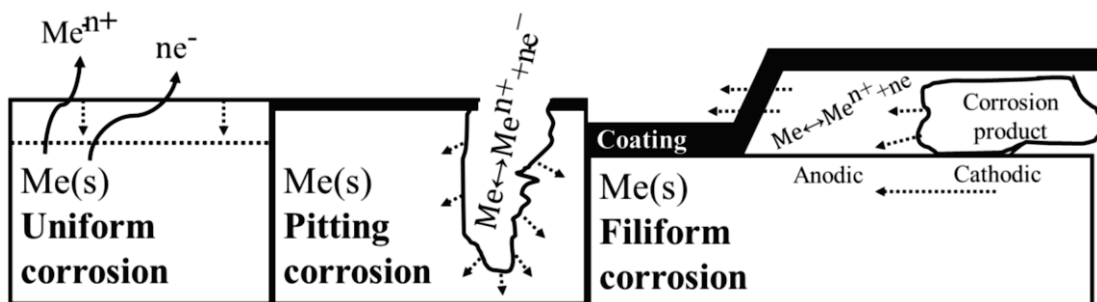


Figure 1.8. Corrosion types.

Filiform corrosion is commonly seen on defected areas of coated metals. Anodic and cathodic reactions take part at the defect until the electroneutrality is reached within

the system.<sup>17</sup> After the formation of corrosion products, cathodic side of the corrosion reaction will move to the anodic side. The new anodic side of the reaction will occur on a random site depending on oxygen and humidity permeation and this process will result as a worm like corrosion product filaments.

### 1.2.4. Corrosion of Tinplate

Surface of a tinplate may include mixed galvanic cells due to the surface heterogeneities such as non-uniform layers, deep or shallow scratches, coating discontinuities, impurities etc. As a result, industrial tinplate samples may not show the ideal structure type as Figure 1.3.

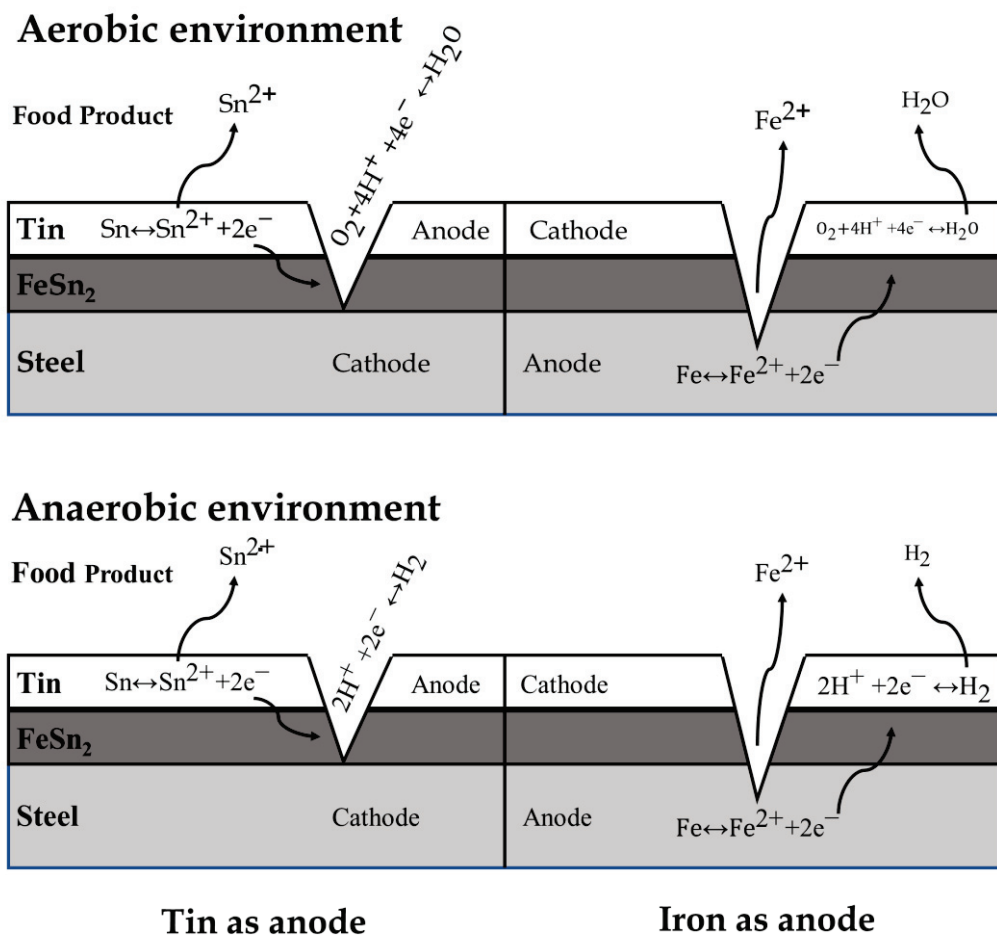


Figure 1.9. Tin as anode(left) and cathode(right) for the representation of different corrosion reactions on tinplate in different oxygen containing media.<sup>14,18</sup>

### 1.3. General Insights of Organic Coating Degradation

A recently published review by Lyon discussed corrosion protection with organic coatings and coating degradation mechanisms.<sup>19</sup> They mentioned that coating failure can be seen on both damaged and intact areas. Main parameters that need to be improved for better corrosion performance were stated as ionic resistance of the coating, adhesion of the coating to the substrate and preventing the formation of pathways which leads to failure.

Studies showed that kinetics of ionic diffusion along the coating-metal interface controls the overall rate of disbonding.<sup>20</sup> Coating adhesion is a necessary, but not sufficient condition for good coating performance. Cathodic disbonding is a chemical effect and can be controlled by interface and binder chemistry. In general, at local anodic phases corrosion tends to give rise to anodic undermining of the coating, while at local cathodic phases coating failure tends to occur via cathodic delamination.<sup>21</sup>

#### 1.3.1. Permeability Properties of the Coatings

Oxygen and water permeability studies reviewed by Sangaj and Malshe<sup>22</sup> showed the exact relationship between permeability and corrosion protection performance of coatings is still unclear. Some of the reasons limiting the measurement of exact permeability and further studies are;

- Variety of components in the paint system, for example different pigments, their dispersion and amount in the coating may significantly affect the permeability.
- Additives like surfactants, dispersing agents may change hydrophilic/hydrophobic properties of the system, resulting increased water-soluble components may change the permeability of the coating.
- Film formation method i.e. air drying, solvent evaporation, chemical crosslink, stoving may affect the permeability of the coating.
- Curing conditions significantly affects the permeability. An example of epoxy-tar coating cured at high temperatures failed earlier than cured at room temperatures due to susceptibility to ageing. Opposite of above-mentioned example, increased crosslinking with stoved enamels may reduce permeability properties.



- The chemical integrity of the binders may change due to water or oxygen, resulting hydrolysis reactions and/or relaxation of the polymer.

Polarity of the different substrates may also affect the corrosion performance of the same coating due different alignment of the polar groups at the interphase i.e. metal/coating or coating/air.

Crosslinking should generally decrease permeability of the water molecules except the scenarios which crosslinking introduces polar groups.

Organization of polymer groups also has an influence on permeability. Similar solvent containing systems were able to be cured within more favorable molecular alignment.

Calculation of water sorption from effective capacitance from Brashers-Kingsbury equation gives different results depending on the frequency due to the non-ideal behavior at lower frequencies(bode plot).<sup>23,24</sup>

### **1.3.2. Cathodic Delamination**

Cathodic delamination of the organic coatings on steel i.e. local alkaline attack due to the reduction of oxygen with water producing OH<sup>-</sup> is a considerable threat and the focus of many corrosion scientists.<sup>25</sup> Ion transport through organic coating is a critical step for cathodic delamination and preventing ion diffusion is a critical role of organic coatings. It can happen via intact coating or defected area with the one or more of the following steps; oxide reduction of the surface, alkaline hydrolysis of the polymer and weakening of the interphase. For polymer hydrolysis mechanism, it was proposed that very thin layer still adheres to the metal and the fracture occurs in the polymer groups.

## **1.4. Investigation of Organic Coating Degradation with EIS**

Electrochemical impedance spectroscopy become a widely used technique to investigate deterioration of organic coatings after 1970.<sup>13</sup> Main advantages of EIS technique are;<sup>26</sup>

- Prediction of corrosion in early stages
- Non-destructive measurement

- More detailed information about the corrosion mechanism compared to DC methods

### 1.4.1. Basics of EIS

The term of electrical resistance and its relation between current and the potential is well-known as Ohm's law as given in Equation 1.7.

$$R = \frac{E}{I}$$

Equation 1.7. Ohm's Law.

However, it can only be used for ideal resistors. For an ideal resistor, resistance is not a function of frequency. For real systems, impedance is used, whose resistance is a function of the frequency of the applied voltage or current perturbation. Therefore, impedance can be considered as the alternating current analog of the resistance, which is a property of direct current systems. Impedance can be measured via alternating (frequency dependent) perturbation (where the perturbation can be in terms of the voltage or the current) of a system that is small enough to keep system pseudo steady-state and large enough to measure current with low errors.

In potentiostatic EIS measurements, where the perturbations is in terms of the voltage, the perturbation and measured current at a time  $t$  can be expressed as following equations (Equation 1.8) and Figure 1.10 in which  $E_0$  is amplitude of the perturbation,  $\omega$  is radial frequency,  $f$  is the frequency,  $\phi$  is the phase angle and  $Z_0$  is the impedance magnitude;

$$E_t = E_0(\sin\omega t)$$

$$\omega = 2\pi f$$

$$I_t = I_0(\sin\omega t + \phi)$$

$$Z = \frac{E_t}{I_t} = \frac{E_0(\sin\omega t)}{I_0(\sin\omega t + \phi)} = Z_0 \frac{(\sin\omega t)}{(\sin\omega t + \phi)}$$

Equation 1.8. AC perturbation and measured current at a time t.

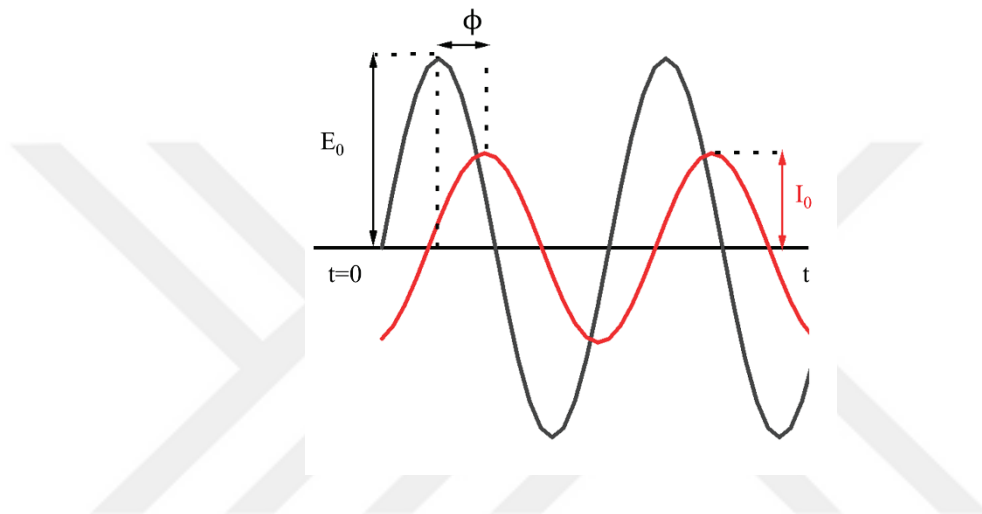


Figure 1.10. Sinusoidal current response to the potential perturbation.

If  $E_t$  vs  $I_t$  plotted, an oval shaped graph can be obtained which is known as Lissajous figure. Electrochemical impedance spectroscopy measurements include the measurements as Figure 1.10 for a range of frequencies usually between 100,000 Hz to 0.01Hz.

It is also possible to express impedance function in the complex plane due to the Euler's relationship,  $\exp(j\phi) = \cos\phi + j\sin\phi$  as Equation 1.9.

$$E_t = E_0 \exp(j\omega t)$$

$$I_t = I_0 \exp(j\omega t - \phi)$$

$$Z(\omega) = Z_0 \exp(j\phi) = Z_0(\cos\phi + j\sin\phi)$$

Equation 1.9. Impedance representation as complex number.

### 1.4.1.1. Plotting of the Data

There are two common approaches for plotting EIS data; Nyquist plot and Bode plot. In Nyquist plot, real and imaginary parts of the impedance data are plotted on x and y axis respectively. Frequency of the data points are in increasing order with increasing real impedance. Phase shift and impedance magnitudes also can be observed in the same plot. Nyquist plot is shown in Figure 1.11a. One drawback of Nyquist plot is that frequencies are not shown directly on the plot. In Bode plots, impedance magnitude and phase shift are plotted with respect to frequency. Bode plots of impedance magnitude and phase shift are shown in Figure 1.11b and Figure 1.11c respectively.

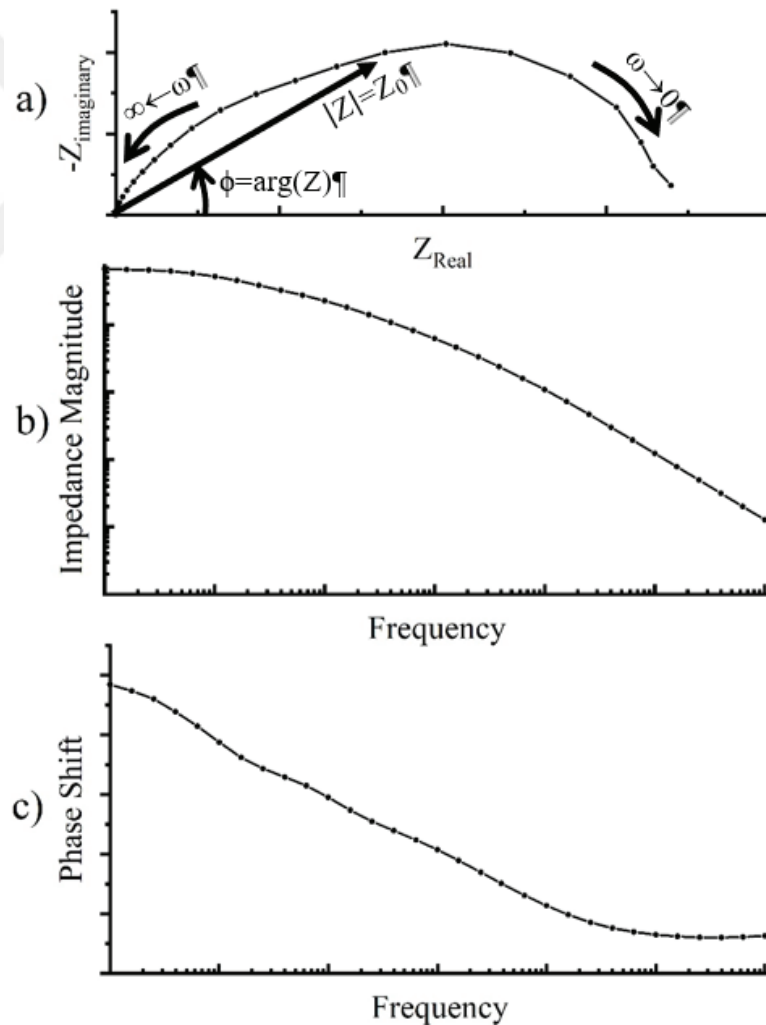









Figure 1.11. Different plotting techniques of EIS data a) Nyquist plot, b) Impedance magnitude of Bode plot, c) Phase shift of Bode plot.

After executing EIS experiment, the data is usually fitted to an equivalent electrical circuit model to be able to comment and have a deeper understanding of the electrochemical and physical properties of the system. Electrical circuit elements are used to simulate electrochemical processes. These elements are shown in Table 1.2 in which  $Y_0$  is the admittance(not a function of frequency),  $n$  is the power of the constant phase element,  $B$  is the diffusion factor given by  $B=\delta/D^{0.5}$ .<sup>13</sup>

Table 1.2. Electrical impedance elements.<sup>13</sup>

Element	Symbol	Schematic Expression	Impedance Expression
Resistance	R		R
Capacitance	C		$\frac{1}{j\omega C}$
Inductance	L		$j\omega L$
Warburg	W		$\frac{1}{Y_0(j\omega)^{0.5}}$
Constant Phase Element	Q		$\frac{1}{Y_0(j\omega)^n}$
Open Finite Length Diffusion	O		$\tanh \left[ \frac{B(j\omega)^{0.5}}{Y_0(j\omega)^{0.5}} \right]$
Bound Finite Length Diffusion	T		$\coth \left[ \frac{B(j\omega)^{0.5}}{Y_0(j\omega)^{0.5}} \right]$

Above mentioned impedance elements can be connected in two different ways; series and parallel as shown in Figure 1.12. With the electrical impedance elements as mentioned in Table 1.2, the total impedance function is fitted to the experimental data.

a)  $\text{---} Z_1 \text{---} Z_2 \text{---} Z_3 \text{---}$   $Z_{\text{Total}} = Z_1 + Z_2 + Z_3$

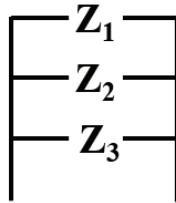
b)   $\frac{1}{Z_{\text{Total}}} = \frac{1}{Z_1} + \frac{1}{Z_2} + \frac{1}{Z_3}$

Figure 1.12. Sum of impedance elements as a) series b) parallel.

There are few commonly accepted criteria about constructing equivalent electrical circuits;<sup>13,27</sup>

- I. All elements must have a physical meaning.
- II. As few as possible elements should be used i.e. if removing an element does not change the validity of the fit, then it should be simplified.

## 1.4.2. Significance of the Passive Elements

The physical meaning of the commonly used impedance elements to model coating degradation are explained briefly in this section.

### 1.4.2.1. Electrolyte Resistance $R_e$

Electrolyte resistance or uncompensated resistance is the resistance between reference electrode and working electrode. It reduces as the ionic concentration increases.<sup>13</sup> Common electrolyte resistance values fall between 1 to 50 ohms.

### 1.4.2.2. Coating Resistance $R_{\text{coat}}$

There is a consensus in the literature that coating resistance is a measure of coating porosity and water penetration.<sup>13,19,23</sup> Porosity in this definition represents both

microscopic and nano-sized pores present in the coating resin. It is also mentioned as  $R_{\text{pore}}$  in the literature.

### 1.4.2.3. Coating Capacitance $C_{\text{coat}}$

Coating capacitance can be calculated from the Equation 1.10 in which  $\epsilon$  and  $\epsilon_0$  are the dielectric constants of the coating and vacuum respectively. Dielectric constant of water is 80 and most coatings are between 3-4.

$$C_{\text{coat}} = \epsilon \epsilon_0 \frac{A}{d}$$

Equation 1.10. Coating capacitance.

Due to the difference between dielectric constants, water uptake of the coating can be measured via coating capacitance via Equation 1.11 where  $C_{c(t)}$  is the coating capacitance at a time,  $C_{c(0)}$  is the initial dry capacitance of the coating and  $\epsilon$  is the relative permittivity of the water.

$$\phi = \frac{\log \frac{C_{c(t)}}{C_{c(0)}}}{\log \epsilon}$$

Equation 1.11. Brasher-Kingsbury equation, used for the calculation of  $\phi$ , the ratio of water penetrated with respect to free pore volume of the coating.<sup>27</sup>

### 1.4.2.4. Diffusion $Z_w$

Diffusion can result as an impedance called Warburg impedance. It is usually attributed to oxygen diffusion of the cathodic reaction however it can be diffusion of the corrosion products. It can be observed as a line with 45° slope in the Nyquist plots.

Comparison of Warburg coefficient ( $\sigma \sim 0.7Y_0$ ) and  $R_{ct}$  can define whether if the reaction is under charge transfer controlled or diffusion controlled. When the ratio of  $R_{ct}$  to  $\sigma$  is greater than 10, it is charge transfer controlled, lower than 0.1 it is diffusion controlled.<sup>13</sup>

Warburg definition in Table 1.2 assumes that the a.c. diffusion layer thickness (of the low frequency perturbation) is much less compared to d.c. Nernstian diffusion layer thickness. When they are comparable, the Warburg impedance definition is better expressed as open finite length diffusion or bound finite length diffusion. The difference can be observed in Figure 1.13.

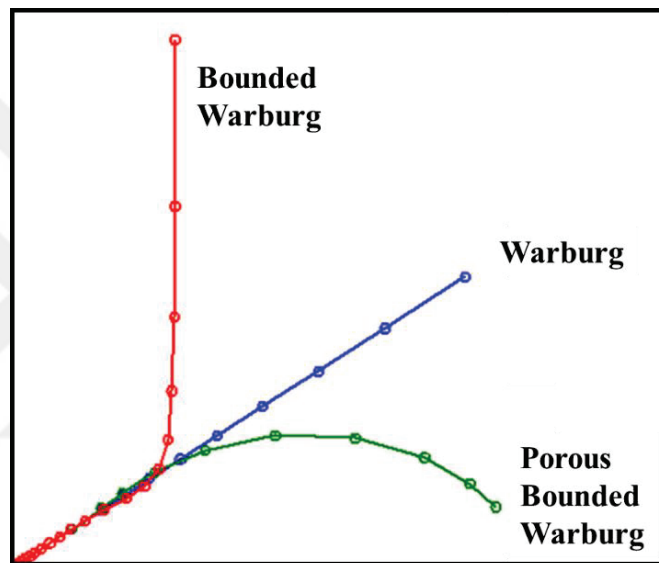


Figure 1.13. Nyquist plot of different diffusion elements.<sup>28</sup>

#### 1.4.2.5. Double Layer Capacitance $C_{dl}$

Formation of a double layer is mentioned in Figure 1.6. Magnitude of the double layer capacitance depends on many factors such as electrode potential, temperature, ionic concentrations, types of ions, oxide layers, electrode roughness, impurity adsorption etc.<sup>29</sup> It is commonly agreed that double layer capacitance is a measure of delaminated coating area<sup>13</sup> or electrochemically active area. It is not possible to fit double layer capacitance without observing the second time constant. Ratio of the delaminated or



electrochemically active area  $A_d$  can be calculated in Equation 1.12 in which  $C_{dl}^0$  is the double layer capacitance of the bare metal.

$$A_d = \frac{C_{dl}}{C_{dl}^0}$$

Equation 1.12. Calculation of electrochemically active area.<sup>13</sup>

#### 1.4.2.6. Charge Transfer Resistance $R_{ct}$

Charge transfer resistance is the reaction resistance at the limit of infinity frequency. To model a simple corrosion reaction,  $R_p$  and  $R_{ct}$  are the same i.e. at the different frequencies. However, in complex corrosion reactions, they can have different values.

Low values of  $R_{ct}$  mean high corrosion reaction rates and usually observed at the later stages of the degradation.

#### 1.4.2.7. Constant Phase Element

Capacitors in the electrochemical systems usually behave non ideally. To be able to create a better fit, an empirical constant  $n$  is used. It is very common to use constant phase elements instead of capacitors for modelling coating degradation systems.<sup>29</sup>

### 1.4.3. Common Equivalent Electrical Circuit Models

There are few common equivalent electrical circuit models that are reported in the literature to simulate coating degradation as shown in Figure 1.14. Model I is called pure capacitive behavior and it is commonly used to fit initial stages of coating degradation. Model II is single time constant, usually used to fit water uptake of the organic coating. Model III is two time constant, usually used to fit corrosion initiation along with water uptake. Model IV is single time constant with diffusion.

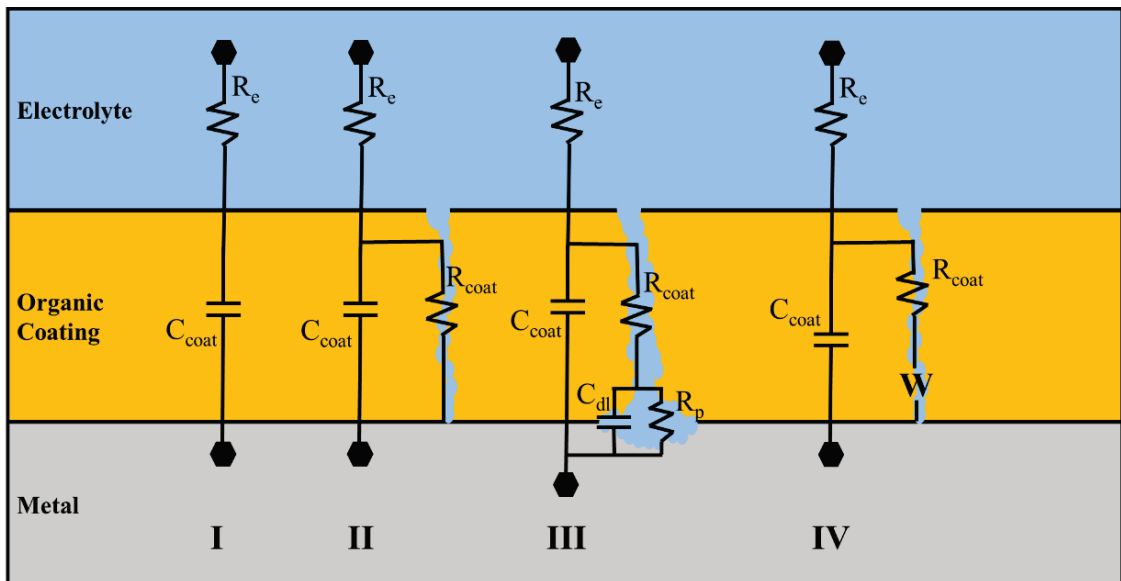


Figure 1.14. Common equivalent electrical circuit models for coating degradation I) pure capacitive behavior II) single time constant III) two time constant IV) single time constant with diffusion.

Nyquist spectra of the common equivalent electrical circuits mentioned in Figure 1.14 are shown in Figure 1.15.

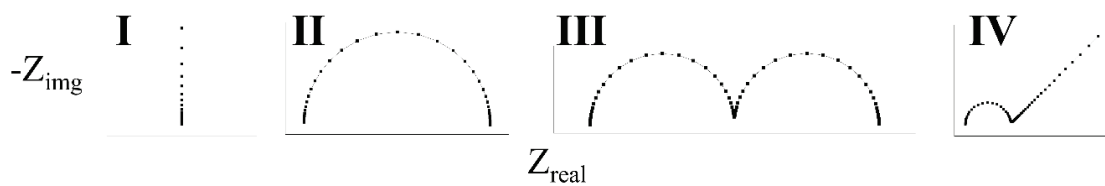


Figure 1.15. Nyquist spectra of common electrical circuits.<sup>13</sup>

More complex models (such as more than two time constant are also reported many times for modelling more complex corrosion behaviors as shown in Figure 1.16.

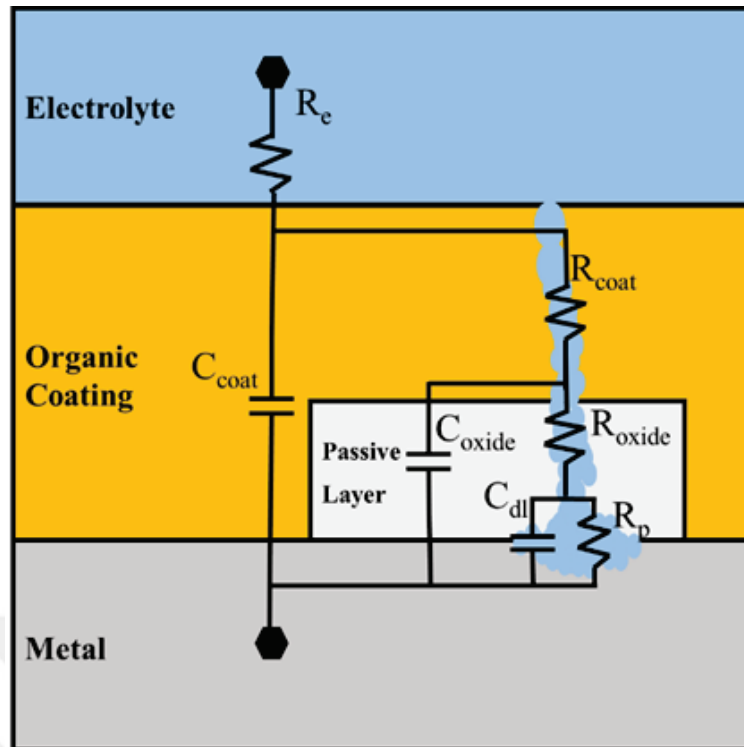


Figure 1.16. Equivalent electrical circuit with 3-time constant.

#### 1.4.4. Commonly Accepted EIS Parameters for Better Understanding of Coating Degradation

Amirudin and Thierry reviewed more than hundred publications about EIS investigations of degradation of polymer coated metals.<sup>13</sup> Substitution of CPE instead of capacitance, significance of coating resistance and usefulness of breakpoint frequency are common in most papers. They mentioned that breakpoint frequency and coating resistance are critical because they are both obtainable in early stages of degradation and the information is related with coating delamination. There were many observations controversial with in present publications. Therefore, the proposed equivalent circuits should be confirmed with other experimental techniques.

Breakpoint frequency is expressed as the highest frequency of the 45° phase shift is observed. When the phase angle is 45°, the resistive and reactive impedances are equal. Assuming that, Equation 1.13 can be obtained to measure the ratio of delamination.

$$f_b = f_b^0 \frac{A_{delaminated}}{A}$$

Equation 1.13. Relation of Breakpoint frequency and delaminated area.

Bonora, Deflorian, and Fedrizzi investigated complex coating-metal interactions with EIS. 3.5% sodium chloride and 0.3% sodium sulphate was used as the electrolyte in EIS measurements.<sup>27</sup> The authors observed that the thickness of the coating may hide the electrochemical behavior, i.e., impedance may not be measured with available EIS instruments due to very high values. This situation may lead to difficulties in finding the best equivalent electrical circuit. So, the coating thickness could be lowered to achieve a more convenient EIS data. Authors also suggest that all the elements in the equivalent electrical circuit should have a physical meaning and circuits should be built as simple as possible. This means, if removing an element does not change the validity of the data, then it should be removed. Meaning of the common EIS parameters were explained by the authors also. Coating capacitance ( $C_c$ ) changes with the water uptake of the coating due to the difference of the dielectric constant of the water and the coating. Ratio of the penetrated water in the coating ( $\phi$ ) was calculated with Equation 1.11 The authors mentioned that  $\phi$  reaches a constant value after an immersion period and this time period contains information about the barrier properties of the coating as shown in Figure 1.17.

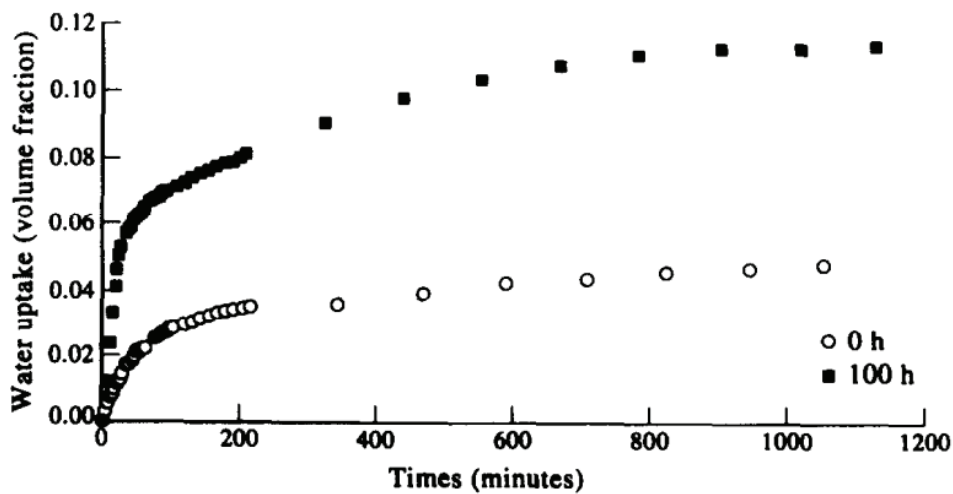


Figure 1.17. Water uptake trend for a polyester coated galvanized steel before and after 100h of UV radiation.<sup>27</sup>

The trends with pore resistance( $R_p$ ) with respect to time is inversely proportional to the defect area evolution according to the authors. Charge transfer resistance( $R_{ct}$ ) is inversely proportional to the corrosion rate and the surface area under corrosion. Double layer capacitance( $C_{dl}$ ) contains information about the wet area of the metal. By comparing  $C_{dl}$  values of bare metal and the sample, it is possible to evaluate the delaminated area  $A_d$  as shown in Equation 1.14

$$\text{Ratio of the Delaminated Area} = \frac{C_{dl}}{C_{dl\ ref}}$$

Equation 1.14. Calculation of delaminated are with double layer capacitance.<sup>27</sup>

#### **1.4.5. Statistical Confidence of EIS Data**

Tait pointed out that the reproducibility of EIS data can be an issue.<sup>30</sup> Collecting data before samples reach steady state may lead to higher errors in further calculations. As shown in non-corroding EIS data of 30 different measurements in Figure 1.18, impedance values between  $3 \times 10^5$  and  $10^6 \Omega\text{cm}^2$  were measured. . With the corroding samples, the error margin could be as high as  $\pm(Z) \times 10^3 \Omega\text{cm}^2$  (three order of magnitudes different than average impedance).<sup>30</sup> Also, for coating thickness, it was observed that there may be homogeneity issues. An example of varying coating thickness from 4 to 8 microns along  $10 \text{ cm}^2$  area was shown. This shows that homogeneity of the coating should also be investigated. With considering mentioned issues, replicate samples, monitoring open circuit potential, and capacitance magnitudes can be used to develop more accurate estimations of system durability.

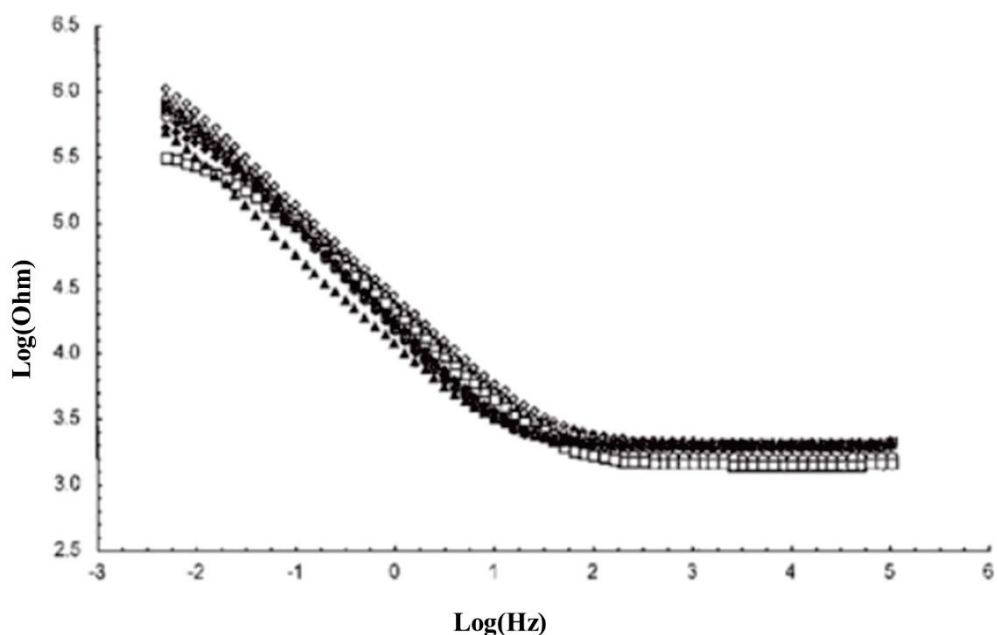


Figure 1.18. EIS measurements of non-corroding epoxy coated tin plate.<sup>30</sup>

#### 1.4.6. Weathering of Coatings

Deflorian compared artificial weathering of the organic coatings regarding salt spray, UV exposure.<sup>31</sup> Before weathering, all samples had around  $10^{10} \Omega\text{cm}^2$  coating resistance. UV exposure of 1000 h did not contribute enough to degrade studied coatings, impedances were not changed, and coating resistance reduced to  $10^9 \Omega\text{cm}^2$ . Only fluoropolymer based top coating degraded and it was proved with FTIR that significant band stretch of C-F only. After exposure to 500h salt spray chamber, coating resistance was reduced to  $10^6 \Omega\text{cm}^2$  for all samples. The difference between the samples are noticed for the high impedance of ZnAl substrate compared to pure Zn. After investigation of natural weathering, authors found that samples are subjected to more wetting time than salt spray i.e. artificial wetting and less solar power than UV chamber i.e. solar power. There was a  $\pm(Z) \times 10^2 \Omega\text{cm}^2$  error margin between the same coating naturally weathered in different climates.

## CHAPTER 2

### LITERATURE SURVEY

In this chapter, relevant studies about can coating industry, tinplate and electrochemical impedance spectroscopy were summarized and compared.

#### 2.1. Investigations and Reported Problems of Can Coating Industry

Charbonneau examined the failures of variety of three-piece food cans in the market with SEM and EDX analysis as case studies.<sup>12</sup> His cases include rapid detinning, pitting corrosion, cosmetic corrosion, flaking of enamel, stress-corrosion cracking. He used square root of the ratio of peak intensities of tin(L $\alpha$ ) and iron(K $\alpha$ ) to understand tin coating weight from EDX. Charbonneau points that industrial grade tin-plates may vary in tin coverage. An example he studied was a 5.6 g/m<sup>2</sup> tin weight, varies from 1.7 to 10.3 g/m<sup>2</sup> even in 100  $\mu$ m scale. This indicates that surface evenness should be investigated. Another method he used involves ICP analysis of the food samples to find trace metals. He pointed that nickel contamination increases the chance of pitting corrosion by comparing different samples that contains low(0-5 ppm) and high(10-20ppm) nickel content in the food media. Another observation that Charbonneau made was contamination of copper in the weld areas promotes stress corrosion cracking.

Tin thickness of a can may vary from inside to outside(1.5 microns to 0.3 microns).<sup>32</sup> Filiform corrosion can occur from outside of a can and may lead to the failure of the can. Also, cosmetic corrosions such as Sulphur stains occurs when the iron or copper forms metal sulfide with the Sulphur in the food media. This will not lead to failure of a can usually however, due to the complaints from the customer it has an economic impact. Each case that were investigated by Charbonneau in this paper, involves different food-container interaction. Corrosion mechanisms were not discussed in detail. As shown in Figure 2.1 tin discontinuities were observed in micron levels which leads to early failure of a can.<sup>33</sup>

Exterior exposure to sulfur dioxide and hydrogen sulfide were reported as promoting stress corrosion cracking in tin plate cans.<sup>34</sup> Exterior corrosion effect of cans

with main atmospheric pollutants in the area as Cl, SO<sub>2</sub>, NO<sub>2</sub> were examined. Relative humidity, storage conditions and seasons, pollutant concentration were found to affect exterior stability of a can.<sup>35</sup>

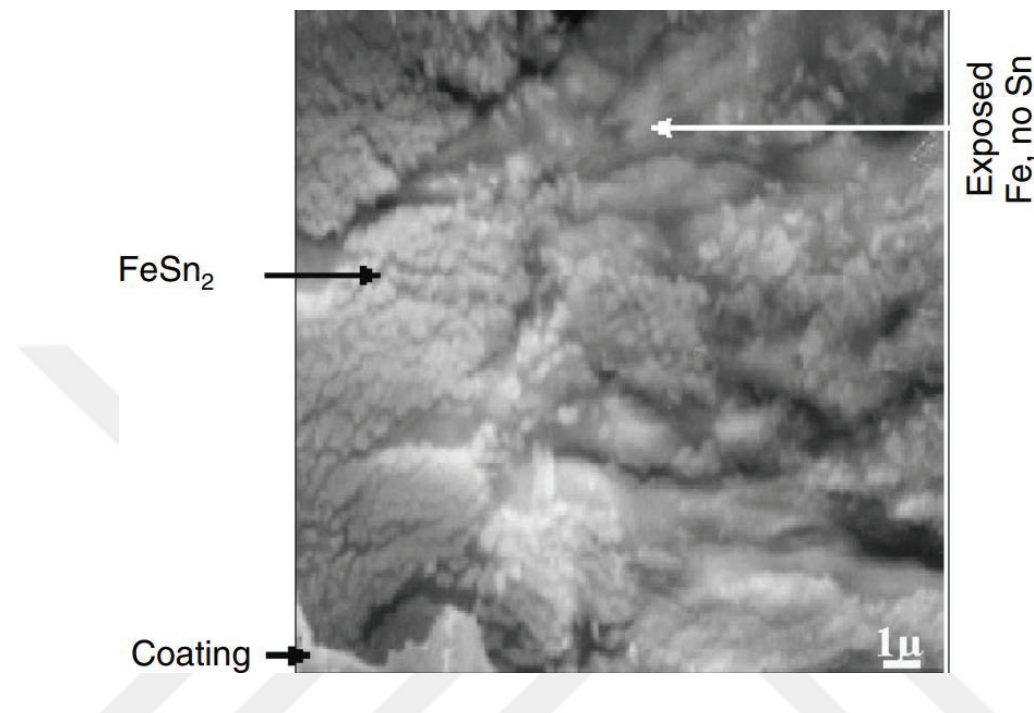


Figure 2.1. An example of tin discontinuity in a food can.<sup>33</sup>

### 2.1.1. Electrochemical Impedance Measurements of Real Cans and Simulations

There are numerous studies which investigated electrochemical behavior of the commercial cans and their performance.<sup>11,12,32,36–39</sup> They include electrochemical study with a physical test or spectroscopy to understand corrosion mechanism in more detail. The main difference of internal corrosion of a can compared to atmospheric corrosion is the presence of aggressive media in the can, i.e. food and anaerobic conditions. Following studies are present for can coating industry.

Two different lacquered system along with different chromate pretreatment weights and applications were studied with sea food by Catala.<sup>40</sup> Lacquering conditions include double coat for both systems. One includes two coats of epoxy-phenolic with



aluminum flakes, other includes a thicker organosol top on epoxy-phenolic base. The corrosion performance of the thicker lacquered system was found superior however it was not clear whether this was due to the thickness of the coating or different coating properties. Corrosion mechanisms of mussels and tuna was found to be different. Corrosion currents of tuna and mussel containing cans were found to be higher than 100 nA/cm<sup>2</sup> and lower than 3 nA/cm<sup>2</sup> respectively. In tuna containing cans, dissolved iron and tin was found to be lower than 10 ppm however for mussel containing cans, no tin was detected, and dissolved iron was found around 30 ppm for all lacquer and pretreatment samples even though lower corrosion current density of mussel containing samples (<3 nA/cm<sup>2</sup>). High iron content with no tin indicates pitting corrosion of mussel containing samples which is a considerable threat in the can coating industry. Pure capacitive behavior observed for even 100 day immersed thicker lacquered systems containing mussels even though higher than 20 ppm of Fe were measured. In tuna containing samples this value is lower than 10 ppm of Fe. Fluctuations in the EIS measurements were attributed to continuous blocking and unblocking of defects with corrosion products which is hard to prove without surface analysis. Authors also used DC corrosion of aged samples to be able to understand the corrosion currents. Unexpectedly, there was not a relation observed between dissolved iron/tin content and the corrosion current of the cans. Different pretreatments include chromium passivation by dipping and cathodic treatment of different chromium weights. There was not a significant relation between corrosion performance and different pretreatments.

Commercial food cans were investigated by Bovard with EIS.<sup>41</sup> It was mentioned that usually cans are examined visually and evaluated with an ASTM standard D714-87 "Standard Test Method for Evaluating Degree of Blistering of Paints" after two-year pack test which was considered as an industry standard for food cans. Bovard, Burleigh and Smith investigated 8 different aluminum food cans with different food compositions with EIS after two-year pack test. The pH range of the foods was 3.3-6. Two electrode EIS measurements were conducted in-situ (with the food it-self) with the same aluminum alloy of the food cans. As a corrosion performance indicator, low frequency impedance ( $\text{Log}(Z)_{0.04 \text{ Hz}}$ ), break-point frequency ( $f_{bp}$ ) and percent ideal behavior i.e.  $C_{(t)}/C_{\text{initial}}$  were chosen to extract information from an entire EIS spectrum by the authors.<sup>42</sup>  $\text{Log}(Z)_{0.04 \text{ Hz}}$  is approximately equal to the charge transfer resistance ( $R_{ct}$ ) and coated steel food cans which have  $R_{ct}$  less than  $10^7 \text{ } \Omega\text{cm}^2$  have a container service lifetime (CSL) shorter than a year,  $R_{ct}$  higher than  $10^9 \text{ } \Omega\text{cm}^2$  have a CSL of longer than

two years showed by Tait.<sup>43</sup> Ideality of the coating was calculated with the ratio of the areas under the bode plots of real and ideal impedance curve as shown in Figure 2.2. It was shown by the authors, initially the coatings were near perfect as they behaved like a pure capacitance however they degraded over time. All the three indicators showed matching results with the visual inspection. The performance of the coating was pH dependent(food).

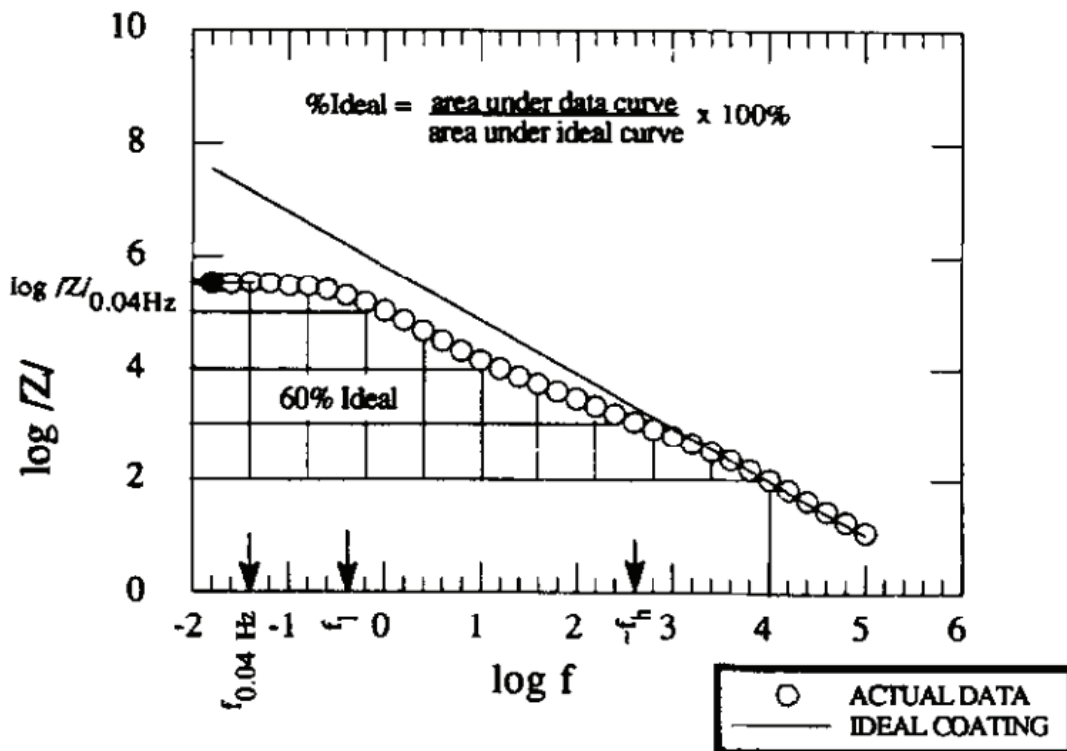


Figure 2.2. Calculation of ideal percentage behavior of a degraded coating with bode plot.<sup>41</sup>

PET laminated and conventional organosol lacquered ECCS samples were investigated with EIS by Buttrey.<sup>39</sup> PET laminated cans were found to be significantly more resistant to corrosion. Authors used a novel technique which involves EIS measurements of autoclaved cans without opening them. This process involves seaming the caps with electrodes. Along with EIS, authors measured oxygen concentration at the head space area of the cans, however electrode seamed cans showed significantly higher oxygen concentration(6%) compared to control cans(1%) due to the oxygen ingress. The

used equivalent circuit model is III of the Figure 1.14. EIS data showed that  $R_{ct}$  values were inversely related to the oxygen concentration due to the corrosion reaction of the iron, while  $R_{pore}$  values remained relatively unaffected. It was found that for laminated cans, initial  $R_{pore}$  values greater than  $6.2k\Omega$  performed well after prolonged shelf life storage and  $R_{pore}$  value drops significantly in 30 days of immersion as shown in Figure 2.3. Authors also reported increasing thickness in PET laminated ECCS samples have increased corrosion resistance as expected.

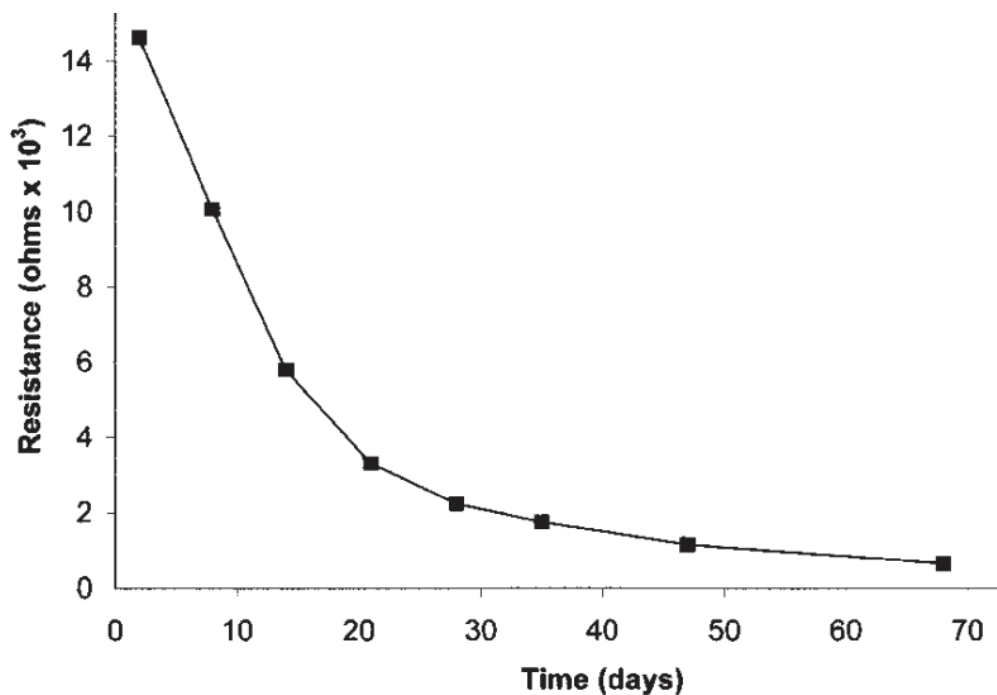


Figure 2.3. Pore resistance values with respect to immersion time.<sup>39</sup>

Variety of the can samples with different coatings were investigated by the authors with EIS.<sup>37</sup> A phosphate buffer solution prepared from ortho-phosphoric acid and sodium hydroxide adjusted to pH value of 6 was used as an electrolyte solution for EIS measurements. It was reported that higher pore area will lead to lower values of  $R_{pore}$ . Similar equation as Equation 1.14 to calculate delaminated area from double layer capacitance is proposed. Double layer capacitance found to be the most useful method for quality evaluation of the cans by the authors. Also, cans were investigated as initial, DC aged and long-term electrolyte aged states. Wetted metal surface area calculations

from EIS showed that 12-month shelf aged and 10h electrolyte aged samples show closer values than DC aged samples. Initial measurements were found to be useful for new cans however electrolyte aging gave the best precision in performance prediction among the methods.

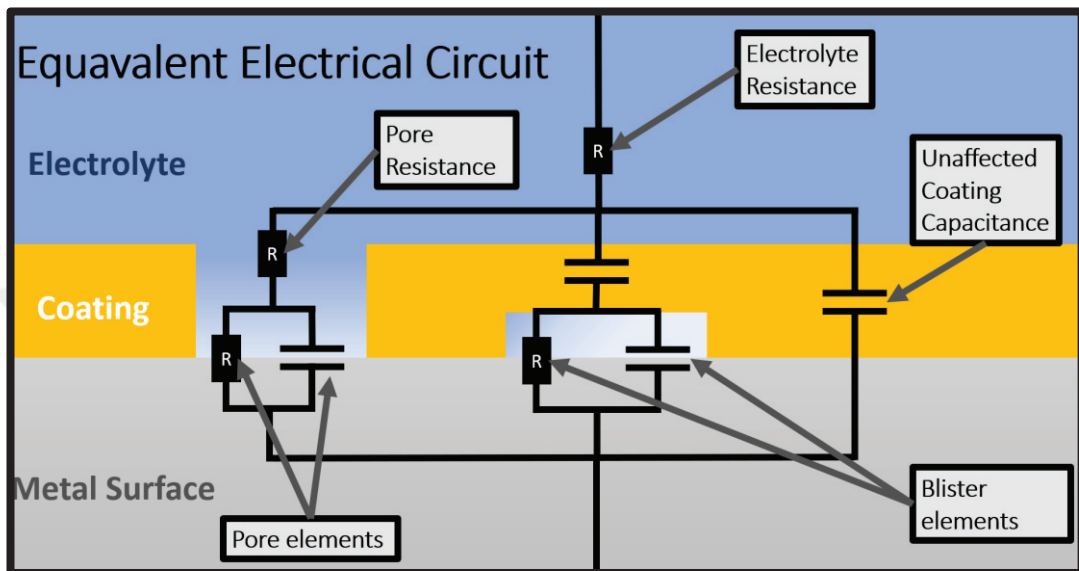


Figure 2.4. A complex equivalent electrical circuit model<sup>37</sup>

Typical values of common circuit elements were given in Table 2.1 for the chosen equivalent electrical circuit as shown in the Figure 2.4.

Table 2.1. Common equivalent circuit elements and typical values.<sup>37</sup>

Element	Description	Related To	Typical Value
$R_e$	Electrolyte resistance		1-2 $\Omega$
$R_{pore}$	Pore resistance	Pore area in coating	5-50 $\Omega$
$R_{ct,pore}$	Charge transfer resistance	Corrosion state of metal	$10^4$ - $10^6$ $\Omega$
$C_{ct,pore}$	Double layer capacitance	Delaminated metal area	$10^{-8}$ - $10^{-6}$ F
$R_{ct,blister}$	Charge transfer resistance	Corrosion state of metal	0.1-100 $\Omega$
$C_{ct,blister}$	Double layer capacitance	Wet metal surface	$10^{-10}$ - $10^{-9}$ F
$C_c$	Coating capacitance	Coating thickness, Water content	$10^{-8}$ - $10^{-7}$ F

Zumelzu investigated corrosion performance of the PET laminated ECCS, aluminum plated and epoxy-phenolic lacquered tinplates immersed in 0.1M pH 3.85 acetic acetate media(0.6 acetic acid roughly).<sup>44</sup> The atomic absorption spectroscopy results showed that, dissolved tin and iron amounts are significantly higher in epoxy-phenolic cans. BET analysis showed that pore size of the epoxy-phenolic lacquered cans was twice as much large compared to PET laminated cans. This result is also confirming electrolytic porosity test results in which the current of the epoxy-phenolic lacquers were 20 times higher than PET laminated cans.

Another study of Zumelzu includes investigation of 1% lactic acid as aging electrolyte for PP and PET coated ECCS samples.<sup>45</sup> It was found that lactic acid affects the structural integrity of both polymers, investigated with FTIR. Ethylene and carbonyl groups of PP coating were changed after the aging with lactic acid. Deformation vibration of the benzene ring observed at  $630\text{ cm}^{-1}$  for PET coating which indicates significant degree of chemical alterations done with lactic acid.

Zhou investigated epoxy-phenolic lacquered tin plate as energy drink beverage which includes citric acid, taurine, saccharose, essence, benzene sulfonic acid sodium salt, citric yellow etc. and pH is between 3 and 3.2 with only EIS and Electrochemical Noise measurements.<sup>46</sup> Corrosion potential as a function of immersion time was plotted. It becomes close to uncoated panel after a year. Corrosion mechanisms were investigated with EIS and classified into three stages; Stage I is the wetting of the organic coating with one time constant. Stage II is the corrosion initiation beneath the coating with two-time constants. Tin coating started to degrade at Stage II. Stage III is the corrosion extension with three-time constants. As shown in Figure 2.5, after 220 days of immersion, corrosion of steel was started. After a year of immersion, the coating was heavily damaged, and the steel corrosion dominated system were observed. Warburg impedance element were not discussed by the authors.

Wang investigated corrosion mechanism of commercial cans containing coffee with EIS, EN, AFM and ICP/MS.<sup>47</sup> ICP-MS results of tin and iron released in the can were parallel with the electrochemical impedance spectroscopy data. Lower impedance valued samples have higher tin and iron release in their media. EIS measurements of the beverage can degradation can be seen in Figure 2.6. In the first month, single capacitive loop with high impedance value is observed which indicates protective properties of organic lacquer. Impedance data of the first month is modelled as  $R_e(R_cQ_c)$ , II of the Figure 1.14. After the first month second capacitive loop is observed which indicates tin

and iron dissolution to the media (parallel connected  $R_{ct}$  and  $Q_{dl}$ ). Impedance data of the latter stage is modelled as III of the Figure 1.14. After 12 months of immersion, the first capacitive loop decreases as an indication of loss of the protective abilities of the organic coating ( $R_c$ ).  $R_{ct}$  is decreased with respect to immersion time which indicates the increase dissolution of iron and tin.

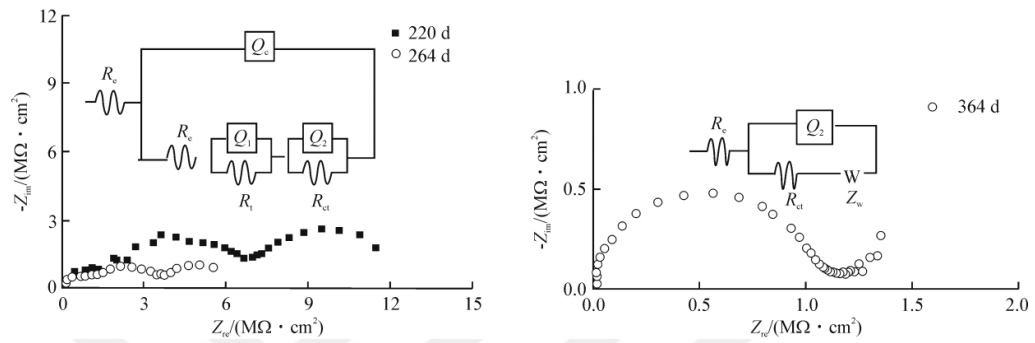


Figure 2.5. Nyquist plot of epoxy-phenolic lacquered energy drink, corrosion stage III.<sup>46</sup>

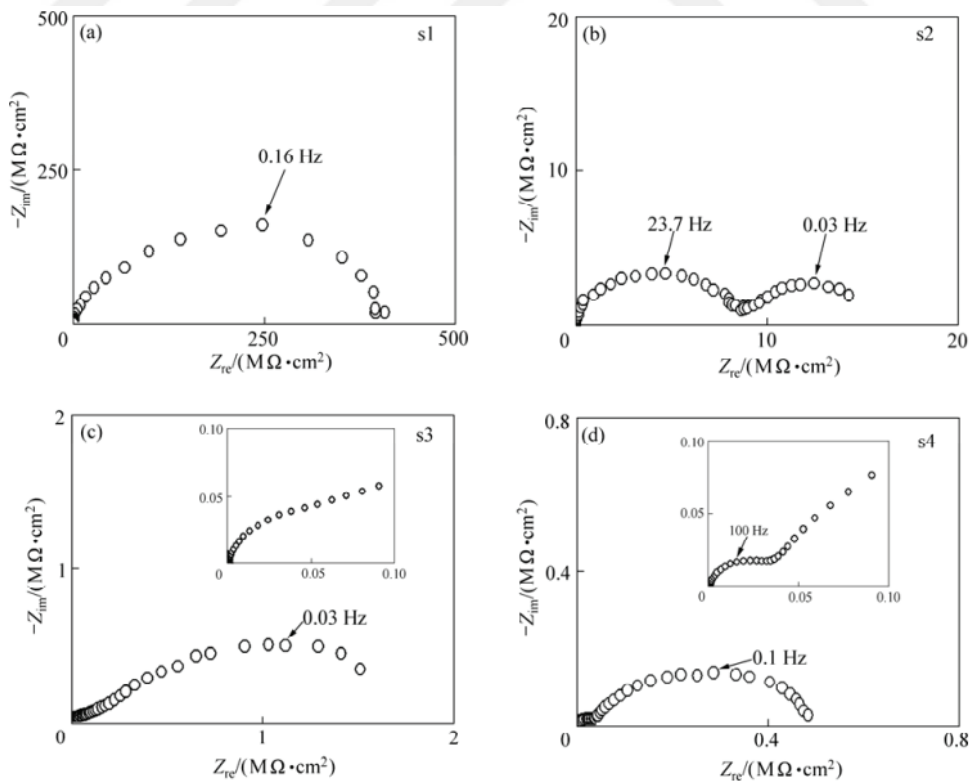


Figure 2.6. Nyquist plots of beverage cans with different storage time: a)1 month, b)3 months, c) 12 months, d)12 months with defect.<sup>47</sup>

Doherty & Sykes investigated degradation of epoxy-phenolic lacquered ECCS samples with scanning kelvin probe(SKP), scanning acoustic microscopy(SAM) and EIS.<sup>48</sup> The samples were immersed in 1% NaCl solution. They pointed out that pore resistance decreased rapidly in the first 5 hours as shown in Figure 2.7.

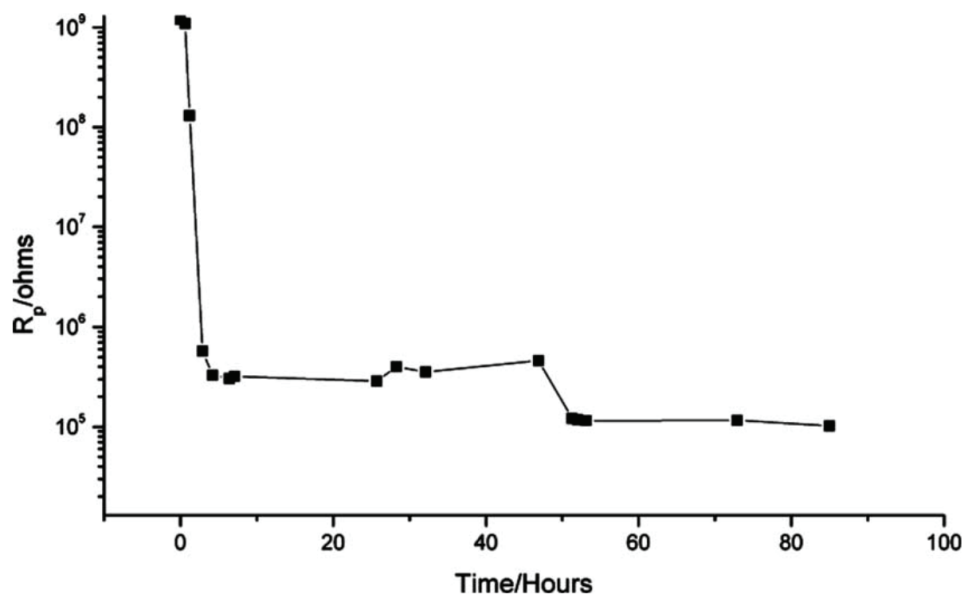


Figure 2.7. Pore resistance of epoxy-phenolic lacquered ECCS immersed in 1% NaCl solution with respect to time.<sup>48</sup>

Authors proposed a model in line with previous scientific work which involves pore blocking by corrosion products(rust) and then the formation of the blisters in Figure 2.9. After blister formation, corrosion products undergo the reaction which is shown in Figure 2.8 as cathode reactants. Standard electrode potential of the reaction was between 0 and – 400 mV. Authors proved that with the scanning kelvin probe images which shows the blister area around -350 mV and optical microscope images which shows the transition between red rust to black magnetite.

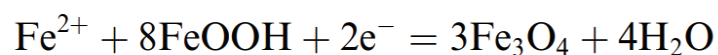


Figure 2.8 Reduction of rust to magnetite.<sup>48</sup>

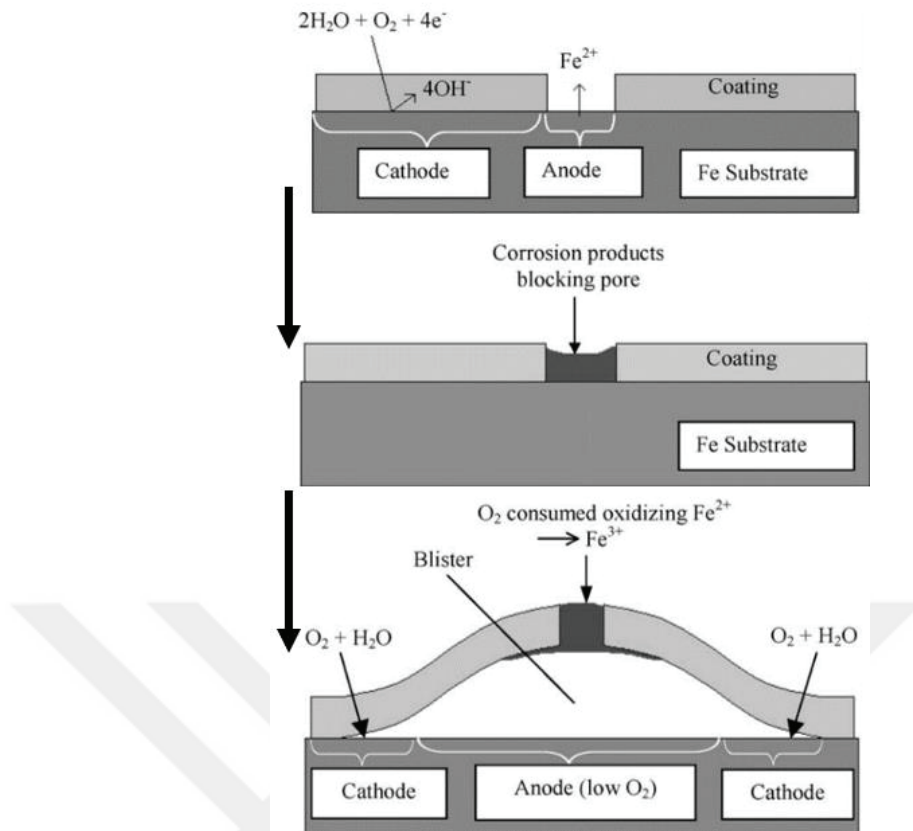


Figure 2.9. Evaluation of the coating surface as blister formation.<sup>48</sup>

Authors also observed the disappearance of the Warburg impedance after they immersed the plates 0.1 M citric acid for 50h which were before immersed for 170h in 1% NaCl. Nyquist plots of the mentioned phenomena is shown in Figure 2.10.

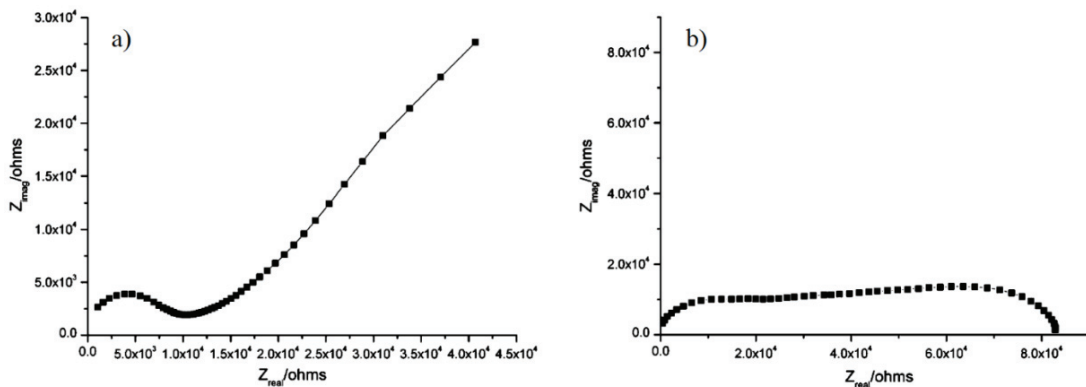


Figure 2.10. Before(a) and after(b) immersion of 0.1 M Citric acid of epoxy-phenolic lacquered ECCS plates.<sup>48</sup>



When a corrosion site becomes blocked with rust, new anodic sites are formed, and the rust becomes the cathode reactant. Citric acid unblocks the pore and due to this, the corrosion reaction no longer continued under the diffusion control.

## 2.2. Surface Structure and Electrochemical Properties of Tinplate

Corrosion performance of different passivation techniques on tinplate were investigated by Almeida including conventional chromium and more environmentally friendly Titanium, Cerium, Zirconium and Oxalate based pretreatments.<sup>38</sup> Methods include DC corrosion, polarization and visual observations after aging with a variety of electrolytes. Visual investigation of Titanium and Cerium was found to be close to conventional chromium pretreatment. As shown in Figure 2.11, Titanium and DCD pretreatments have lower corrosion currents than Zirconium and Oxalate pretreatments. Authors mentioned insufficient thicknesses of the pretreatments to cover the whole surface and it should be improved for better protection however the thickness of the pretreatments were not measured. For all passivated tinplates, metallic tin with Sn(II) and Sn(IV) oxidation stages were confirmed on the surface.

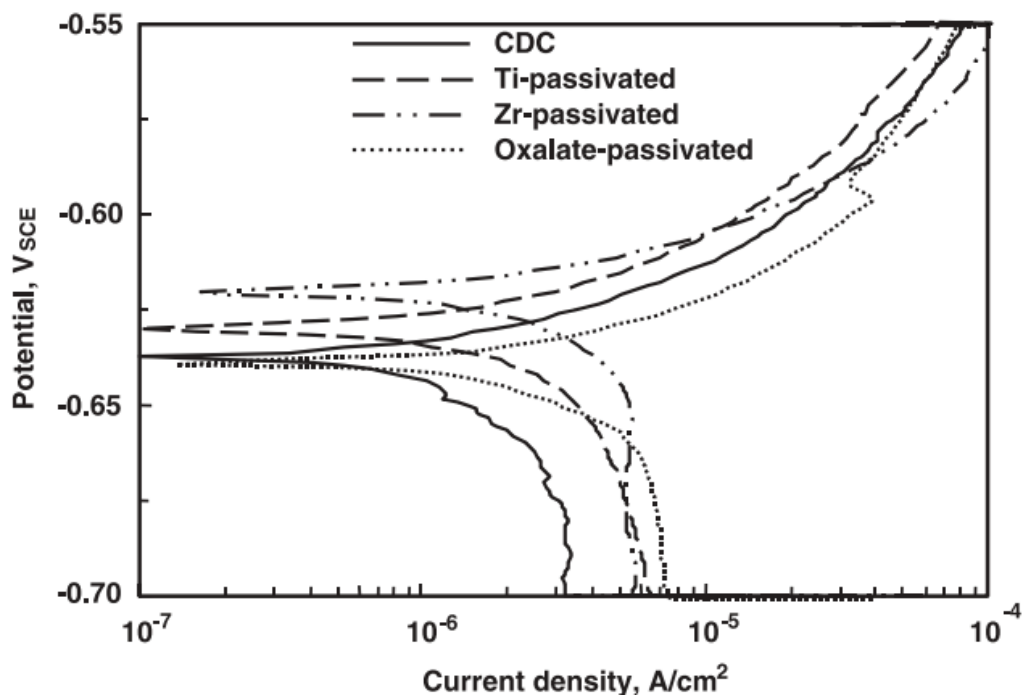


Figure 2.11. Polarization curves of different passivation on tinplate.<sup>38</sup>

Wang showed that the chemical passivation film distributes more uniformly on an uneven tinplate surface than the electrolytic passivation film as schemed in Figure 2.13<sup>49</sup>. For electrolytic passivated samples, Ra values increased from 22 to above 40 microns while dipped samples only increased to 27 microns, measured with profilometer. According to the profilometer roughness data, authors concluded that the film is thicker on the microscopic bulges than that in the microscopic valleys, and the thickness difference increased with longer passivation time. For chemical passivation, surface contamination is less and has more desirable composition as shown in Table 2.2.

Structure model of ideal tinplate consists of nanometer scale thick Cr and Sn oxides, micrometer scale Sn and FeSn<sub>2</sub> alloy and mm scale base steel as shown in Figure 2.12.

Table 2.2 Chemical composition of a tinplate surface.<sup>49</sup>

<b>Tinplate Sample</b>		<b>Cr(OH)<sub>3</sub></b>	<b>Cr<sub>2</sub>O<sub>3</sub></b>	<b>Cr</b>	<b>Cr(VI)</b>
Chemical passivation	3 s	–	100.00	–	–
	6 s	–	100.00	–	–
Electrolytic passivation	3 s	48.82	41.44	6.55	3.18
	6 s	51.03	41.89	4.88	2.20

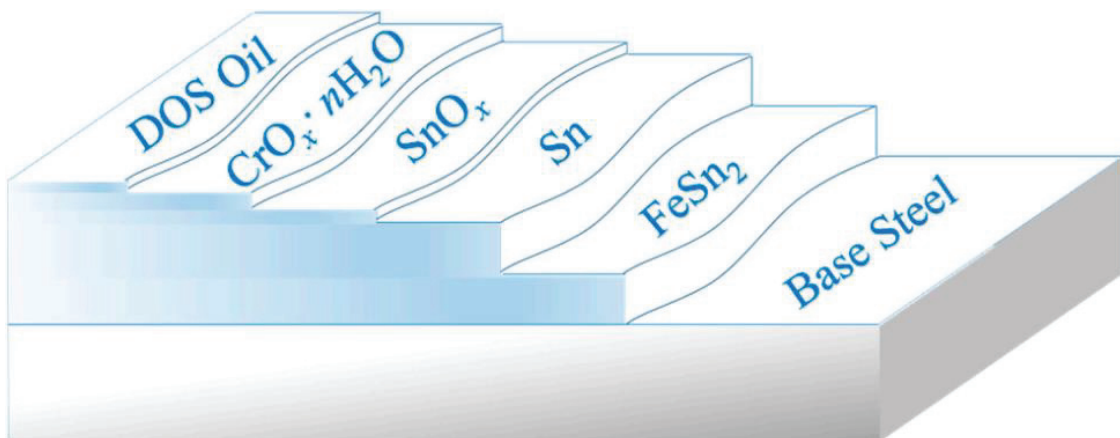


Figure 2.12. Structure model of the tinplate surface and interface.<sup>49</sup>

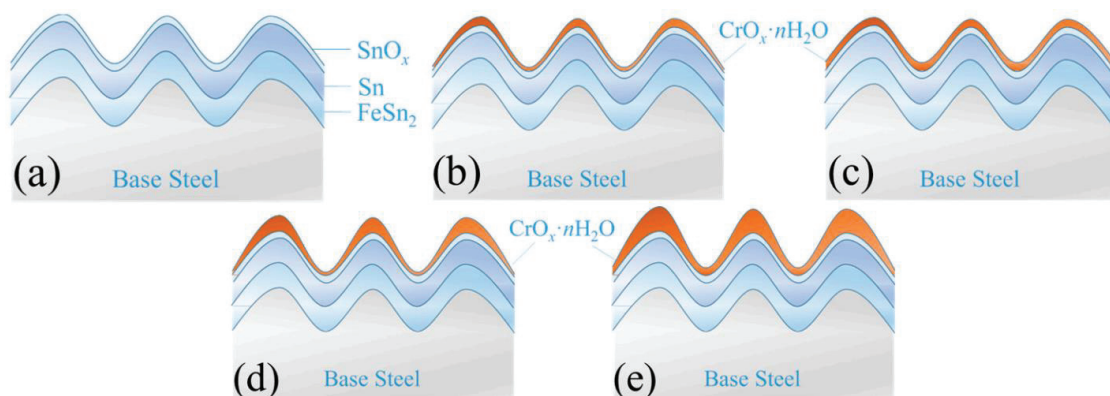


Figure 2.13. Schematic diagram of structure models of the tinplate treated with (a) reflowing before passivation; (b,c) chemical passivation for 3 s and 6 s, respectively; and (d,e) electrolytic passivation for 3 s and 6 s respectively.<sup>49</sup>

Thickness of the passivation film were not measured by Wang because the film is very thin, and since the thickness distribution of the film on the tinplate surface is uneven, combined with large base roughness, it is difficult to find a test method to accurately detect the thickness of the passivation film.

Almeida et al. investigated the corrosion effect of titanium passivation technique over traditional chromium passivation on metal food packaging with EIS, EDX and SEM.<sup>11</sup> Following electrolytes were used;

- 1% citric acid and 0.5% tartaric acid;
- 2% citric acid and 10% sucrose;
- 3% acetic acid and 1% NaCl;
- 1% citric acid and 3%NaCl;
- 1% lactic acid;
- 3 g/L L-cysteine chlorhydrate neutralized with a 1% solution of Na<sub>2</sub>CO<sub>3</sub>

EDX measurements of the plates before and after aging by the tomato paste resulted without a significant difference which means there were not any corrosion or corrosion product related changes observed on the surface of the plate. EIS measurements of different passivated samples which were aged for 7 days in citric acid show different corrosion mechanisms as shown in Figure 2.14, which show the importance of passivation

on the corrosion protection. Authors also compared industrially accepted tests such as MEK double rub, color change, cross-cut adhesion, enamel rater porosity, gloss and visual comparison with EIS and EDX data. Electrochemical and spectroscopic data were supported by conventional evaluation methods. The corrosion mechanisms were not discussed in detail.

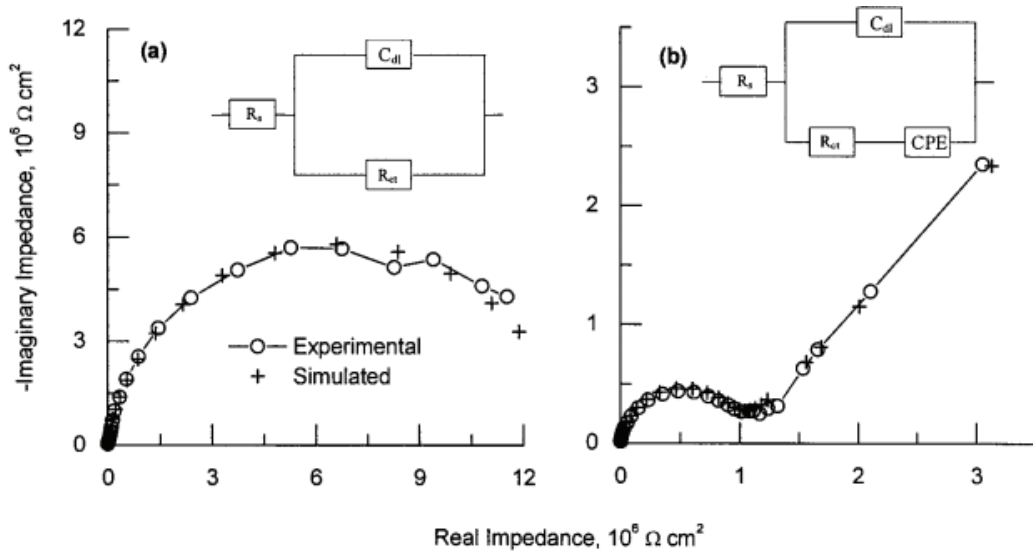


Figure 2.14. Nyquist plots for lacquered tinplates after 7 days of immersion in citric acid solution a) titanium passivated b) chromium passivated.<sup>11</sup>

A recent publication by Melvin showed that increasing the tin coating weight reduces the surface roughness for all the surfaces.<sup>50</sup> Industrial samples with different tin coating weights were investigated. White Light Interferometer(WLI) was used to measure roughness. As the tin coating weight increases, the difference between the roller finish induced topologies reduces. At the first 4 nm of the surface of the commercial tin plate, main compounds are chrome hydroxide, chrome oxide, tin oxide, and a small quantity of metallic tin and chrome. CrOx may provide the bonding sites between the lacquer and the substrate, this organic/inorganic surface bond is not the cause of lacquer/tinplate failure according to the XPS data of scratch and unscratched surfaces as shown in Figure 2.15.

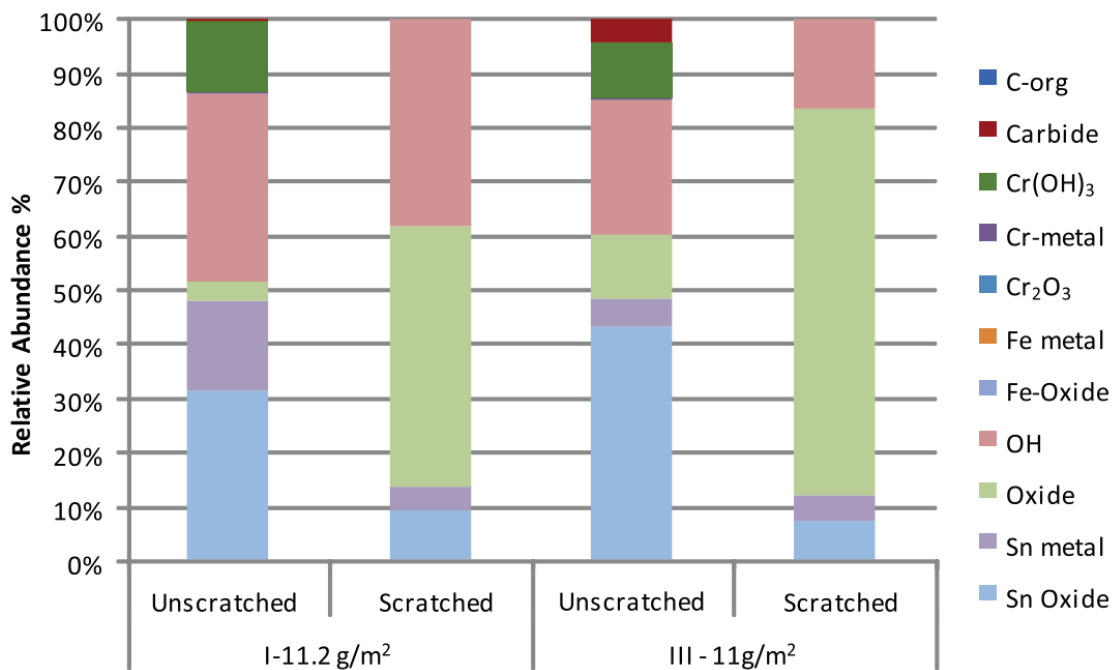


Figure 2.15. XPS Surface composition by weight of scratched and unscratched coated tinplate.<sup>50</sup>

There was a relation between SnO<sub>x</sub> and Sn weight, as 0.145 mg/m<sup>2</sup> SnO<sub>x</sub> per g/m<sup>2</sup> Sn. The composition in the valley created by the scratch and within the scratch, there is no evidence of any chrome species (metallic, oxide, or hydroxide) indicating that these have been removed by the stylus i.e. adhesion scratch tester as shown in Figure 2.15. There is no exposed iron at the surface indicating that the failure has occurred above the iron and the iron/tin intermetallic layer. The primary difference in the surface chemistry is an increase in the oxides associated with the tin oxide formation. Authors did not find a correlation between the surface roughness and the measured adhesion and that the underlying macrostructure of the texturing roll surface (ground or shot blasted) does not play a significant role in the adhesion. The primary means of adhesion failure has proven to be the brittle tin oxide layer between the tin surface and the chrome passivation layer. Caiazzo detected tin free surface(iron) in 36nm sputtered EDX measurements.<sup>51</sup> The thickness of the different layers is determined according to Standards EN 10202 by galvanostatic polarization of the tinplate in 1 M HCl. Calculated free and alloyed tin was shown in Table 2.3. Increased free tin did not contribute to thicker alloyed tin.

Table 2.3. Free Tin and Alloyed tin calculated results via equation

Sample	Free Sn <sup>a</sup> , nm	Alloyed Sn <sup>a</sup> , nm	Total Sn
A	215 ± 05	124 ± 06	339 ± 08
B	211 ± 13	106 ± 05	317 ± 14
C	426 ± 06	138 ± 14	564 ± 15
D	936 ± 49	49 ± 09	985 ± 50
E	1061 ± 65	193 ± 08	1254 ± 66

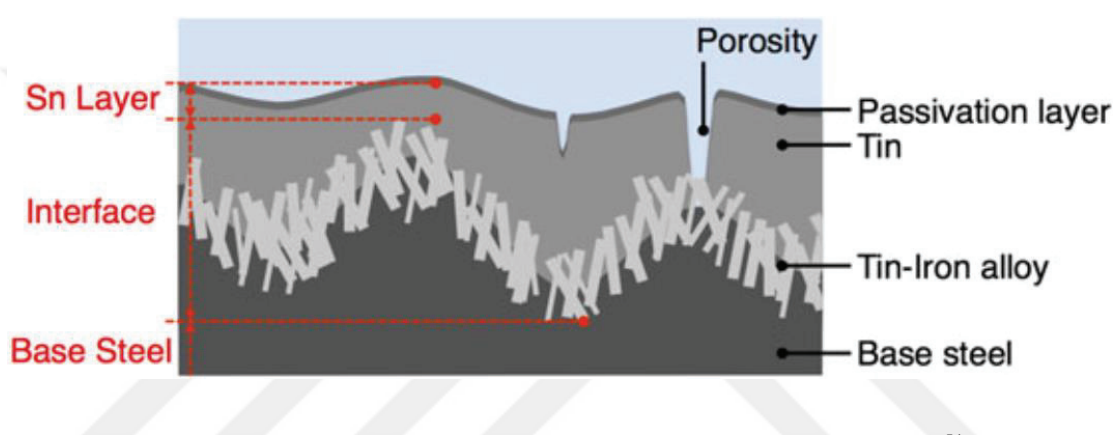


Figure 2.16. Model of the tinplate proposed by Caiazzo et. al.<sup>51</sup>

Despite the chemical inertness of the FeSn<sub>2</sub> phase, its needle-like structure limits its corrosion protection capabilities since iron is exposed through the inter-needle spaces. The iron-tin alloy layer should be expressed as diffusion interface with iron, tin and iron-tin alloy coexist together as shown in Figure 2.16.

Mora investigated 311 passivation(cathodic treatment in sodium dichromate) applied commercial tinplate samples.<sup>52</sup> 5.50 mg/m<sup>2</sup> of total chromium consisted of 1.27 mg/m<sup>2</sup> of metallic chromium and 4.23 mg/m<sup>2</sup> of oxides. Chromium was in the form of oxide as Cr<sub>2</sub>O<sub>3</sub> and hydroxide [Cr(OH)<sub>3</sub>]. Metallic and hexavalent chromium were not observed in XPS data. XPS depth profiles showed that, hydroxides(chromium) are located at the outer surface and oxides(Tin and chromium) located at the inner surface. SnO and SnO<sub>2</sub> were also observed for passivated and unpassivated samples however instrumentation was not allowed to distinguish between them due to the close binding energies.

Electrodeposited tin with different coating mass were investigated by Wu.<sup>53</sup> Iron contamination in the pretreatment solution may rise corrosion problems. Main surface oxides are  $\text{Cr}_2\text{O}_3$  and  $\text{Cr}(\text{OH})_3$  and  $\text{Cr}_2\text{O}_3$  located at the outer surface.

30 nm of the surface of the commercial tinplate with dip chromate treatment had been investigated with XPS.<sup>54</sup>  $\text{Cr}_2\text{O}_3$ ,  $\text{SnO}$ ,  $\text{Cr}(\text{OH})_3$ , metallic Sn and a small amount of metallic Cr found as mixed. Majority of the layer consists of  $\text{Cr}_2\text{O}_3$  and it was found in whole surface as shown in Figure 2.17. Metallic chromium was only found in the deeper and  $\text{Cr}(\text{OH})_3$  on the top of the layer(8nm according to sputtering rate of pure Sn is about 21 nm/min). Metallic tin was found in whole layer however  $\text{SnO}$  exists in 0-15nm below the surface only.

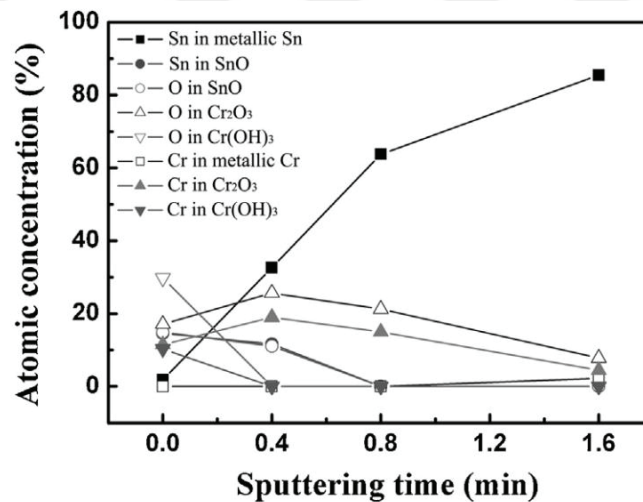


Figure 2.17. Atomic concentration of the elements on the sputtered tinplate.<sup>54</sup>

Corrosion performances of unlacquered food grade tin plates were investigated by Benitez<sup>55</sup>. 10 g/L of citric acid and 13 g/L NaCl regulated to pH=4.0 by the addition of NaOH was used as synthetic food media. Determination of the exposed iron of the tin coating was measured with the current evolved after applying a potential step of 1.2V between specimen and reference electrode. The method is based on the activation of the exposed iron only at the applied potential. Free tin and alloyed tin amount were measured with galvanostatic oxidation of the metal in 1:10 HCL at 6.26mA/cm<sup>2</sup>. A typical electrochemical potential of a tin plate was shown in Figure 2.18 and due to this alloyed tin will not be attacked while free tin is available.

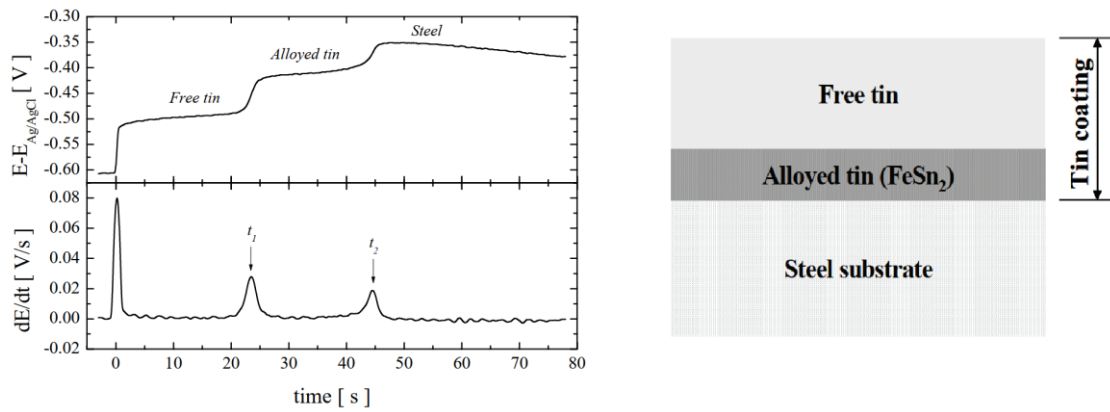


Figure 2.18. Electrochemical potential of galvanically oxidized tin plate.<sup>55</sup>

Nitrate ions fasten dissolution rate, creating pores in the free tin coating and increases total porosity as shown in Figure 2.19 and  $\text{Cu}^{2+}$  in the solution leads to increased tin coating porosity.

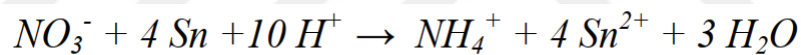


Figure 2.19. Dissolution of tin.<sup>55</sup>

### 2.2.1. Nano Characterization of Coating Degradation

Morsch proved that regardless of the application method, the dry thickness and water uptake capacity of the epoxy-phenolic can coating increases with increased curing temperatures as the cross-linking degree increases.<sup>56</sup>

Degradation mechanism of epoxy-phenolic can coating were investigated by Morsch.<sup>57</sup> Nano-scale fluctuations in crosslinking density occur within thermoset epoxy resins. Also, water uptake of epoxy-phenolic resins heterogeneous at the nanoscale. Ion transport was found to occur across the intact coating which indicates ion penetration is not only dependent of water-induced degradation. Morsch showed that deionized water affects the morphology of the coating faster and more intense than 5% NaCl as shown in Figure 2.20 . This shows that ionic species(Na, Cl) does not significantly affect the



degradation mechanism of epoxy-phenolic can coating. They advised investigation of bonding at substrate-coating interface and substrate potential effect as the driving force for ion transport to be able to understand corrosion initiation better.

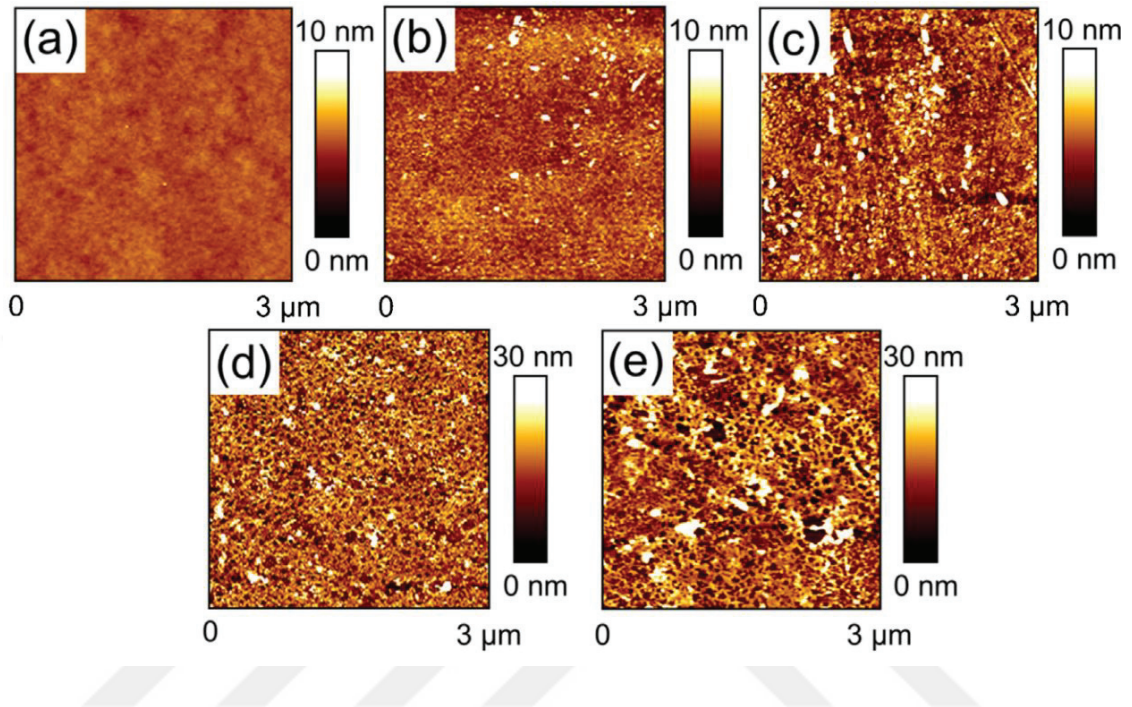


Figure 2.20. AFM Spectra of the degradation of epoxy-phenolic can coating applied on polished steel applied on polished steel <sup>57</sup> a) unaged, b) after 7 days immersion in 5% w/w NaCl, (c) after 21 days immersion in 5% w/w NaCl electrolyte; (d) after 7 days immersion in deionized water and (e) after 21 days immersion in deionized water.

Kefallinou investigated degradation mechanism of epoxy-phenolic can coating with EIS, LEIS, SEM and cathodic polarization.<sup>58</sup> Water uptake of the coatings were calculated using Brasher-Kingsbury Equation 1.11. It was noted that after formation of corrosion sites, capacitance errors increased which leads to uncertain water uptake calculations. Delamination resistance of the coatings were investigated with cathodic polarization of the coated tin plates for 3h in 0.85M NaCl solution. It was found that 10 min. cured samples were delaminated, and 30 min. cured samples were intact even though increased water absorption capacity due to higher cross-linking degree and swelling. It was proposed that this issue is due to increased degree of interfacial cross-linking Water

uptake measurements after corrosion initiation may lead questionable results due to increased capacitance errors. Electrochemical properties of coating were directly related with coating thickness and curing degree. Water uptake capacities were increased due to interfacial crosslinking and swelling from 3% to 8% of total coating volume for 10 min and 30 min samples respectively using Brasher Kingsbury equation with dry EIS capacitance values. It was not possible to measure instant water uptake with conventional wet EIS measurement. There are three possible stages of water absorption stage proposed by the authors.

- 1) Water uptake of instantly available free volume increases with increased curing.
- 2) Water diffusion to smaller pathways, was measured with EIS, 2% of coating volume was filled with water for all samples regardless of curing degree. This was attributed to polymer-network rearrangements may occur and this leads to slight increase in dielectric constant of the coating.
- 3) Establishment of connection with the substrate,

It should be noted that, it was not possible to delaminate coated ECCS plates. This indicates that coating lamination resistance is highly dependent on the substrate finish and metallic coating deposition. It was proposed that interfacial resistance could be a sensitive measure for total coating performance. Authors proposed that increased delamination resistance and corrosion performance of higher curing degree samples were due to enhanced metal-polymer bonding which prevents water and ion contact with the metal substrate. Effect of surface roughness and tin-iron alloy thickness were not investigated by this study which can be a function of corrosion performance.

### **2.3. Aim of the Study**

Investigated literature and the customer requests in the can coating industry points out that there is an increasing demand for more sustainable alternatives for conventional i.e. BPA containing can coatings. In the competitive can coating market, commercialization of alternative studies also takes time due to industry standards. A faster, systematic and objective approach that will contribute to the identification of factors responsible for the anti-corrosive behavior designed lacquers will contribute to the coating manufacturer and can producer.

Therefore, the aim of this study is to answer the following scientific questions:

- 1) What is the effect of electrolyte type on the corrosion mechanism of bare (non-coated) tinplate?
- 2) What is the effect of coating type on the corrosion mechanism of tinplate?

In order to answer the questions, the anti-corrosive behavior of tinplate is investigated as a function of electrolyte and coating type, by performing electrochemical measurements using Electrochemical Impedance Spectroscopy measurements. Afterwards, the changes in corrosion (electrochemical) activity as a function of electrolyte immersion time is related to structural changes occurring on substrates, as measured by Scanning Electron Microscopy (SEM), Energy Dispersive X-ray (EDX) and Atomic Force Microscopy (AFM).

## CHAPTER 3

### EXPERIMENTAL

Overall experimental procedure on the samples is shown in Figure 3.1.

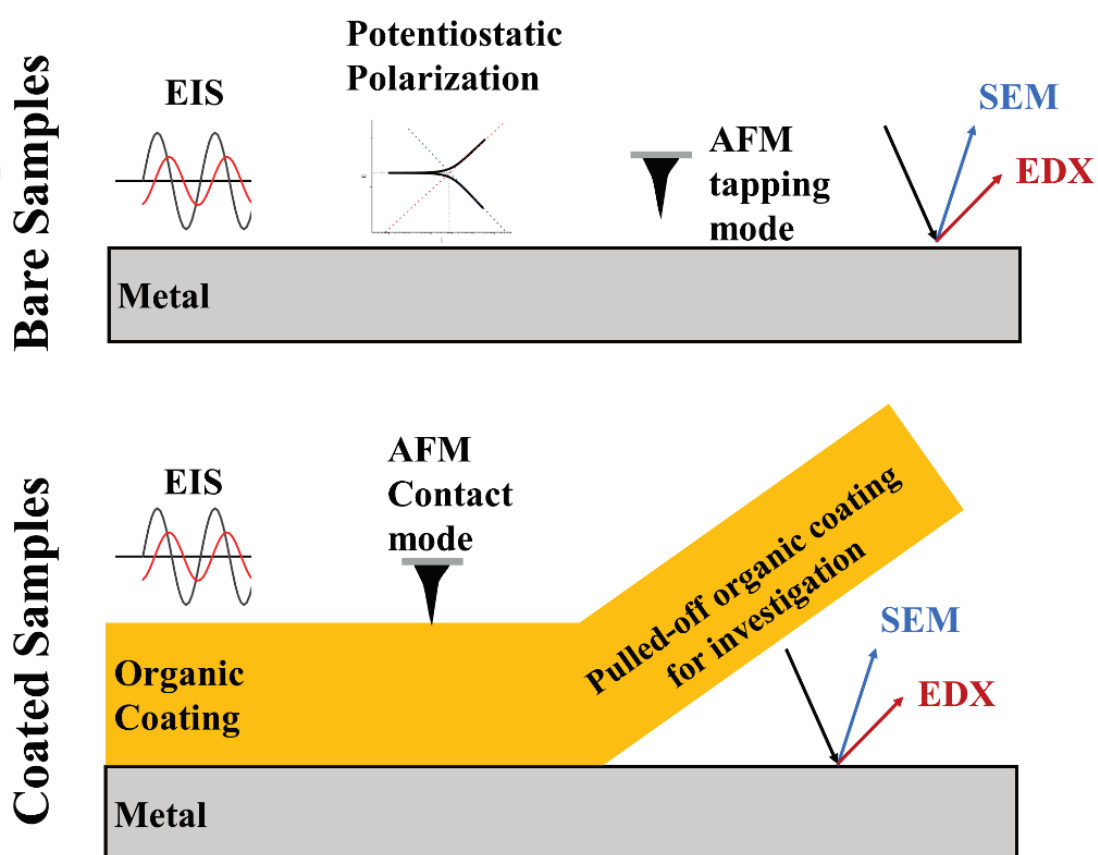


Figure 3.1. Experimental procedure of the thesis.

#### 3.1. Aging Electrolytes

Following electrolytes are used to investigate bare tinplate corrosion;

- I. 3% NaCl + 1% Citric acid
- II. 1% NaCl + 3% Acetic acid
- III. 0.1M NaCl(0.58%)

IV. 0.1M NaCl(0.58%) + 0.1M Acetic acid(0.6%) + 0.01M Citric acid(0.19%)

V. 1% NaCl + 1% L-cysteine

To prepare aging electrolytes, DI water is heated to 80°C with a commercial kettle and mixed in a polypropylene container. Electrolyte I, II, and V are commonly used to evaluate coating resistance to different food compositions in the can coating industry. Electrolyte III is a common aging solution to simulate atmospheric corrosion that are used in academic research<sup>13</sup>. Electrolyte IV is an electrolyte composition tried for this project. Coated panels were only aged with electrolyte IV. Electrolyte III and V was not investigated further with electrochemical impedance spectroscopy due to the difference of the pH of the electrolytes. pH of only lower than 3 were investigated with this study.

Granulated citric acid anhydrate 99.91% as citric acid, glacial acetic acid %100 as acetic acid, Sodium Chloride %99 as NaCl was used.

### **3.2. Aging Bare Tinplates**

Industrial samples were gathered from the current customers of Toyoink. They were commercial packaging steel however, the tin thickness, surface treatment and finishing types were not investigated further. Control sample was supplied from QLAB as Qpanel DT-46 tinplate with 311 passivation(Sodium Dichromate) between 4 to 7 mg/m<sup>2</sup> chrome and 5.6 g/m<sup>2</sup> tin coating. The samples were cut with a metal scissor and the sides were sealed with a heat resistant tape TESA 4657 to hinder the corrosion.

Aging tinplates were done on two different instruments. The Gamry paint cell and full electrolyte immersion in a jar. Two methodology has different degradation intensity, which was visually observed and had different EIS results. Minimum of three EIS measurements were made for jar aged tinplates. They usually corroded faster. This variation is attributed immersion of two sides of the plate. This means anodic and cathodic reactions can occur at both sites independently since tinplate is an inductor metal. Single measurement was made for Gamry paint cell aged tinplates. There was a limited oxygen intake and only one side for both anodic and cathodic reactions to be able to occur which is more accurate simulation of tinplate corrosion. An adverse side of paint cell method is, it disables other users to use the potentiostat and paint cell because measurement and aging occurs simultaneously with a pre-programmed sequence. The data of only Gamry paint cell aged bare tinplate samples are used to model the corrosion behavior.

### 3.3. Aging Coated Tinplates

Two different lacquer composition was investigated. These are Epoxy-Phenolic and Polyester-Phenolic-Isocyanate will be mentioned further as EP and PE systems respectively. Both systems were not commercialized yet.

The coatings were applied with a spiral bar coater(Kbar-3) with a dry thickness between 5 and 6 microns and cured at 205 °C for 12 minutes.

Oxygen has a critical role in corrosion. Cans are filled in good practice to minimize oxygen content. To be able to achieve this, fillers usually pack the food at high temperatures(80-90°C) and minimize the air in the can by filling as much volume as possible. To be able to simulate this process, both side lacquered tin plates are fully immersed in jars at hot fill conditions(80°C) and closed immediately with 1-2 cm headspace and then sterilized in an autoclave unit at 121°C for 1h as usually seen with most food cans.

### 3.4. Electrochemical Measurements

Electrochemical measurements were conducted on Gamry Interface 1010B Potentiostat/Galvanostat with the Gamry paint cell in a Faraday cage as shown in Figure 3.2. EIS measurements were performed with in 0.01 to 10000 Hz range with an AC amplitude of 1 mV for bare plates and 5 mV for coated plates with respect to their open circuit potential in their aging solution. Potentiodynamic polarization were performed between -0.2V to 1V vs open circuit potential with a scan rate of 0.4 mV/s.

For immersed samples, 2 measurements were made. EIS measurements were carried out for the samples that are aged on the paint cell simultaneously during the aging period with 1-hour periods for bare samples and 2-hour periods for coated samples. For sterilized samples 3 EIS measurements were made. They were carried out immediately after the sterilized jar was opened. This is important for stable oxygen levels as in the jar. Aging electrolytes in the jars were used as an electrolyte for EIS measurements.

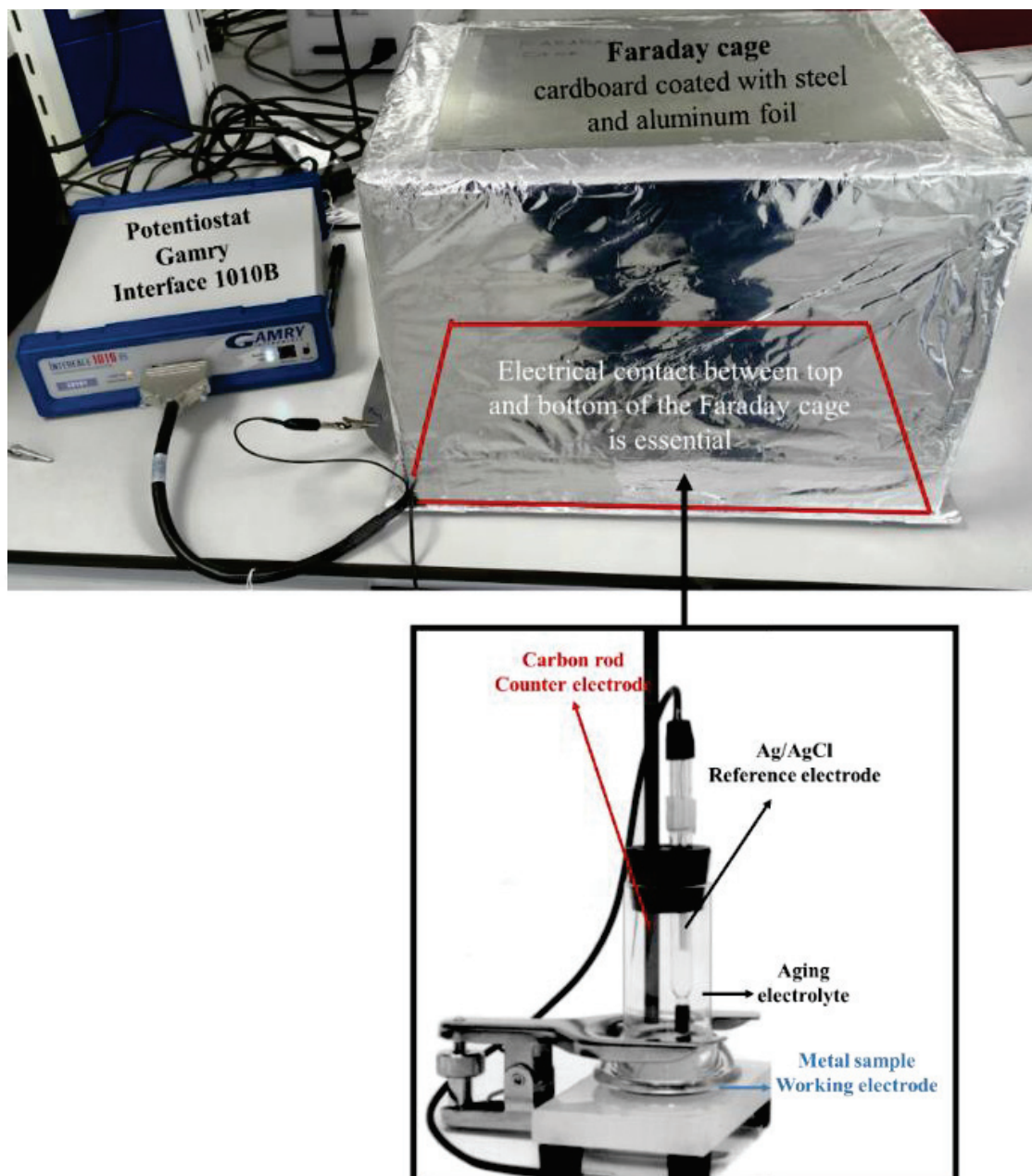


Figure 3.2. Experimental setup for electrochemical measurements.

### 3.5. SEM and EDX Measurements

SEM uses a focused beam of high-energy electrons to create an excitement signals at the surface of solid specimens. Signals derived from electron-sample interactions contain information about the sample including morphology , chemical structure, and orientation of materials<sup>59</sup>.

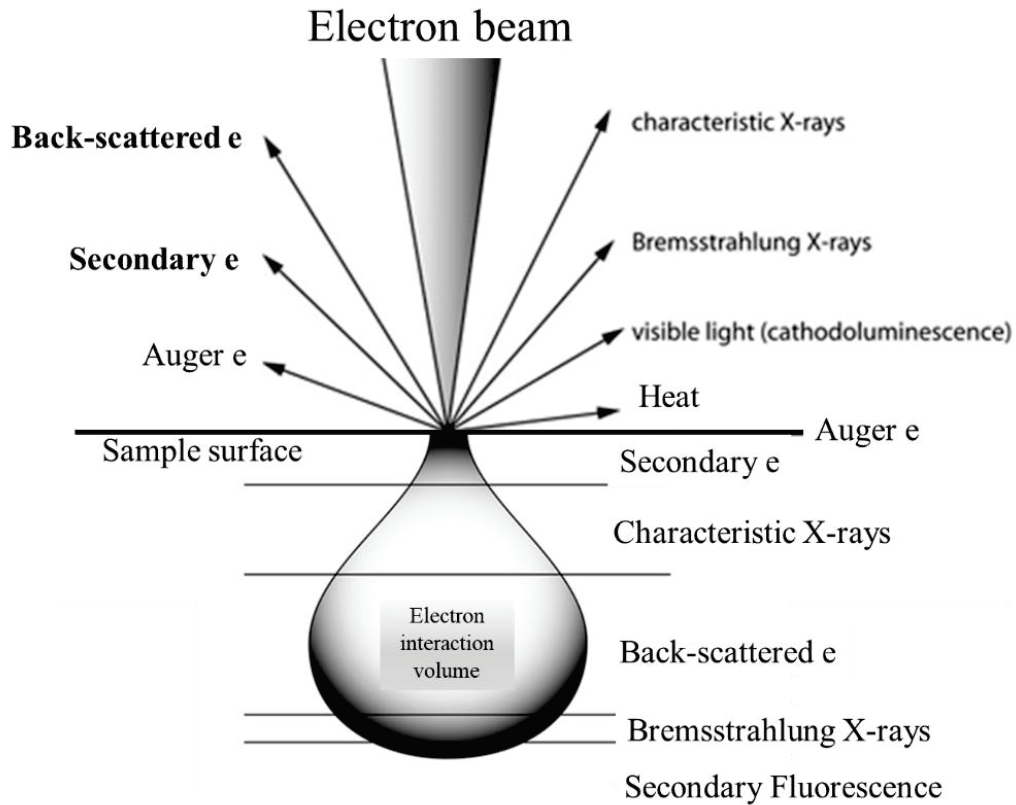


Figure 3.3. Electron sample interactions.<sup>59</sup>

Backscattered electron images and secondary electron images are used. As shown in Figure 3.3, backscattered electron penetration depths are higher than secondary electrons. Penetration depth of the electron beam can vary between 1 to 5 microns. Due to this property, information about 1 to 5 microns are included in data. Unfortunately, it is hard to confirm nanometer level oxide species with bulk EDX analysis.

SEM measurements were carried out with FEI QUANTA 250 FEG. 1x1cm cut pieces were investigated with 15-20 kV penetration density in SEM and EDX measurements.

### 3.6. AFM Measurements

AFM is a scanning probe microscope. A cantilever with a small enough needle (for desired resolution) is used to scan the surface of the sample. A piezo shaker is used to create an oscillation. A laser beam reflected on the cantilever creates signals about



morphological structure of the surface due to the different height, chemical or physical properties on the surface. There are three main different working modes of AFM.

General working principle and modes are drawn in Figure 3.4. In contact mode, the tip touches the surface of the sample and due to the difference of the height, morphological structure of the sample can be observed. In non-contact mode, the tip is brought very close to the sample and due to the atomic attractive and repulsive forces, the signals are produced. Both height and chemical structure difference can affect the signal. In tapping mode, the tip scans the surface with a defined frequency tapping. After each tap, cantilever is bounced back. The bounce amount can be different due to the material structure such as hardness, toughness etc. This allows the user to identify different chemical structures on the surface if any present with phase degree images and height images as shown in Figure 3.5.

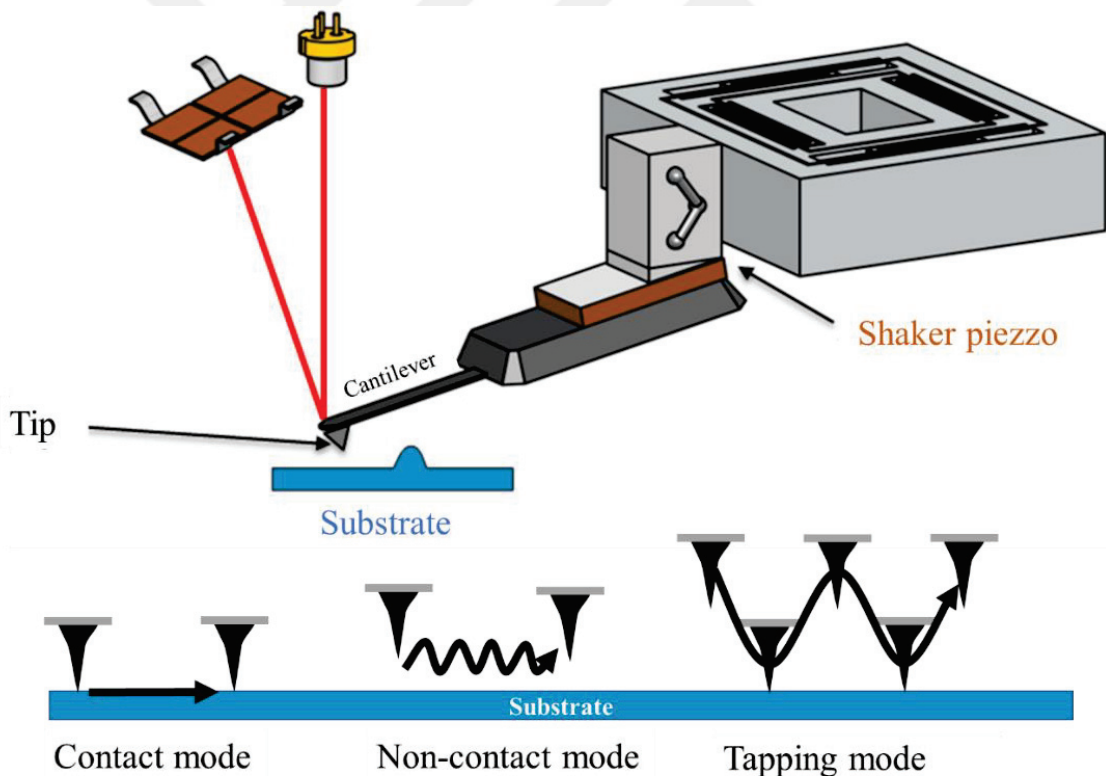


Figure 3.4. AFM working principle and modes.<sup>60</sup>

AFM measurements were carried out with Bruker-MMSPM Nanoscope 8. Bare samples were measured with contact tapping mode with budget-sensors diamond-like carbon coated Tap300DLC with a resonance frequency of 300 kHz and force constant of 42 N/m. Coated samples were measured in scanasyst mode with nanoworld silicon pointprobe with a resonance frequency of 320 kHz and force constant of 42 N/m.

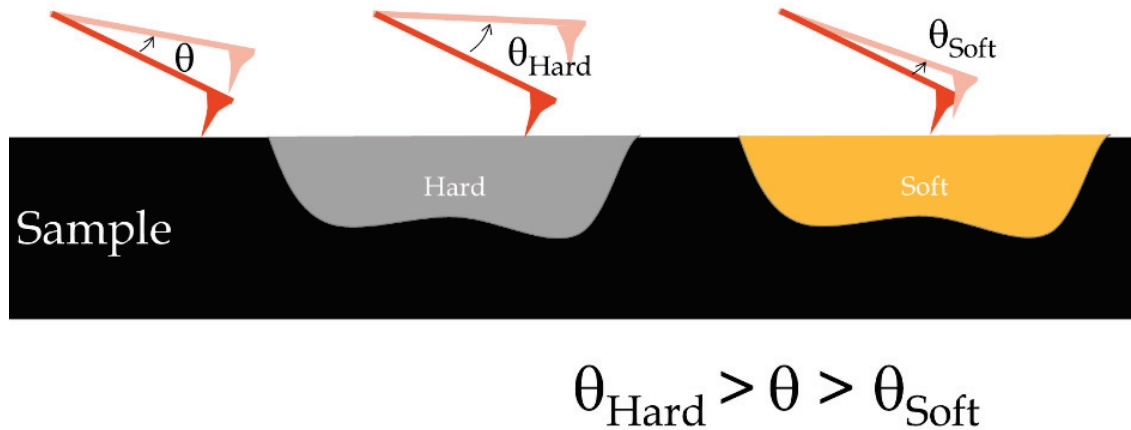


Figure 3.5. Phase angle change according to the hardness of the surface in tapping mode.

# CHAPTER 4

## RESULTS

### 4.1. Packaging Steel in the Industry

Different samples that are used in the food packaging industry were gathered from the relevant customers. Unfortunately, information of surface treatment and tin coating weight could not be gathered. BSE images of the different samples are shown in Figure 4.1.

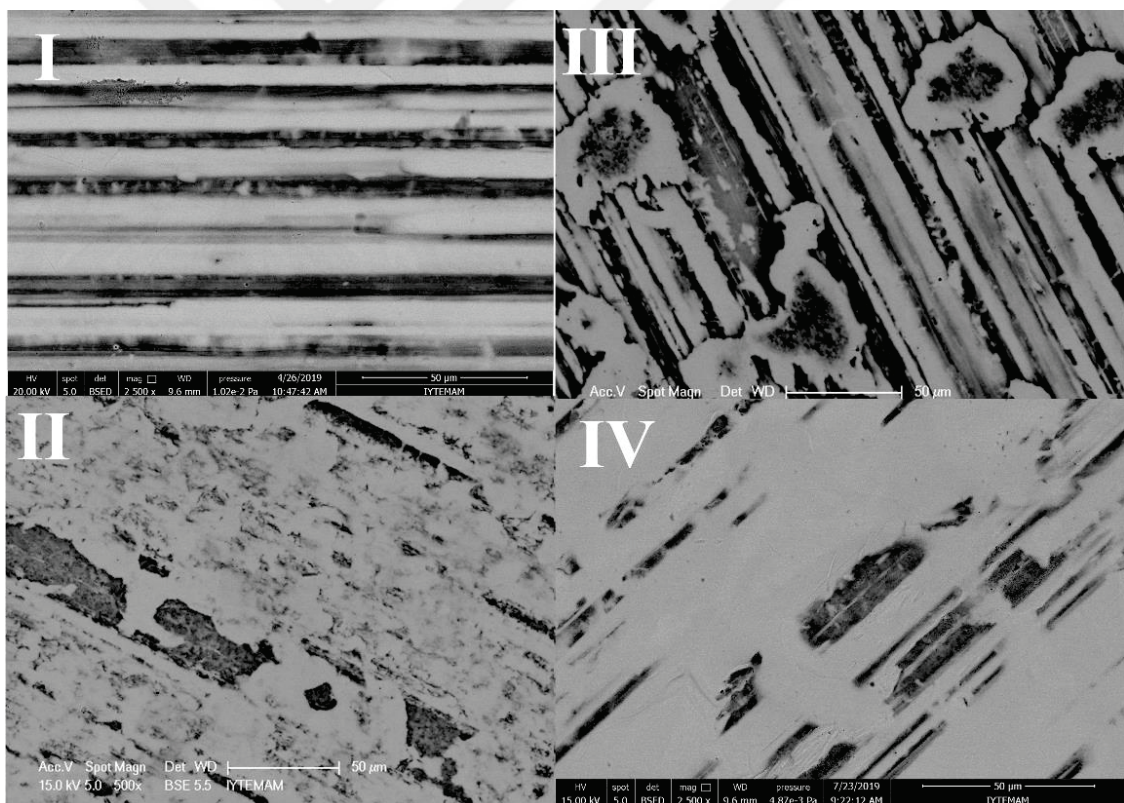


Figure 4.1. SEM(BSED) images of different tinplate samples. I, II, III from Toyoink customers, IV from QLAB.

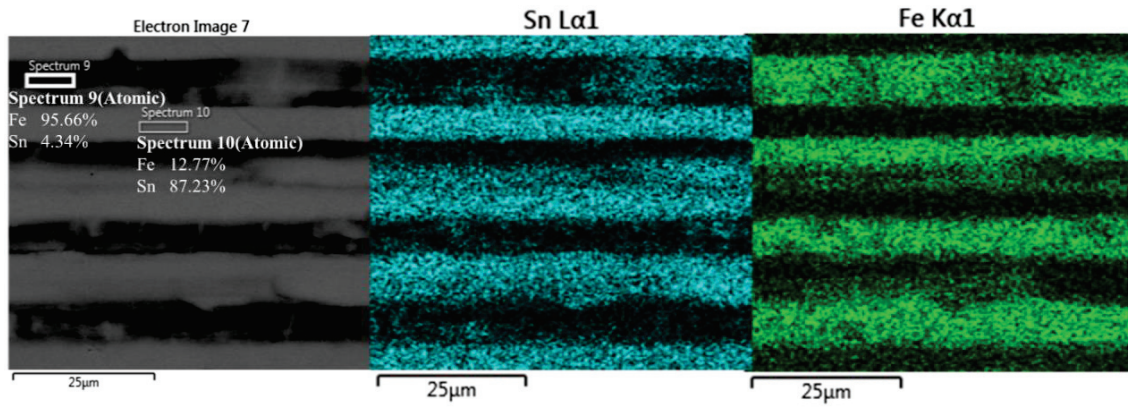


Figure 4.2. EDX mapping of the sample I.

Sample III is the test specimen currently used in the coating laboratory of the formulator, Toyoink. Therefore, it was compared with model tinplate sample IV(QLAB). Bulk EDX analysis of the virgin bare tinplate samples of III and IV can be seen in Table 4.1. The data of higher tin content in the sample IV is also match the BSED images in Figure 4.1.

The sample III were measured multiple times on different locations due to the heterogeneous look observed on SEM images. 3% difference in each element was found which is acceptable since EDX data represents a semi-quantitative measurement.

Table 4.1. Bulk EDX analysis of IV and III samples.

Element Atomic%	III				IV
<b>C</b>	7.52	7.48	7.64	4.92	5.69
<b>O</b>	6.78	8.18	8.30	8.07	12.38
<b>Fe</b>	48.34	47.67	47.42	50.20	19.83
<b>Sn</b>	37.35	36.66	36.64	36.81	62.1

Except the bulk EDX analysis, local fluctuations on the surface were investigated with EDX mapping. In every sample, dark areas were found to be iron rich and light areas found to be tin rich. In dark areas, atomic tin percentage was found to be less than 10%

for all samples. Even though majority of the composition of the dark areas are FeSn<sub>2</sub>, due to the low thickness of the alloy layer, atomic tin percentage is very low.

There are nitrogen traces found in tin rich areas for all samples. Oxygen content was homogeneous for different areas. Atomic oxygen % was found to be increasing with increasing tin content in sample III. For sample II oxygen was not detected. Oxide growth is affected by storage conditions<sup>4</sup>. Since we could not gather this information, the reason for increased oxygen content in sample III was not investigated. Atomic carbon % was found to be increasing with increasing iron content which is attributed to the carbon content in the steel.

The pattern of light/dark grains was found in every tinplate sample. For better understanding of nano level heterogeneities, light grains(tin rich and high ground areas) were investigated with AFM tapping mode. Special attention was given to phase images because it enables the user to understand the different compositions of the surface due to bounce difference in cantilever while tapping. Different morphologies were observed for different samples as shown in Figure 4.3.

Table 4.2. Roughness values of different virgin tinplates.

<b>Samples</b>	<b>I</b>	<b>II</b>	<b>III</b>	<b>IV</b>
Z Range(nm)	33	81	56	39
Ra(nm)	2	7	3	2
Rq(nm)	3	9	4	3

Height wise difference was not significant as shown in Table 4.2. It should be noted that commercial tinplates were very heterogenous to investigate with AFM( is used to investigate nano scale heterogeneities) and Z range is highly affected by the measured position however particle analysis showed that except few high points, surface roughness stays the same for unaged samples. For the all samples, R<sub>a</sub> were found lower than 10nm and Z range were found lower than 100 nm.

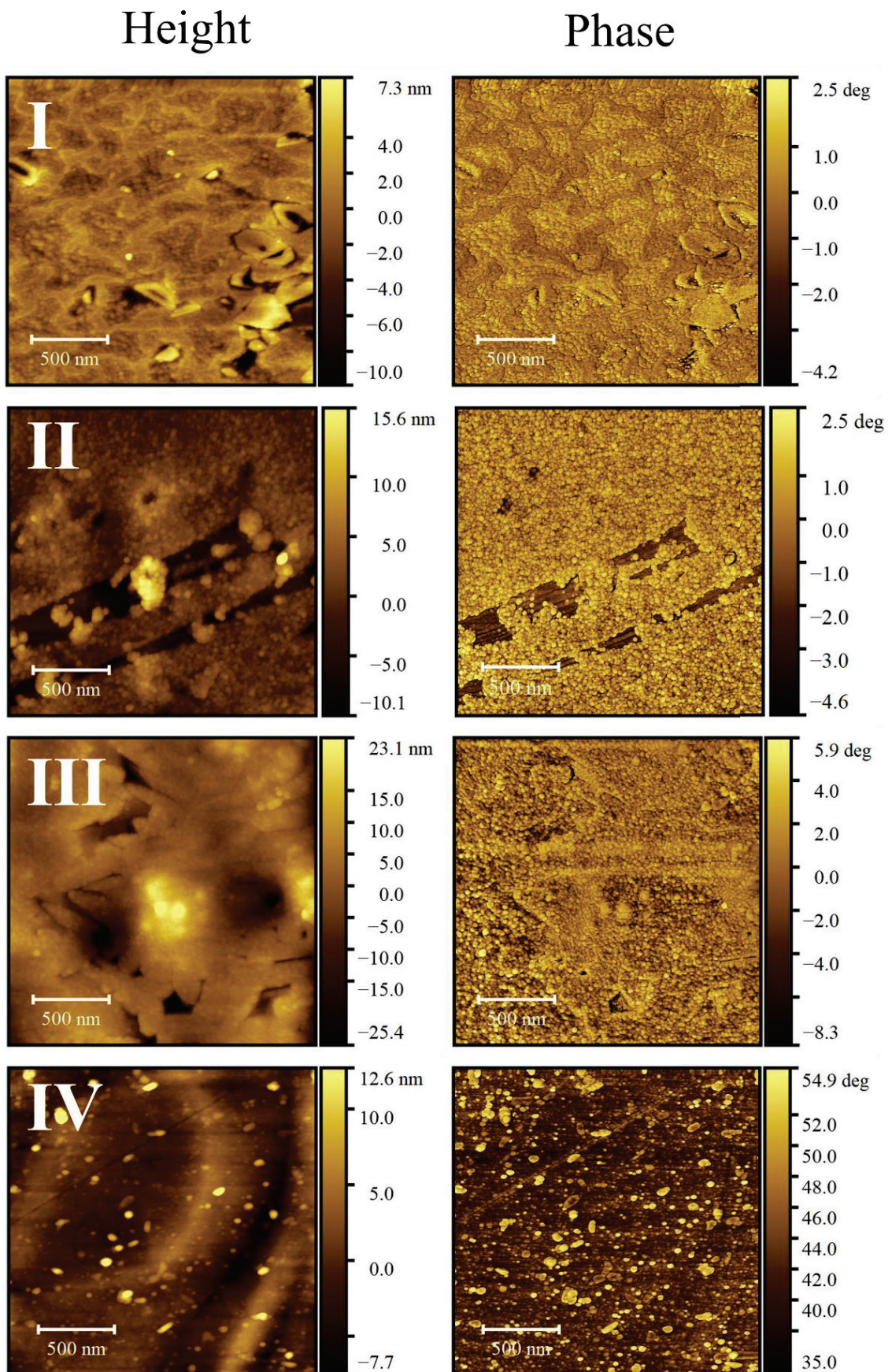


Figure 4.3. AFM phase images of different tinplates.

## 4.2. Corrosion of Bare Tinplate on Different Electrolytes

It was previously reported that aging electrolyte is an important parameter of tinplate corrosion<sup>14</sup>. To be able to select a simulating electrolyte for food media, corrosion of tinplate with a variety of electrolytes were investigated with EIS, DC polarization, SEM and EDX.

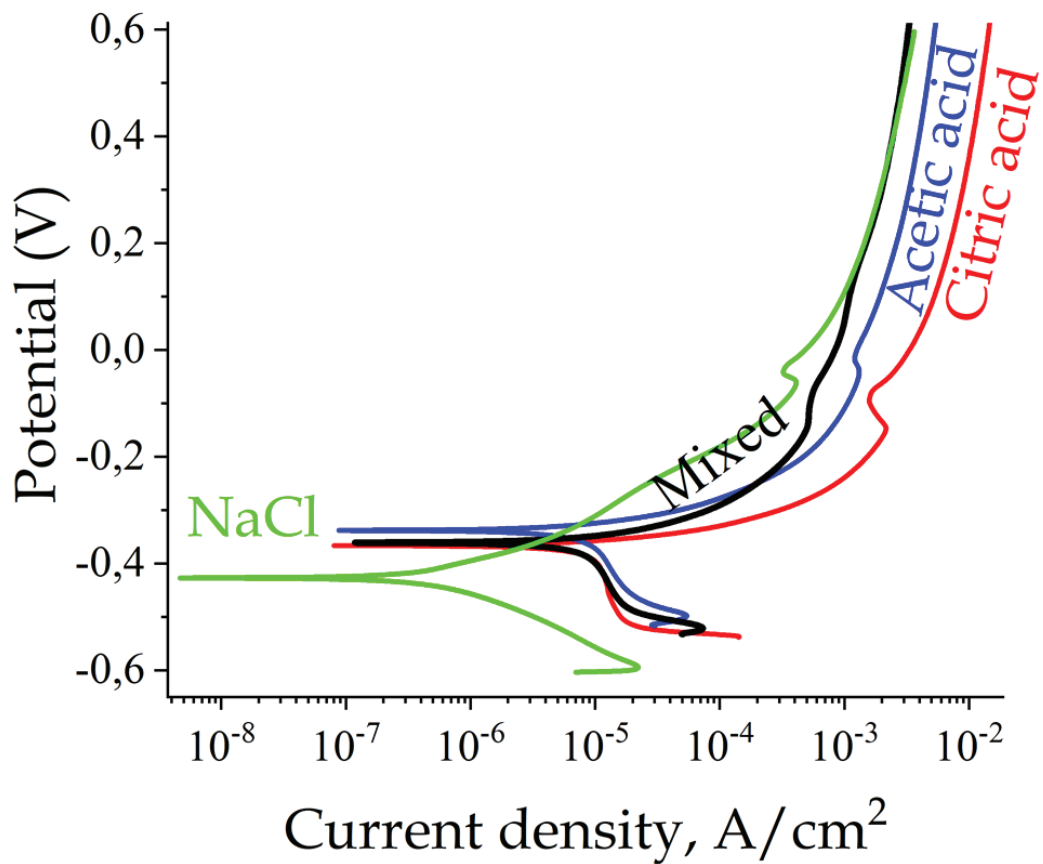


Figure 4.4. Polarization curves of tinplate in different aggressive media.

As shown in Table 4.3 and Figure 4.4, corrosion currents of mono acid solutions were found to be similar and novel mixed electrolyte were approximately twice of these amounts.

Table 4.3. Corrosion current and potential of tinplate in different aggressive media.

	$I_{corr}$ , $\mu\text{A}/\text{cm}^2$	$E_{corr}$ , V	pH	Conductivity mS/cm
0.1 M NaCl	0,924	-0,427	6,68	8,7
0.1 M (0.58%Wt) NaCl 0.1 M (0.6%Wt) Acetic Acid 0.01M (0.19Wt) Citric Acid	<b>46,04</b>	-0,361	2,46	12,5
1% Citric Acid 3% NaCl	23,75	-0,366	2,02	50,4
3% Acetic Acid 1% NaCl	24,66	-0,338	2,50	18,5

#### 4.2.1. 1% Citric Acid 3% NaCl Solution

For citric acid, tin selective corrosion was observed on tinplate with respect to immersion time as shown in Figure 4.5. Even for 1 h of immersion, attacked tin areas were observed. After 24h, free tin containing areas were almost disappeared. This means the tin concentration in the aggressive media is very high and the food is unable to be used. This is the accepted failure point.

As shown in Table 4.4, as the time increases atomic tin percentage decreases which is an indication of dissolved tin as anodic reaction. Oxygen on the surface also increases.

Needle shaped  $\text{FeSn}_2$  were successfully imaged with SEM as shown in Figure 4.6 and Figure 4.8, also match with recent publications<sup>51</sup>. Tin selective corrosion was observed also in 5h aged sample. EDX mapping of citric acid aged samples showed increase in oxygen ratio for 12h and 24h aged samples. Crystal shaped corrosion product in for 12h(III) aged sample include Sn, O, C Na, Cl elements. For 24h aged sample, O and Fe are present together and covers the surface which may indicate passivation of oxides of iron however in this stage, there are not any free tin present and the sample degraded far from acceptable state.



Table 4.4. EDX Data of citric acid immersed bare Qpanel tinplate surfaces.

<b>Element Atomic%</b>	<b>Virgin 0h</b>	<b>1h Citric Acid Immersion</b>	<b>5h Citric Acid Immersion</b>	<b>24 Citric Acid Immersion</b>
<b>C</b>	5.69	5.82	6.88	11.05
<b>O</b>	12.38	12.26	13.87	32.58
<b>Fe</b>	19.83	26.81	33.26	40.99
<b>Sn</b>	62.1	55.11	45.99	8.17
<b>Na</b>				5.18
<b>Cl</b>				2.03



## Backscatter Detector

## Secondary Electron Detector

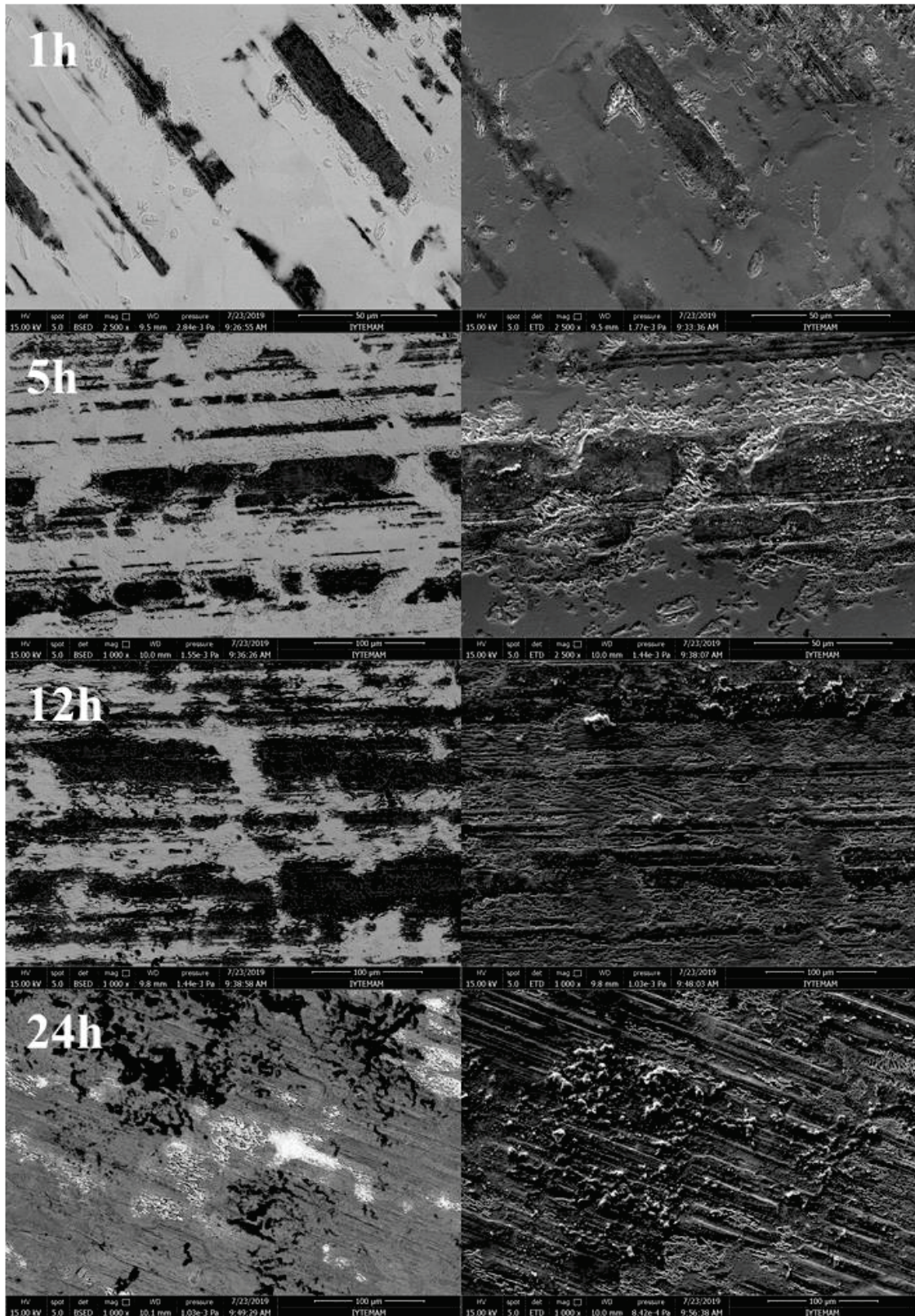


Figure 4.5. SEM images of Citric acid immersion of tinplate with BSE detector (left) and SE detector(right).

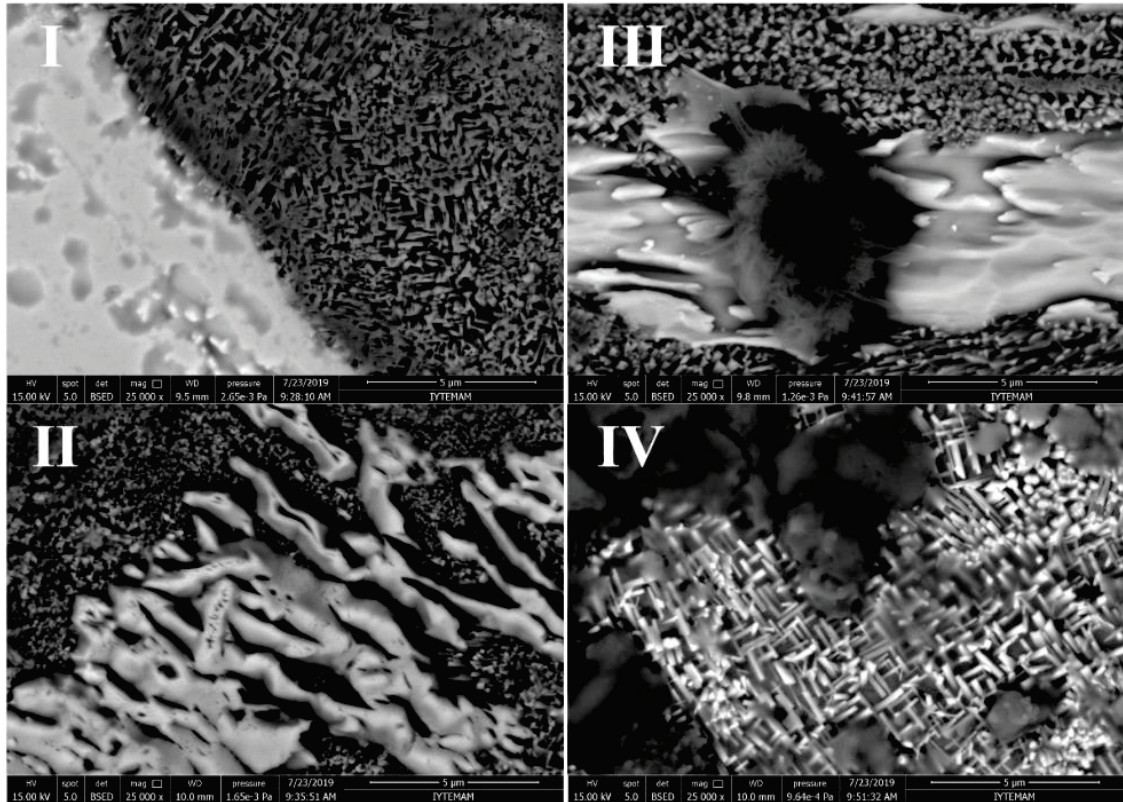


Figure 4.6. Tinplate corrosion in citric acid solution for I) 1h, II) 5h, III) 12h, IV) 24h immersion, bar 5 microns

EIS data of the citric acid aged samples are shown in Figure 4.7. Increased low frequency impedance is observed. Frequency at the maximum phase angles of citric acid aged samples were found to be between 1 and 10 Hz. Phase shift at the frequency range between 1-10 Hz is increased with respect to immersion time. Proposed models and further comments are included in discussion section.

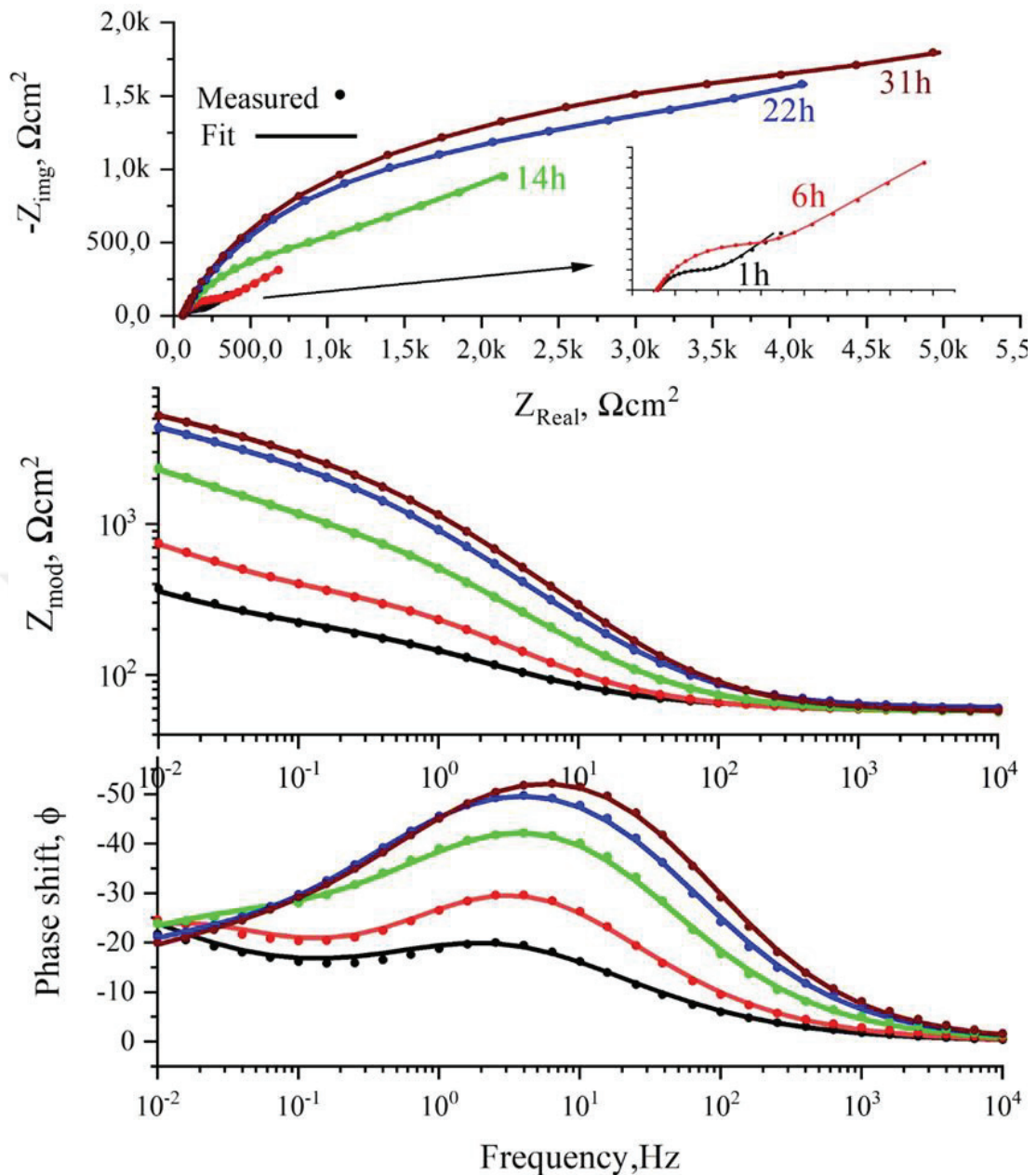


Figure 4.7. EIS data of corroding tinplate in 3% NaCl 1% Citric acid as aging electrolyte.

#### 4.2.2. 3% Acetic Acid 1% NaCl Solution

Different attack compared to citric acid aged samples was observed in acetic acid immersion as shown in Figure 4.9. It was observed in low tin areas. Acetic acid attack has lower rate of tin dissolution compared to citric acid. This data is also match corrosion current calculations from Tafel curves. After 24h of immersion, free tin areas were still

present. Increase in oxygen and iron content were similar compared to citric acid aged samples as shown in Table 4.5.

Table 4.5. EDX Data of acetic acid immersed bare QLAB tinplate surfaces.

Element Atomic%	Virgin 0h	1h Acetic Acid Immersion	5h Acetic Acid Immersion	12 Acetic Acid Immersion	24 Acetic Acid Immersion
C				7.62	11.23
O			20.38	21.84	24.64
Fe	25.87	25.21	20.02	48.90	52.43
Sn	74.13	74.79	59.60	21.63	11.70

Black spots in 5h aged samples in Figure 4.9 and 12h aged sample in showed dense O and C content in the absence of iron and dilute Sn which indicates tin complex substances and tin oxides. Also, in some spots Na and Cl content were found as an indication of NaCl. Oxide species and NaCl usually present together however there are lone examples also present. EDX mapping of the 24h aged sample has very dense O content and covers the majority of the surface as shown in II of Figure 4.8.

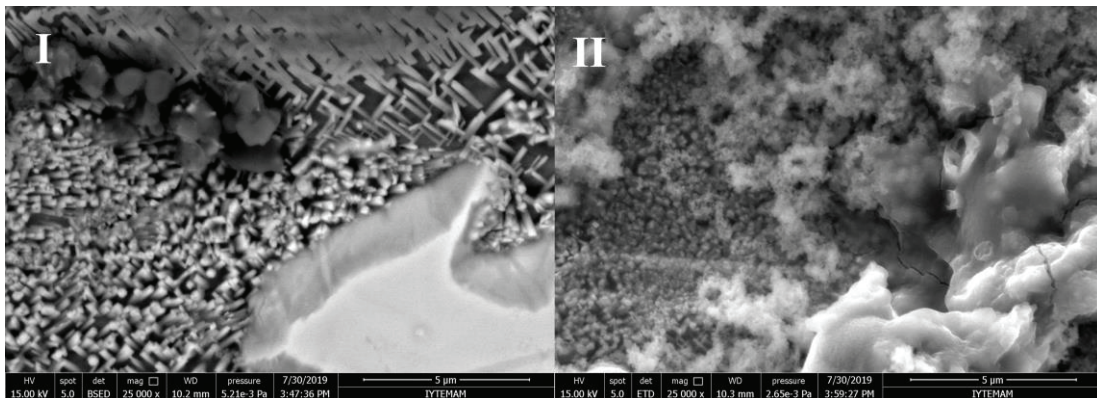


Figure 4.8. SEM images of acetic acid aged tinplates I) for 12h II) for 24h.

# Backscatter Detector

# Secondary Electron Detector

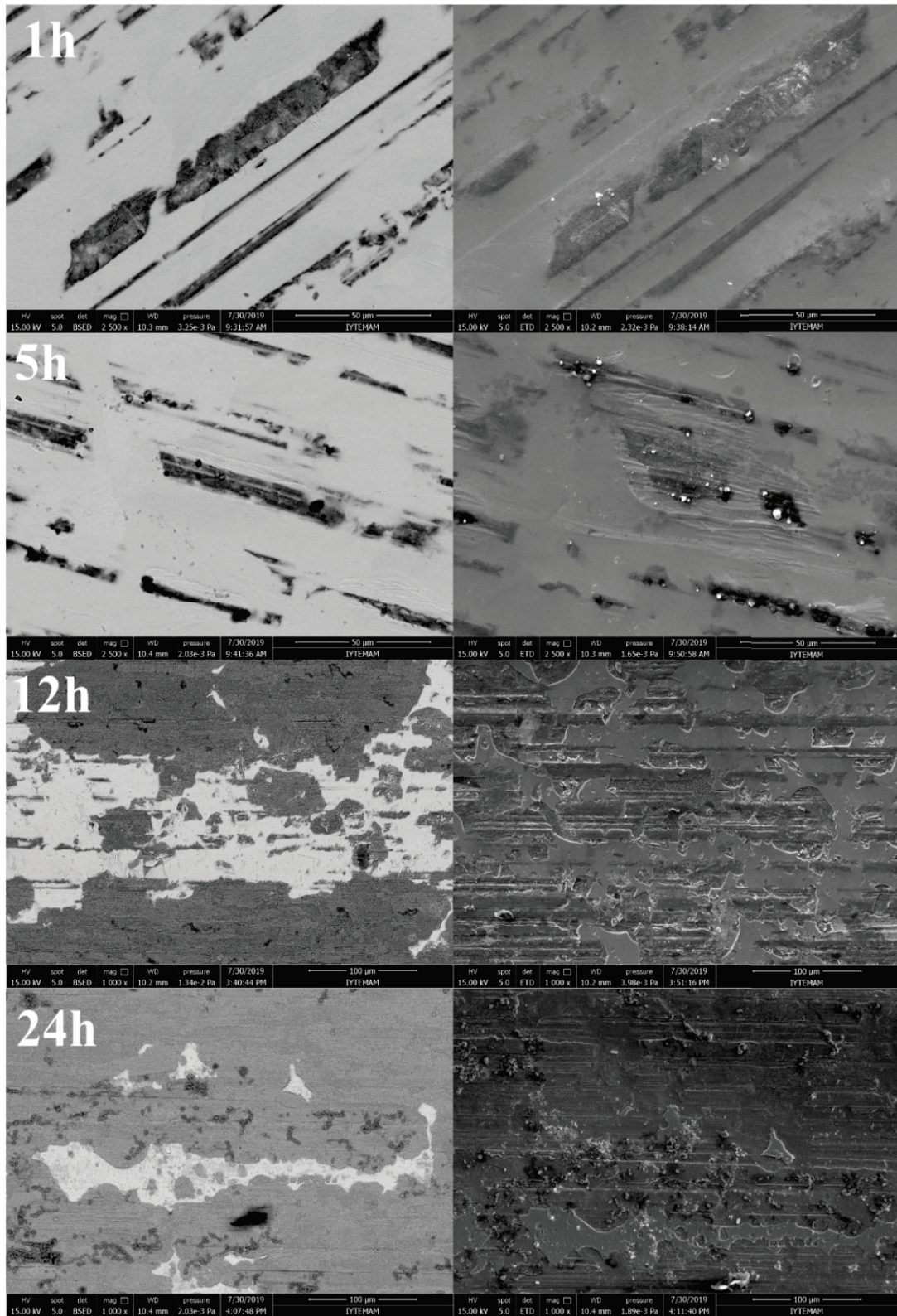


Figure 4.9. SEM images of acetic acid immersed QLAB tinplate.

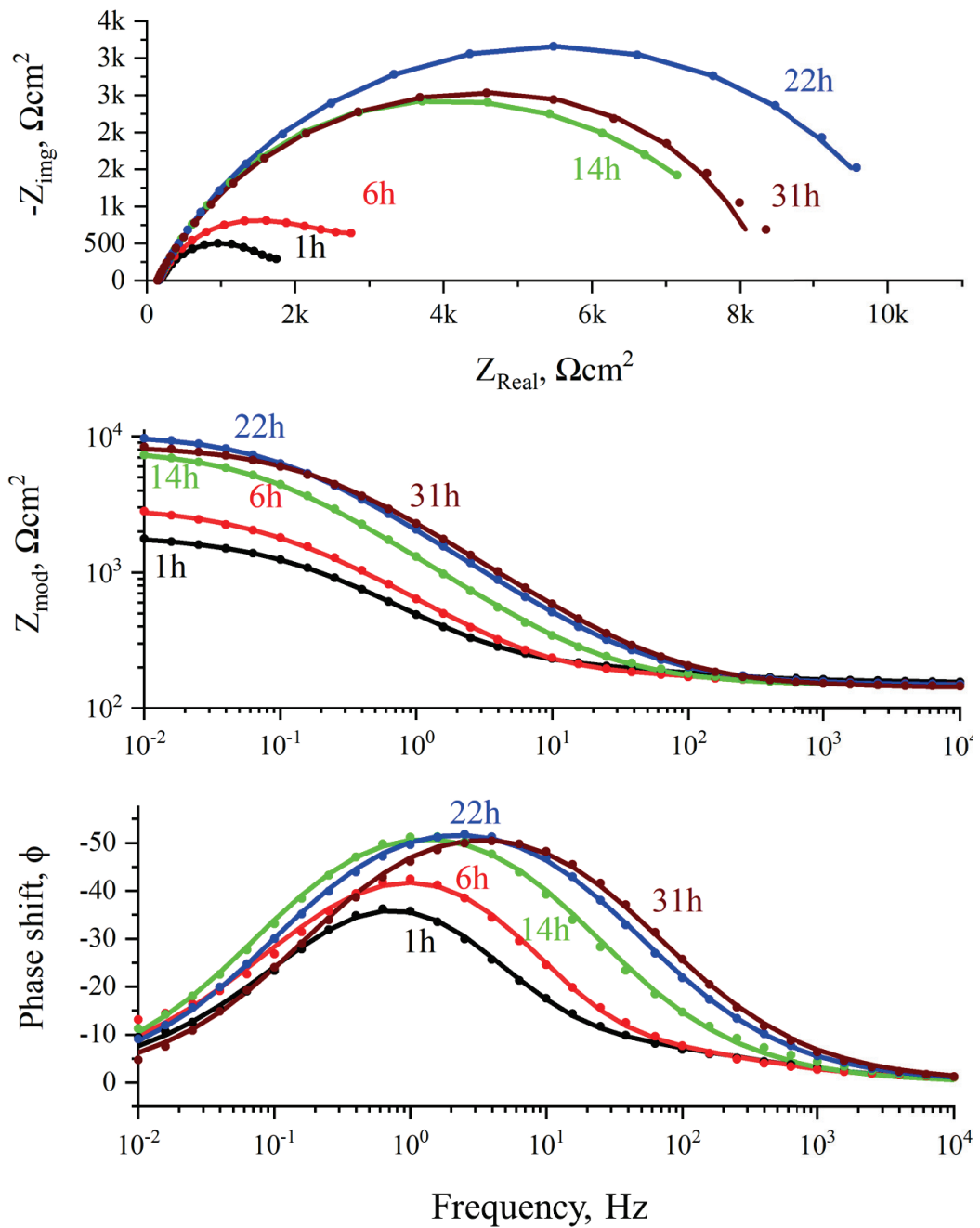


Figure 4.10. EIS data of corroding tinplate in 1% NaCl 3% acetic acid as aging electrolyte.

EIS data of acetic acid aged samples are shown in Figure 4.10. Similar impedance increase was observed as citric acid. Frequency at the maximum phase angles of acetic acid aged samples were found to be 1 Hz. Proposed models and further comments are included in discussion section.

Only 1h aged samples investigated with AFM. The aim of this investigation is to have a better understanding of initiation of corrosion. Nodule shaped morphologies disappear faster with citric acid aging as shown in Figure 4.11.

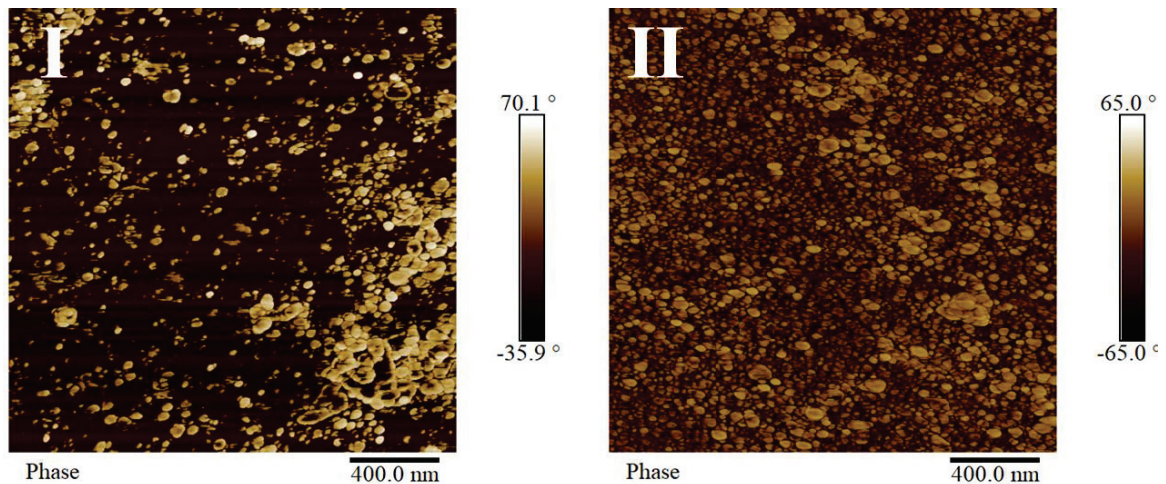


Figure 4.11. AFM phase images of QLAB tinplates immersed in I) Citric acid II) Acetic acid for 1h.

#### 4.2.3. 0.1M NaCl 0.1M Acetic Acid 0.01M Citric Acid Solution

Corrosion observed was similar to citric acid mechanism however significantly faster as shown in Figure 4.12 as there is not free tin available. Free Iron areas and black pits are observable in 10000x magnified image. Due to strong tin dissolution capability, coated tinplates were investigated with this acidic combination.

Bulk EDX data showed low Oxygen and tin but high iron content. This might be an indication of limited passivation availability in this solution which makes it especially useful for testing corrosion performances of organic coatings.

EIS data of the mixed acid aged samples did not show impedance increase at 12h aging as shown in Figure 4.15. After 12h period, impedance increase was observed however compared to mono acid aged samples, less than an order of magnitude increase were observed. Compared to mono acid samples, mixed acid aging had more complex behavior. Another time constant were observed after at 24h.



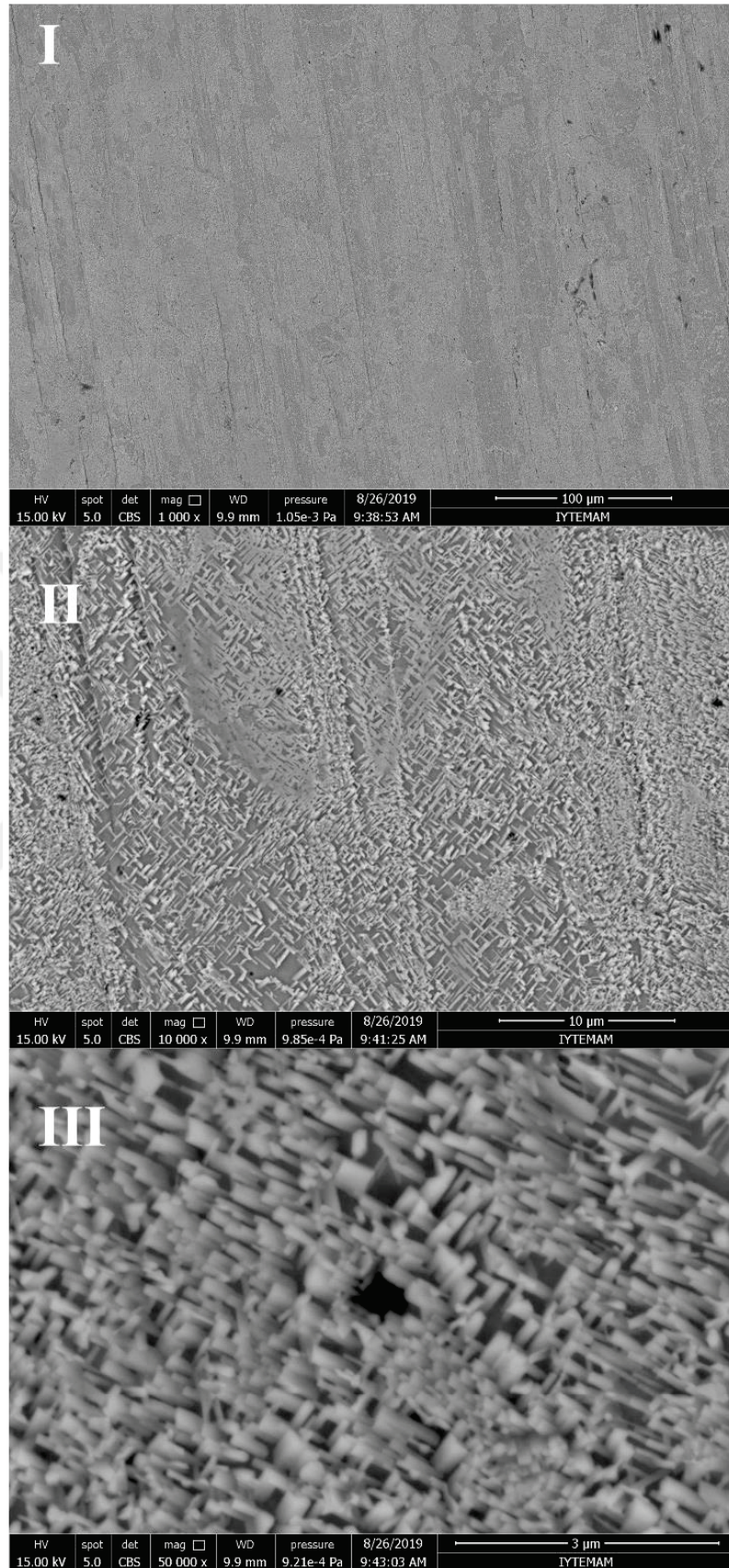


Figure 4.12. 12h aged tinplate in 0.1M NaCl 0.1M Acetic acid 0.01M Citric acid  
 I)1000x II)10000x III) 25000x magnification.

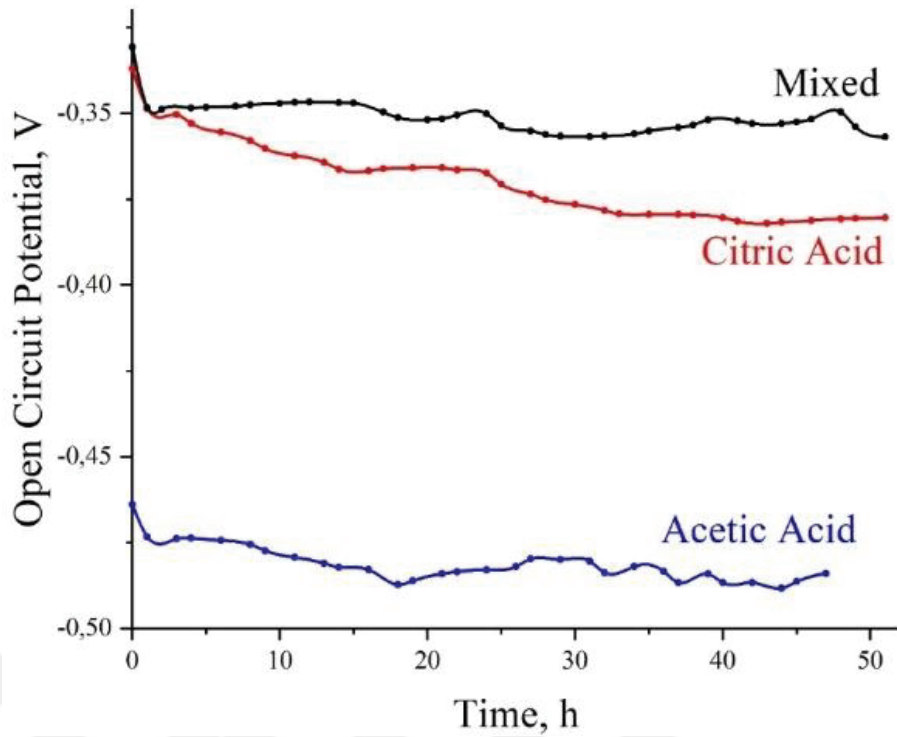


Figure 4.13. Open circuit potential evolution with respect to immersion time of different aging solutions.

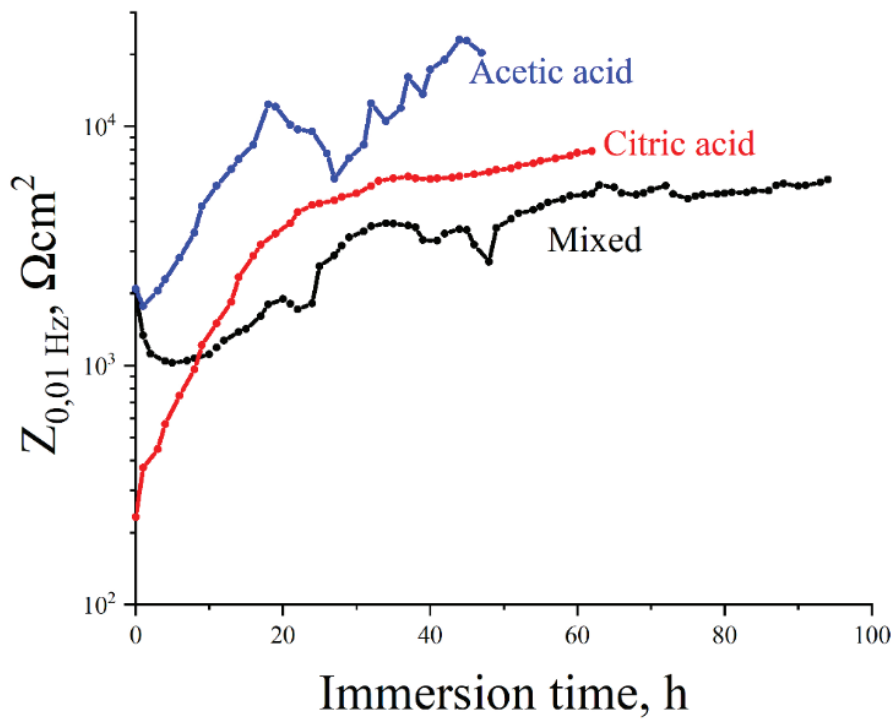


Figure 4.14. Low frequency impedance evolution with respect to immersion time.

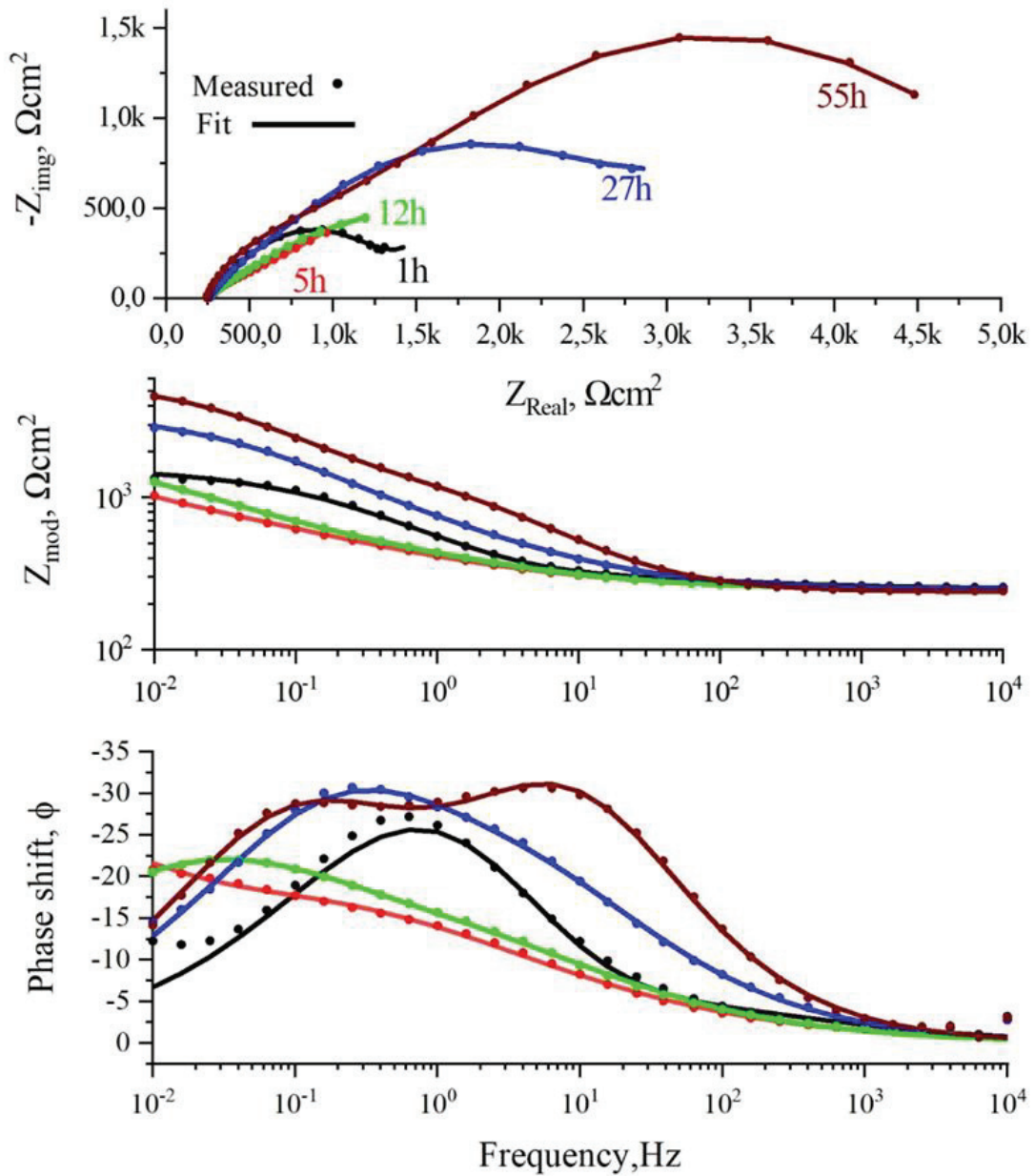


Figure 4.15. EIS data of corroding tinplate in 0.1M NaCl 0.1M acetic acid 0.01M citric acid as aging electrolyte.

Evolution of OCP and low frequency impedance of the different aging solutions is shown in Figure 4.13 and Figure 4.14 respectively. Compared to mono acid electrolytes, novel mix was found to have the most noble behavior of all. OCP value of mixed electrolyte was close to citric acid. Different impedance results were observed for aging methodology i.e. full immersion and paint cell. Common point is the increase of impedance with respect to immersion time. With citric acid aged samples, immediate and

steady impedance increase was observed. With acetic acid impedance increase is followed the second measurement. For novel mix electrolyte however, impedance increase is observed after 10h of immersion.

### 4.3. Corrosion of Lacquered Timplates

Surface morphology degradations and pin-hole like structures were observed with aging for both types of coated samples in AFM images as shown in Figure 4.19, Figure 4.20 and Figure 4.21. Corrosion products of the EP system after 1 month of aging is shown in Figure 4.21.

Samples were investigated with SEM and EDX before and after the aging. Before SEM and EDX measurements, the organic coating was pulled off from the surface to investigate the metal. In bare metal aging, atomic Sn ratio decreases below 10% in 24 h as shown in Table 4.4 and Table 4.5. Bulk EDX analysis of the pulled surfaces is shown in Table 4.6. Atomic Sn ratio before and after aging of was found to be in  $60 \pm 5$  range. Disruptions at the structural integrity of the surface were not observed and detailed images are shown in Figure A.1 and Figure A.2.

Table 4.6. EDX analysis of the pulled-off lacquered surfaces.

<b>Lacquered Qlab Timplate aged with mixed acids</b>	<b>Sn</b>	<b>Fe</b>	<b>O</b>	<b>C</b>
PE t=0	63,22	26,25	5,67	4,86
PE immersion 5 days	59,36	19,69	8,57	12,38
PE after autoclave same day	61,53	20,88	6,93	10,66
PE a week after autoclave	63,64	20,49	9,60	6,27
EP t=0	64,81	20,55	5,90	8,74
EP immersion 5 days	63,04	17,64	7,12	11,85
EP after autoclave same day	61,98	14,95	13,25	9,82
EP a week after autoclave	58,10	16,27	16,76	8,88

Table 4.7. Low frequency impedance values of tested coatings.

$Z_{0,01\text{Hz}}$ $\Omega\text{cm}^2$	Immersion					After Sterilization		
	2h	9h	20h	48h	96h	3h	1 week	1 month
<b>EP</b>	3,06E+08	2,34E+08	2,00E+08	1,19E+08	8,97E+07	1,49E+06	1,14E+06	9,27E+05
Error	2,06E+08	1,28E+08	1,04E+08	4,33E+07	4,71E+07	5,50E+05	1,54E+05	2,28E+04
<b>PE</b>	1,04E+08	8,89E+07	6,46E+07	4,48E+07	3,77E+07	1,33E+06	1,13E+06	1,04E+06
Error	4,79E+07	4,60E+07	3,50E+07	2,24E+07	2,36E+07	2,18E+05	4,87E+05	4,27E+05

Evolution of the open circuit potential with respect to degradation is plotted for immersed and sterilized samples together to compare more clearly in Figure 4.16. 3 samples measured for sterilized samples. Nobler OCP values were observed for polyester coated samples except 3-4 day immersion period. After sterilization, OCP values were decreased and then increased for all samples. There is a discrepancy between the sterilized and immersed samples because decrease followed by increase were not observed for immersed samples. Low frequency impedance values were decreased with respect to immersion time for all samples. After sterilization, low frequency impedance values were decreased to  $10^6 \Omega\text{cm}^2$  level from  $10^8 \Omega\text{cm}^2$  level i.e. two orders of magnitude for each sample. For epoxy coated samples, a mild decrease was observed after sterilization however for PE coated samples, it was not clear. As shown in Figure 4.16 and Table 4.7, standard error of the 1 month aged sterilized PE coated samples, it is not possible to generalize the behavior of the PE coated samples however It should be noted that, corrosion were only observed on EP coated samples as also shown in Figure 4.21.

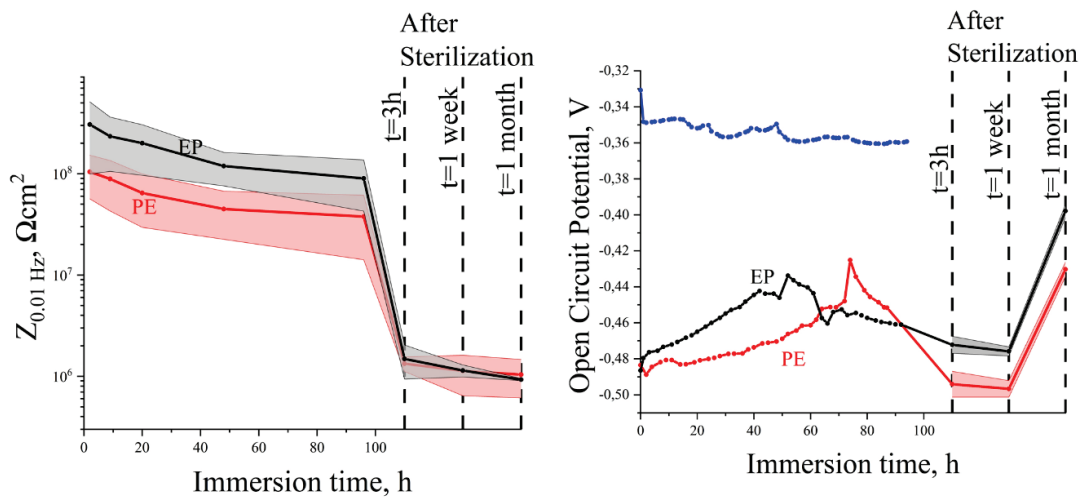


Figure 4.16. Evolution of the OCP and low frequency impedance for coated samples, with standard errors.

EIS data of the coated samples are shown in Figure 4.18 and Figure 4.17 as Nyquist and Bode plots respectively. It should be noted that immersed samples measured 2 times and sterilized samples measured 3 times however only a single representative data was plotted in the figures. To check statistical confidence, multiple measurements were plotted with standard error of the mean (lighter areas) as shown in Figure 4.16.

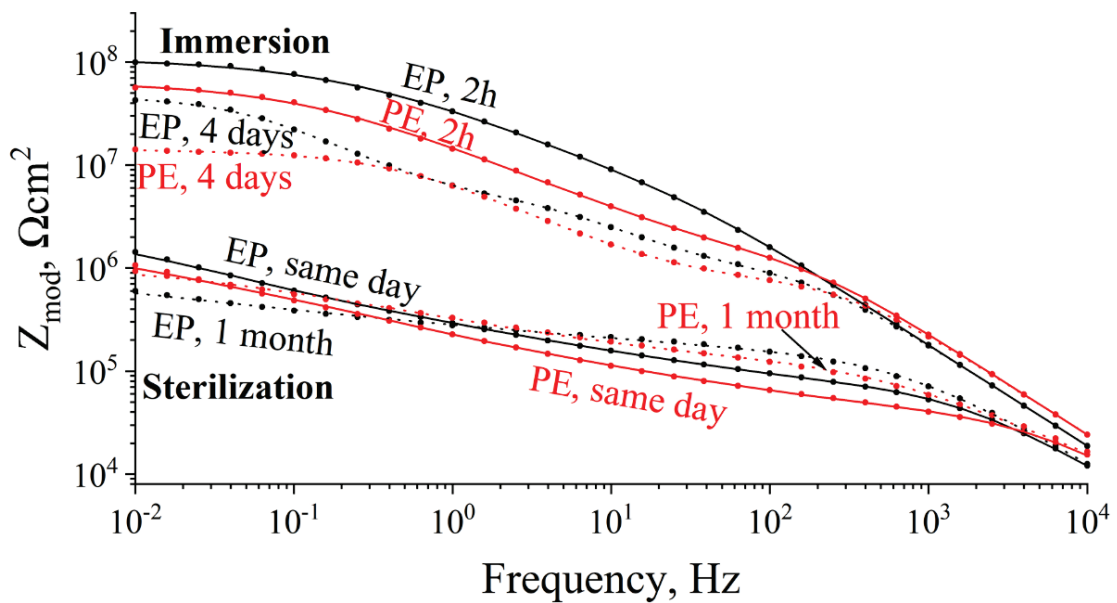


Figure 4.17. Bode plot of fitted models for coated samples.

Immersed PE samples showed time constants at 100 Hz even for 2h of immersion which EP samples did not. It is also confirmed with the breakpoint frequency of 2h immersed PE sample which is 100Hz. For 20h immersed samples, breakpoint frequencies were found as 60 and 200 Hz for PE and EP respectively. These were the points where the formation of a new time constant occurs i.e. real point of the semi-circle on the Nyquist plot. After 4 days of immersion 3 clear time constant plot were observed for both systems. It is previously reported that a variation around  $10^3$  ohm times the magnitude of impedance is common among aged identical samples<sup>30</sup>. Therefore, magnitude difference of the low frequency impedances was not significant to point out. In EP sample, the size of the arc increases with respect to lowering frequencies. In PE sample however, there is a smaller semi-circle at the low frequencies.

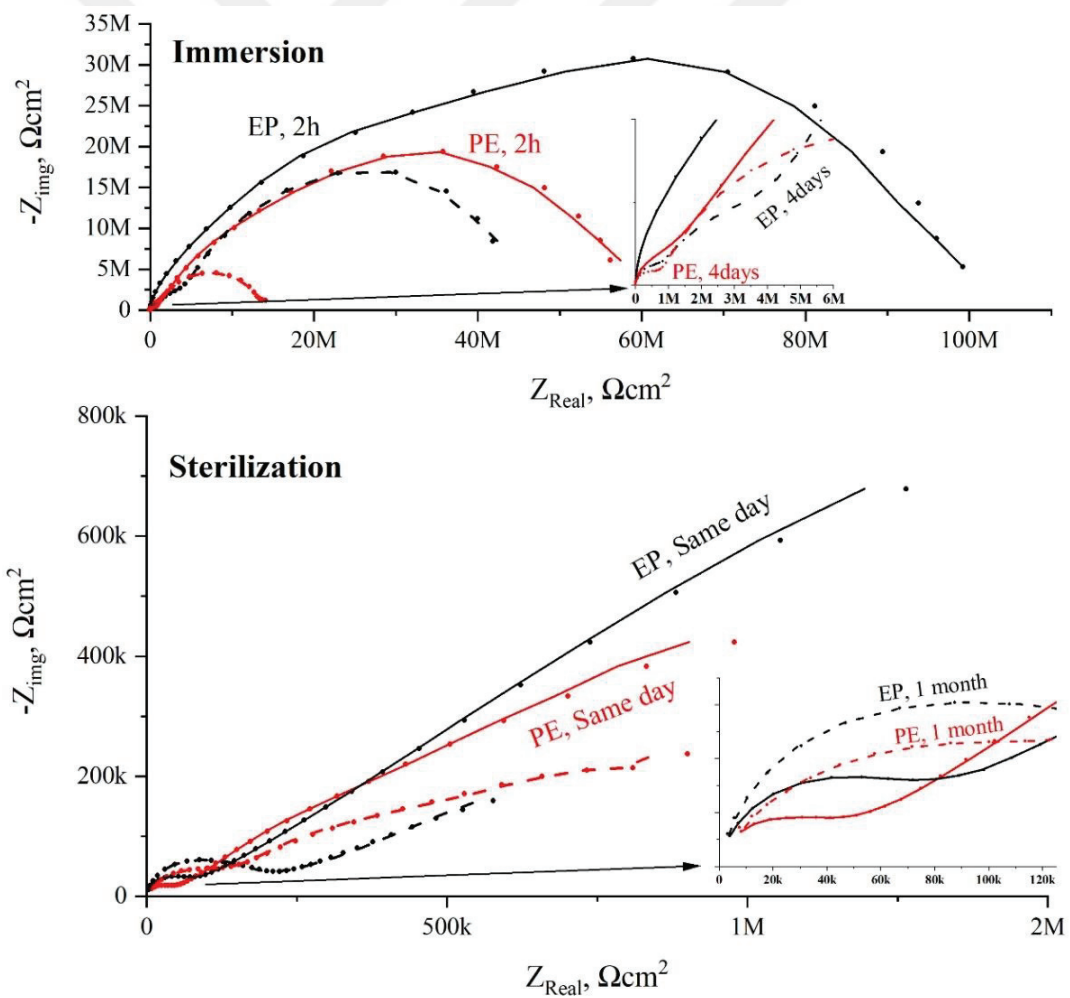


Figure 4.18. Nyquist plot of EIS data for coated samples with fits.

EIS data of sterilized samples were plotted separately, because they were unable to be seen. Similar EIS data were observed for each system that were measured 3h after sterilization. After a week from sterilization, increase in high frequency time constant were observed for each system. Proposed models and further comments are included in discussion.

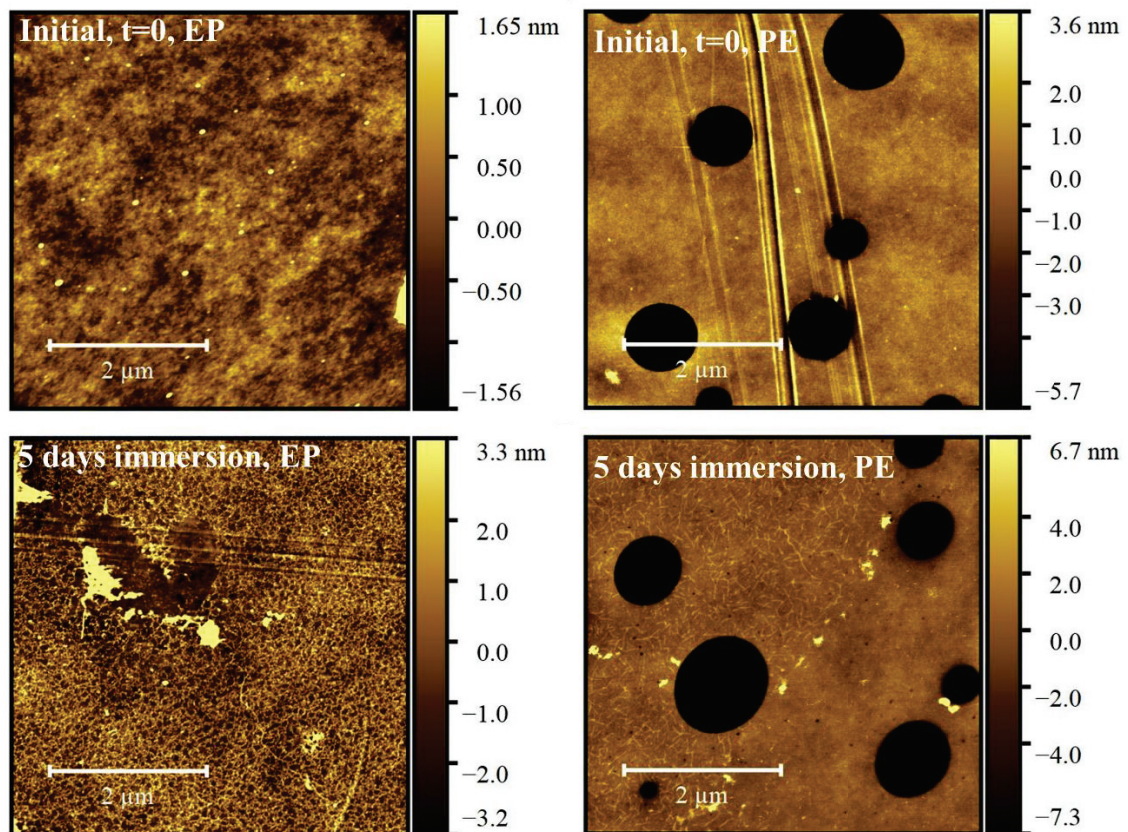


Figure 4.19. AFM images of Epoxy phenolic(left) and Polyester coated(right) tinplates immersed in acidic electrolyte.



Table 4.8. Roughness analysis of EP coated plates.

<b>Roughness analysis of EP plates</b>	<b>t=0</b>	<b>5-day immersion</b>	<b>sterilization</b>	<b>1 week after sterilization</b>	<b>1 month after sterilization</b>
<b>Z Range(nm)</b>	24	44	89	63	70
<b>Ra(nm)</b>	0,42	1,1	2,3	2	2,6
<b>Rq(nm)</b>	0,68	2	0,75	1	1,6

Table 4.9. Roughness analysis of PE coated plates.

<b>Roughness analysis of PE plates</b>	<b>t=0</b>	<b>5-day immersion</b>	<b>sterilization</b>	<b>1 week after sterilization</b>	<b>1 month after sterilization</b>
<b>Z Range(nm)</b>	170	183	184	230	225
<b>Ra(nm)</b>	12	15	5	11	15
<b>Rq(nm)</b>	22	26	14	24	27
<b>Z Range(nm) Manipulated</b>	113	36	71	106	132
<b>Ra(nm) Manipulated</b>	5	0,75	1,2	1,6	4
<b>Rq(nm) Manipulated</b>	7	1,2	2,2	3,5	7

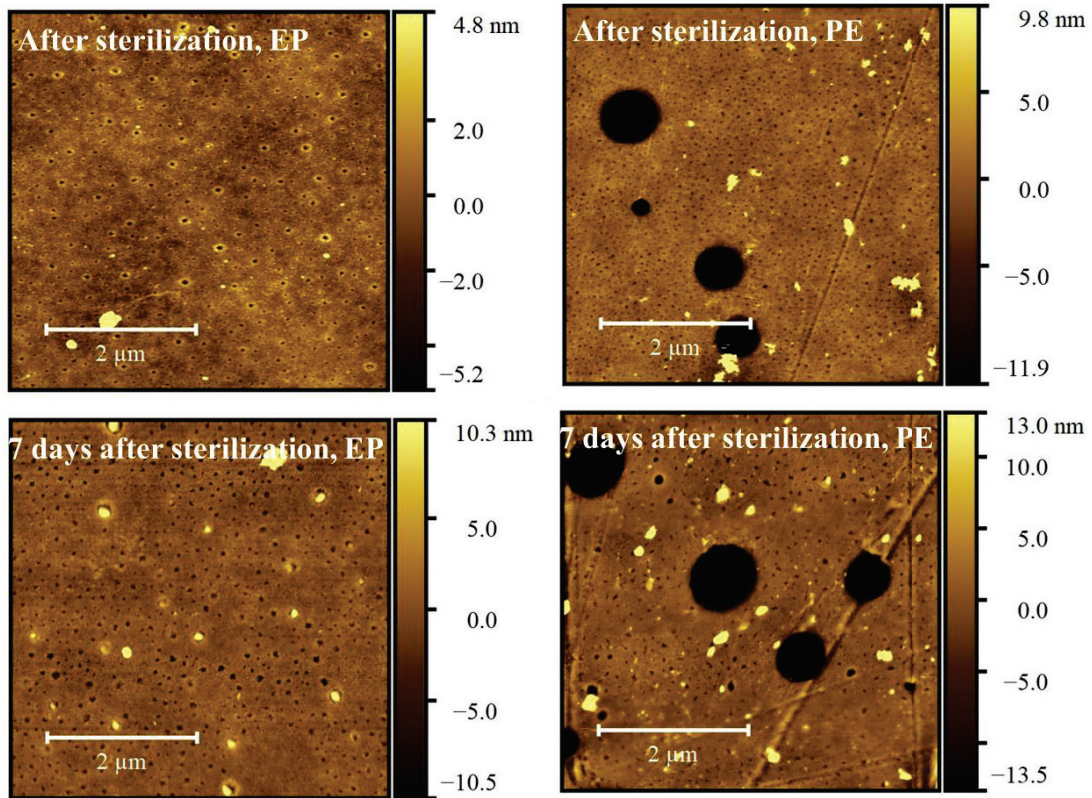


Figure 4.20. AFM images of Epoxy phenolic(left) and Polyester coated(right) tinplates sterilized in acidic electrolyte.

Roughness parameters of aged EP and PE systems were given in Table 4.8 and Table 4.9. respectively. Roughness of PE systems were found to be greater than EP systems. Main reason is the micro craters on PE systems. Therefore, roughness data of PE samples were processed i.e. manipulated in a way that large craters will not be included in data. The results showed that both systems show below 5 nm roughness which is lower than few previous reported systems.<sup>46,57</sup>

After sterilization process, formation of pores between 50 and 100 nm diameter were observed for both systems. Minimum of 2 measurements were made to check homogeneity of the surface. Pore size of EP systems were found to be slightly larger than PE systems. Irregularities of the pore shapes were observed with respect to aging. There are observed high points which match the size of the observed pores, especially in EP systems.

Largest pore diameter was observed after 1 month of aging for PE system however brown deposits were observed in EP systems only as shown in Figure 4.21. Also, larger

defects were observed with optical microscopy images for EP systems. These larger defects(around 5-10  $\mu\text{m}$ ) were not detected with AFM.

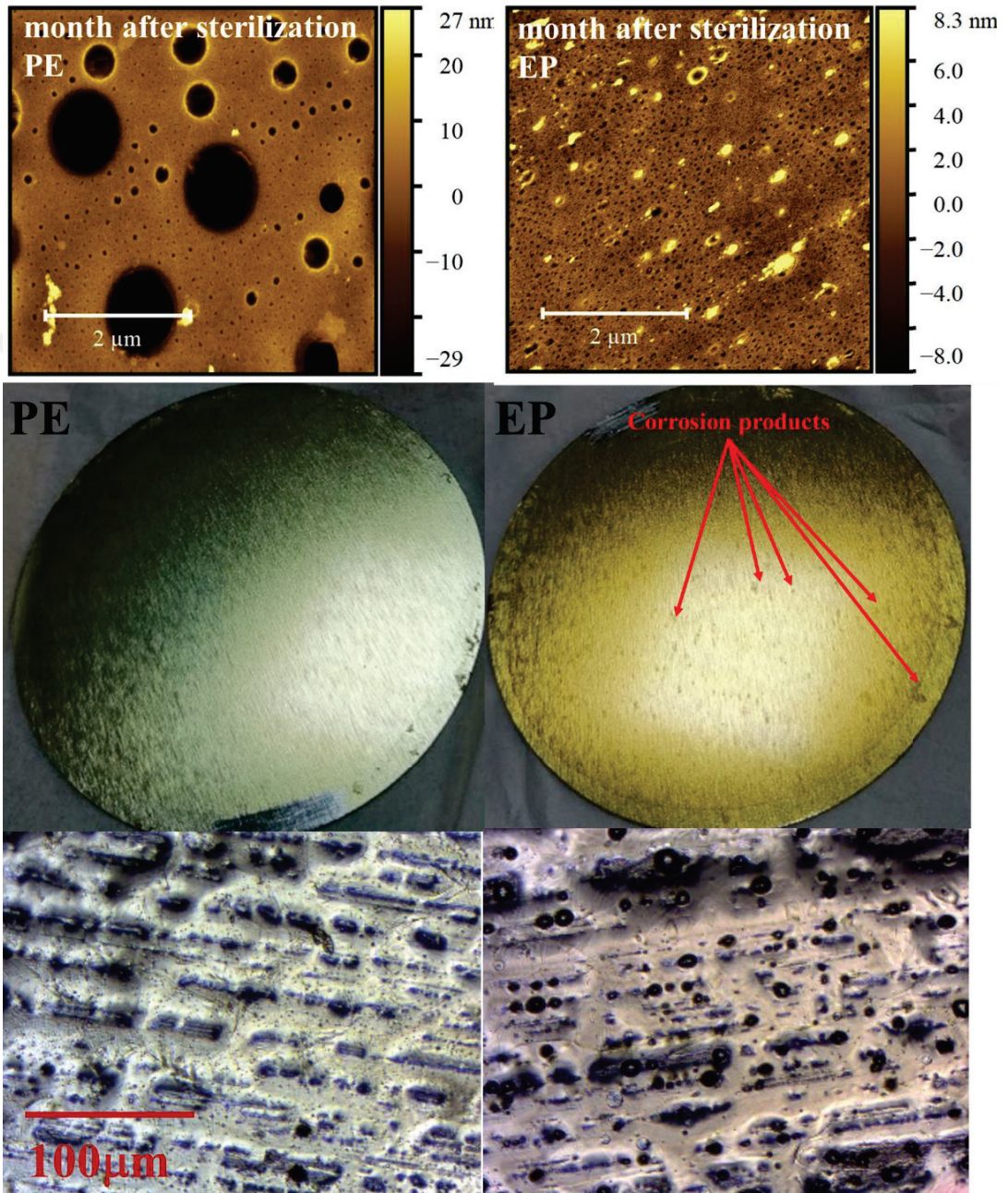


Figure 4.21. Corrosion products on the EP surface, bottom optical microscopy images.

## CHAPTER 5

### DISCUSSION

#### 5.1. Packaging Steel in the Industry

A tinplate can have different surface treatments, tin coating weight, finishing process, annealing process, reflow process, etc. as well known in the literature. Frankenthal et al<sup>8</sup> mention that tin weight does not have a significant effect on tin-iron layer growth alloy which is nobler than tin and iron. Also, Melvin mentioned that surface finish has little importance regarding adhesion performance.<sup>61</sup> However, our SEM, EDX and AFM results indicate surface impurities, morphological irregularities on the surface and composition differences between different industrial samples. For example, Sample II and QLAB(IV) samples showed more homogeneous morphology. A different pattern was observed in III sample and surface heterogeneity in sample I. The absence of nodule shapes in I and III is attributed to surface pretreatment imperfections or different oxide species. For 311 type pretreatments, it was previously reported that outermost layer consists of chromium oxides or chromium hydroxides.<sup>52,53</sup> This is another reason we conducted coated tinplate experiments on QLAB panels.

Brighter areas on back-scatter detector implies higher tin and darker areas implies higher iron content according to mapping results as shown in Figure 4.2. These results are consistent through the previous studies.<sup>62</sup>

#### 5.2. Corrosion of Bare Tinplate on Different Electrolytes

Chemical composition of nodular shaped morphologies at Figure 4.11 could not be detected by our EDX analysis. Numerous studies indicate the topmost layer of commercial tinplate includes chromium and tin oxides/hydroxides.<sup>12,38,50,52</sup> Therefore, it was attributed to disappearing of passivating layer. Same needle shape structure as reported by Caiazzo<sup>51</sup> was observed as shown in Figure 4.6, Figure 4.8 and Figure 4.12.

Migration test procedures and daily practice of coating suppliers include testing with high concentration of citric acid, acetic acid, l-cysteine, NaCl etc. The main purpose

of these electrolytes is creating a visual difference between the studied samples. However, they have different tin-complexing tendency and corrosion mechanism. It was previously reported by Montanari<sup>14</sup> that different concentration of different acids changes the corrosion current of the system. Especially using different acids on the same electrolyte increases the tin complexing attitude i.e. dissolved tin and iron. Even though acid concentrations decrease, combination of acetic acid and citric acid increases the corrosion current compared to mono acid type with high concentration. Also decreased citric acid concentration from 0.05M to 0.01M in 0.1M NaCl and 0.1M acetic acid containing mixture, increased corrosion current observed as shown in Table 4.3.

EIS data was fitted to models shown in Figure 5.1. Following criteria were considered during fitting procedures;

- Physical significance of the elements
- Lower error values compared to physical magnitudes
- Goodness of the fit value lower than 0,005

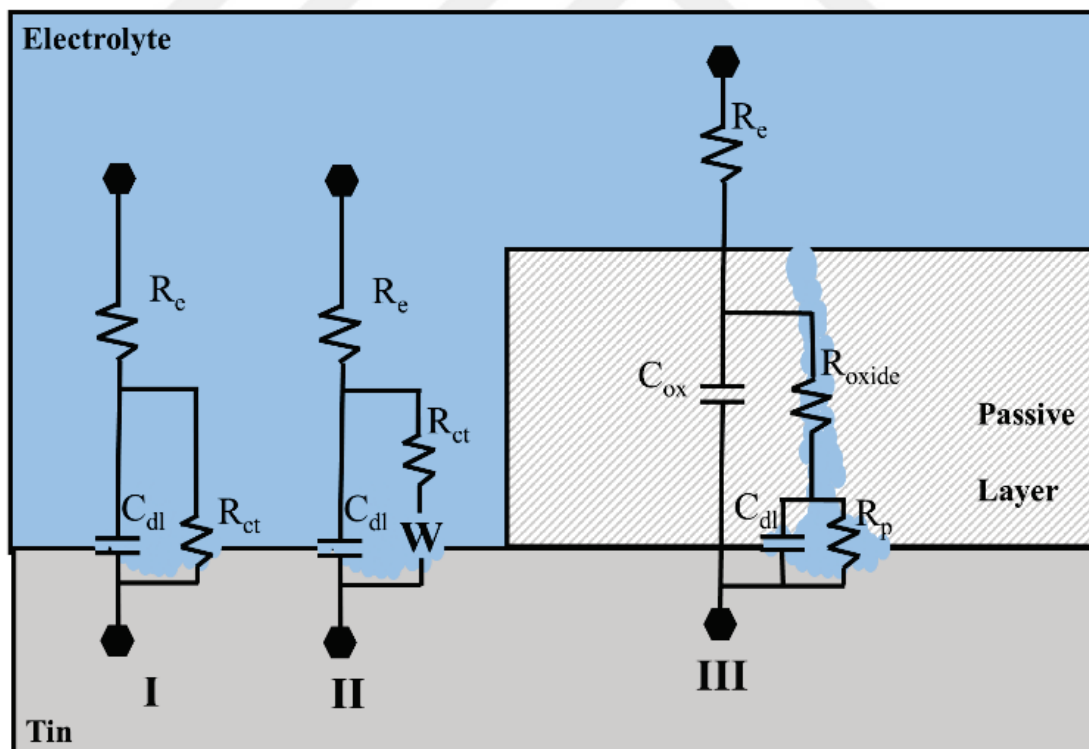


Figure 5.1 Fitted equivalent electrical circuit models for bare tinplate aging.

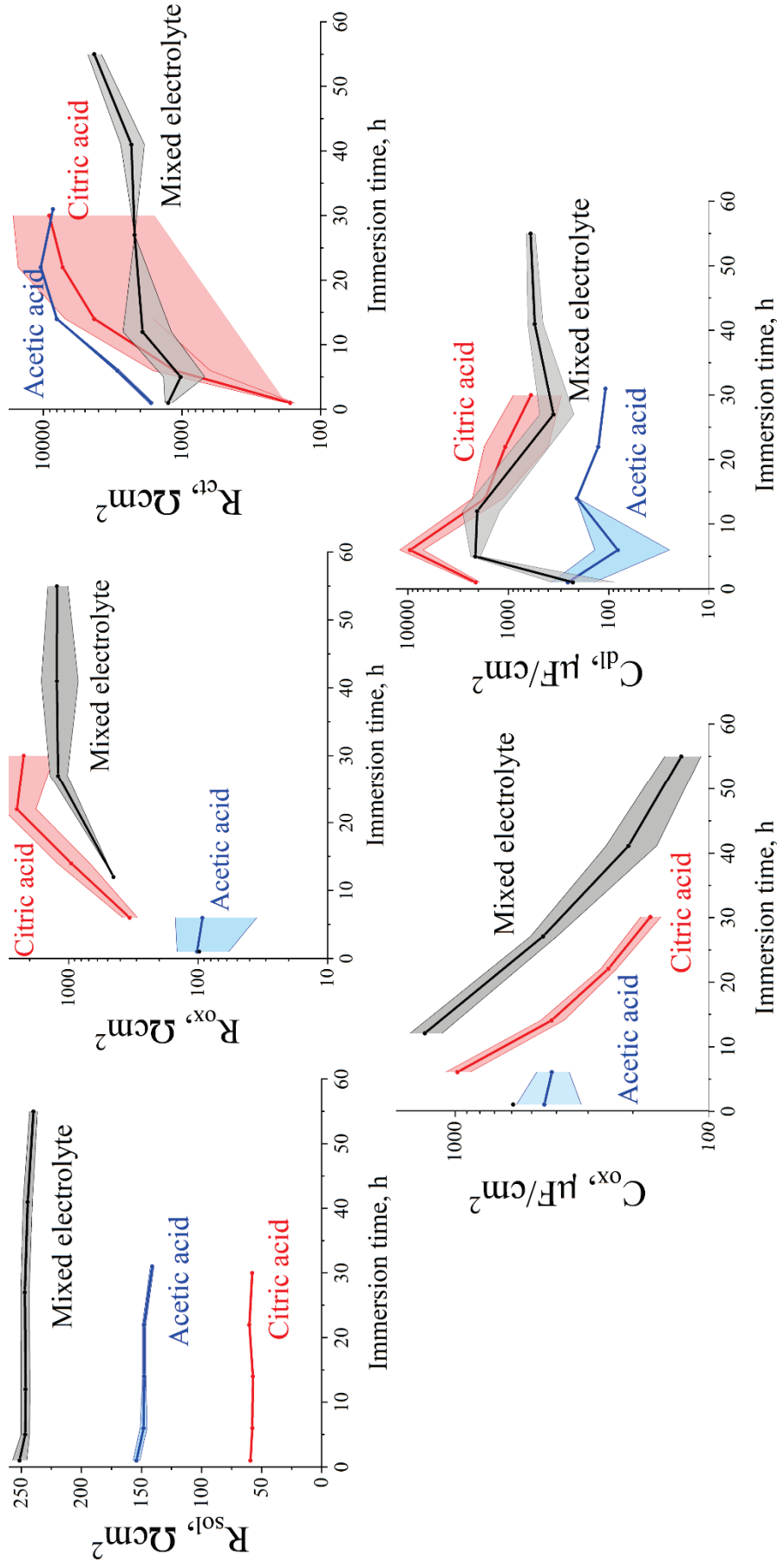


Figure 5.2. Evolution of circuit elements with respect to aging with fitting errors for bare tinplates.

As shown in Figure 5.2, solution resistance was reduced slightly for mixed electrolyte and acetic acid electrolyte in 5h. This may be an indication of dissolution of tin ions to the solution which increases the conductivity as previously reported for steel<sup>13</sup>. Citric acid solution has already 3% NaCl in it, i.e. conductive enough that dissolved tin ions did not contribute to it.

In the initial stages i.e. till 12h of immersion,  $R_{ox}$  and  $C_{ox}$  could represent passive layer. It was previously reported that in acidic conditions tin is anodic to iron.<sup>14,55</sup> SEM images are consistent with the literature also. Therefore, it is expected that tin dissolution as the dominated reaction is observed in EIS. For better understanding, ICP-MS could be used along with electrochemical measurements to characterize dissolved ions. At the later stages of immersion, increase of  $R_{ox}$  and decrease of  $C_{ox}$  were observed. It could be deposition of tin-complex corrosion products which partially passivates the surface as shown in Figure 4.6. Another reason could be the reduction of the free tin amount.

At early stages of aging in citric acid containing electrolytes, low frequency of the data was fitted to Warburg impedance. Since the systems were sealed i.e. limited oxygen intake, it was expected that after oxygen consumption in cathodic reactions, the system will be controlled by diffusion briefly. Unfortunately, in acidic systems, it is possible observe corrosion progress due to proton reduction i.e. anaerobic corrosion.<sup>18</sup> Citric acid has tin complexing ability with oxygen<sup>14</sup>, therefore it was expected. Passivation of the surface by a film of tin hydroxide or oxide in complexing(tin) acids were previously reported by Rehim et al.<sup>63,64</sup> Results of increasing impedance and oxide resistance with respect to immersion time are consistent through this study.

Initial increase followed by a decrease at  $C_{dl}$  were observed for mixed and citric acid containing electrolytes. Since it is an indication of electrochemically active area, it can be a result of self-passivating corrosion products. Initial reduction of the charge transfer resistance was observed for the novel mixed electrolyte. Logarithmic growth was observed with conventional electrolytes. Mixing different acids could catalyze tin dissolution reaction or reduce the stability of the possible corrosion products. Tafel measurements and charge transfer resistance results are consistent through each other and literature.<sup>14</sup>

It was verified that increasing acid combination could fasten the dissolution reactions. Using mono acids excessive amount may not always increase the corrosion rate, the surface may become passivated due to the stable corrosion products. Therefore,

it is advised that preparing novel electrolyte systems for realistic simulation of harsh food environment could be beneficial for coating developers.

### 5.3. Corrosion of Coated Tinplate on Different Coating Formulations

Corrosion products were not observed for both coating systems for 4-day electrolyte immersion and 1-week aging after sterilization. However, after 1 month of aging, corrosion products were observed visually as shown in Figure 4.21.

Roughness analysis of the AFM images did not show a significant relevance with increased aging. Increasing coating degradation was observed with increasing immersion time for both types of coatings. After sterilization, 50-100 nm pits were observed on the coatings. This may occur due to the polymer hydrolysis. Introduction of ionic transport pathways and gradual evolution of hydrophilic channels as Nguyen proposed is suspected however these pit patterns were homogeneous through the surface which also proves it is homogeneous at micrometer level. Swelling or increasing roughness were not observed, therefore blister elements<sup>37</sup> were not used in equivalent circuit modelling. Pore diameters of the PE system were found to be larger than EP system at 1-month aged samples however visual coating failure is first seen on EP systems. This indicate coating resistance after sterilization may not be a reliable parameter for corrosion protection from acidic solutions.

Corrosion of tinplates were related to the decreasing tin content and increasing iron content as observed in EDX analysis of bare tinplate aging. The results indicate that corrosion processes did not proceed to the level where they could be detected with EDX analysis. Only slight morphology changes on the tinplate surfaces were observed, which did not reveal enough information about corrosion processes. These SEM images are shown in Appendix section.

Similar EIS spectra were observed for each system. Proposed equivalent circuit models are shown in

Figure 5.4. Magnitudes of the physical elements and fitted models are shown in Table B.2 for Epoxy and Table B.3 for Polyester.



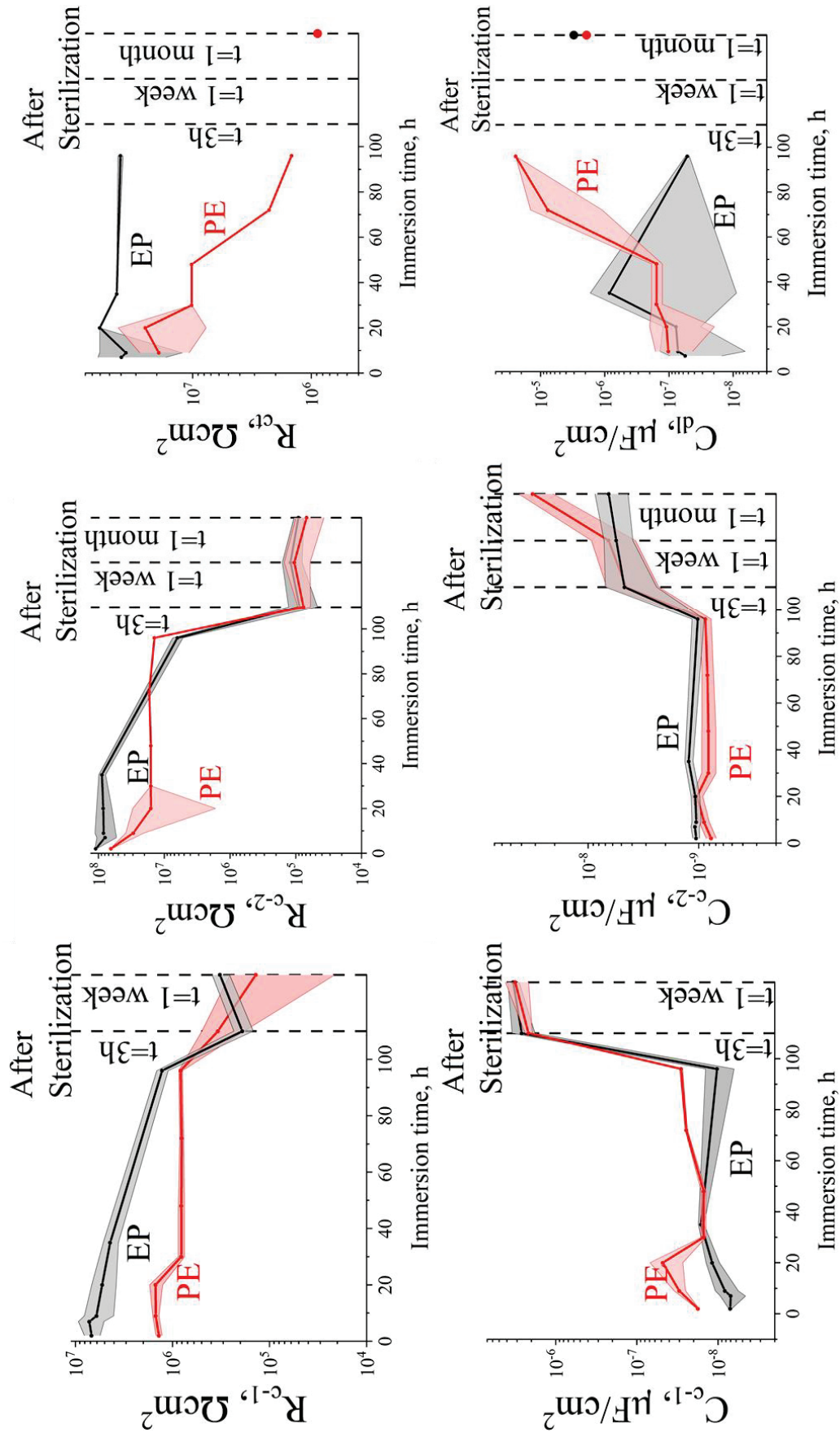


Figure 5.3. Evolution of circuit elements with respect to aging with fitting errors for coated templates.

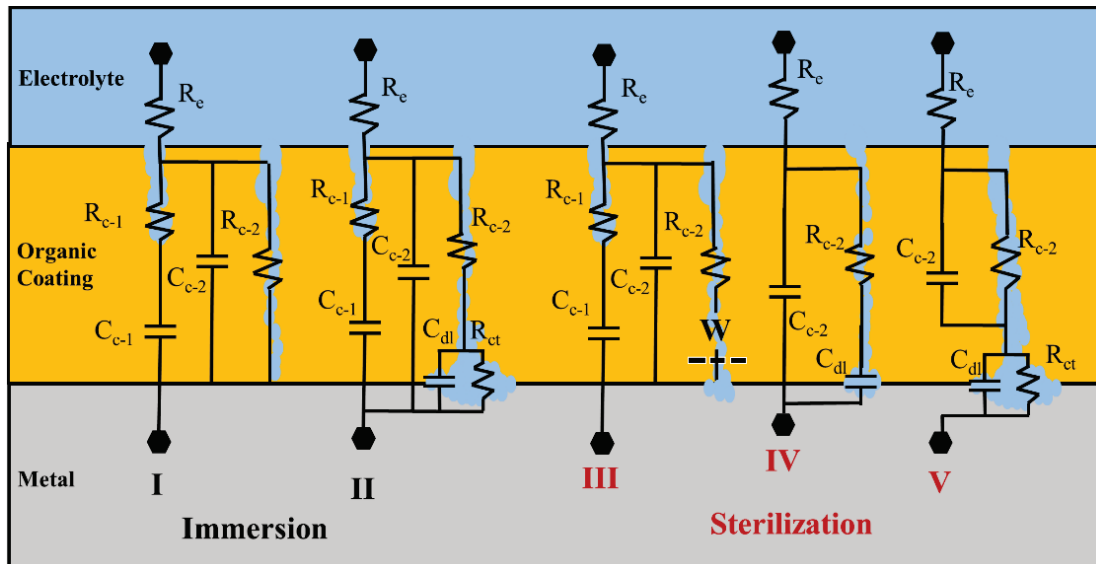


Figure 5.4. Fitted equivalent electrical circuit models for coated tinplate aging.

In the proposed equivalent circuit model,  $R_{c-1}$  represents macropores, and  $R_{c-2}$  represents micropores. These are hypothetical concepts that align with current AFM images. The aim is to model different water uptake mechanisms if any. Comparison of coating resistance elements for PE samples showed a steady behavior after the initial decrease with the immersion. EP samples showed a steady decrease regarding coating resistance with respect to immersion. After sterilization,  $R_{c-1}$  and  $C_{c-1}$  indicate a better performance of PE samples because of the higher resistance and lower capacitance values compared to identically aged EP samples. Compared to the study of Doherty<sup>48</sup>, less dramatic reduction of the coating resistance were observed however the magnitude of the resistance values are consistent through each other. In to the study of Kern<sup>37</sup>, pore resistance values were given within the range of 5-50 ohm which is very low compared to our values.

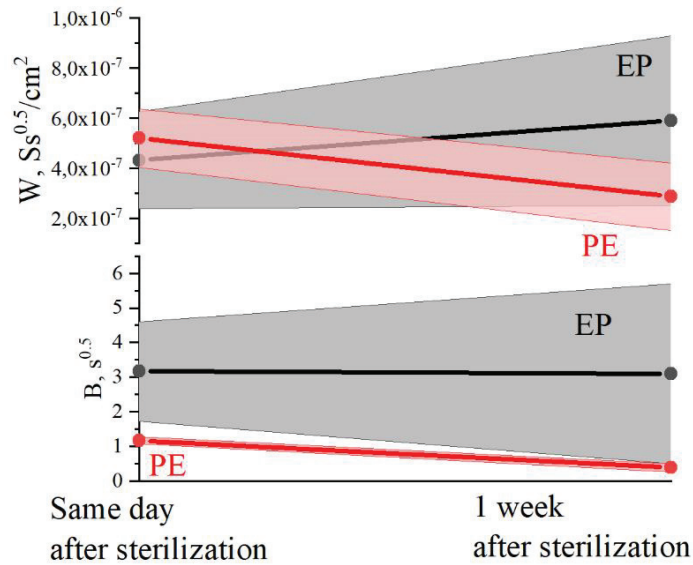


Figure 5.5. Evolution of bound diffusion elements before corrosion products were observed.

Bovard mentioned that<sup>41</sup> samples with lower  $R_{ct}$  than  $10^7 \Omega\text{cm}^2$  is prone to be corroded within 1 year. However, our results indicate that  $R_{ct}$  may not be a corrosion predictive parameter for sterilized samples, in case of diffusion-controlled processes. Porous Warburg were used in this thesis. B parameter in the porous term defines the ratio of diffusion layer thickness to the diffusion constant. As shown in Figure 5.5, B is decreased for PE sample however W also decreased which is an indication of hindered diffusion process. In EP systems, increase of W and constant behavior of B were observed after sterilization which is an indication of easier diffusion through the electrochemically active area. Thus, the lower corrosion resistance of the EP coating after sterilization may be attributed to the diffusion of corrosion products. A month of aging after the sterilization process,  $C_{dl}$  values indicate more electrochemically active area for EP system as shown in Figure 5.3 even though immersion performance of the EP system were better including total impedance. This also indicates that higher electrochemically active area may be the second reason that EP samples shows a lower corrosion resistance, compared to the PE samples after sterilization. These results indicate the importance of coating-interphase area and the diffusion properties for the corrosion protective properties of different coating types.

## CHAPTER 6

### CONCLUSION

In this thesis, the effect of electrolyte and lacquer types on the corrosion mechanism of tinplate were investigated. Our comparison of industrial samples showed that their surface structure could be different, which may influence the corrosion mechanism and make it difficult to have results based on the lacquer and electrolyte type. Therefore, the measurements in the thesis were conducted on QLAB model samples, so that results are not affected from the changing surface composition.

Combination of acid mixtures alters the corrosion mechanism, as indicated from the appearance of different number of time constants, reflecting different rate limiting steps. Corrosion rate was found to be higher for the mixed acid compared to the lower concentrations of mono acids. This is important for can coating suppliers because, simulation of food media alter the coating design.

Surprisingly, the performance of the BPA-NI polyester-based coating were found to be superior compared to epoxy-based coating, after sterilization. EIS spectra of early aging stages by immersion did not reveal this result. Even after 24h immersion of coated plates, 3-time constant EIS spectra were observed for both samples. A complex equivalent circuit was used to model the behavior of the system however only the low frequency elements were consistent through the results of the study.

Nano-pores at the coating surface as a result of aging were imaged with AFM. It was attributed to water uptake or hydrolysis of the polymer. Even though polyester samples have larger pores, corrosion products were not observed on these samples. Modelling of EIS data also revealed that EP sample had a higher diffusion rate of corrosion products and a larger electrochemically active area compared to PE sample after sterilization. These results may indicate that coating-metal interphase, the electrochemically active area and the diffusion properties may be important factors for predicting corrosion protection of different lacquers on tinplate.

## REFERENCES

1. LaKind, J. S. Can Coatings for Foods and Beverages: Issues and Options. *Int. J. Technol. Policy Manag.* **2012**. <https://doi.org/10.1504/ijtpm.2013.050999>.
2. Geueke, B. Dossier – Can Coatings. *Food Packaging Forum.* **2016**. <https://doi.org/10.4067/S0250-71612013000200001>.
3. Watson, J. Can Coating Market To Reach USD 2.71 Billion By 2026 <https://www.globenewswire.com/news-release/2019/08/08/1899339/0/en/Can-Coating-Market-To-Rreach-USD-2-71-Billion-By-2026-Reports-And-Data.html> (accessed Nov 1, **2019**).
4. Turner, T. A. *Canmaking - the Technology of Metal Protection and Decoration*; **1998**. [https://doi.org/10.1002/\(sici\)1099-1522\(199811/12\)11:6<301::aid-pts440>3.3.co;2-0](https://doi.org/10.1002/(sici)1099-1522(199811/12)11:6<301::aid-pts440>3.3.co;2-0).
5. Page, B.; Edwards, M.; May, N. Metal Packaging. In *Food and Beverage Packaging Technology*; Wiley-Blackwell: Oxford, UK, **2011**; pp 107–135. <https://doi.org/10.1002/9781444392180.ch5>.
6. Arcelor Mittal. Arcelor Mittal Packaging Catalogue [https://packaging.arcelormittal.com/repo/Unassigned/CatPack\\_170908.pdf](https://packaging.arcelormittal.com/repo/Unassigned/CatPack_170908.pdf) (accessed Nov 1, **2019**).
7. Barisic, B.; Pepelnjak, T.; Math, M. D. Predicting of the Lüders' Bands in the Processing of TH Material in Computer Environment by Means of Stochastic Modeling. *J. Mater. Process. Technol.* **2008**. <https://doi.org/10.1016/j.jmatprotec.2007.09.054>.
8. Frankenthal, R. P.; Loginow, A. W. Kinetics of the Formation of the Iron-Tin Alloy FeSn<sub>2</sub>. *J. Electrochem. Soc.* **1960**. <https://doi.org/10.1149/1.2427542>.
9. *GIDA İLE TEMAS EDEN MADDE VE MALZEMELERE DAİR YÖNETMELİK*; Resmi Gazete: Turkey, **2018**.
10. European Commission. Commission Regulation (EU) No 10/2011 on Plastic Materials and Articles Intended to Come into Contact with Food. *Off. J. Eur. Union* **2011**. <https://doi.org/10.1016/j.nucengdes.2011.01.052>.
11. Almeida, E.; Costa, M. R.; De Cristofaro, N.; Mora, N.; Catala, R.; Puente, J. M.; Bastidas, J. M. Titanium Passivated Lacquered Tinline Cans in Contact with Foods. *Corros. Eng. Sci. Technol.* **2005**, *40* (2), 158–164.
12. Charbonneau, J. E. Application of Scanning Electron-Microscopy and X-Ray-Microanalysis to Investigate Corrosion Problems in Plain and Enameled 3 Piece Welded Food Cans. *Food Struct.* **1991**, *10* (2), 171–184.

13. Amirudin, A.; Thienny, D. Application of Electrochemical Impedance Spectroscopy to Study the Degradation of Polymer-Coated Metals. *Progress in Organic Coatings*. **1995**. [https://doi.org/10.1016/0300-9440\(95\)00581-1](https://doi.org/10.1016/0300-9440(95)00581-1).
14. Montanari, A. Basic Principles of Corrosion of Food Metal Packaging. In *Food Packaging Hygiene*; **2015**. <https://doi.org/10.1007/978-3-319-14827-4>.
15. Atkins, P.; Paula, J. De. *Atkins' Physical Chemistry 8th Edition*; **2009**. <https://doi.org/10.1021/ed056pA260.1>.
16. Ahmad, Z. *Principles of Corrosion Engineering and Corrosion Control*; **2006**. <https://doi.org/10.1016/B978-0-7506-5924-6.X5000-4>.
17. Cramer, S. D.; Covino, B. S. ASM Handbook: Corrosion - Fundamentals, Testing, and Protection. *Asm* **2003**. <https://doi.org/10.1002/jbm.b.31896>.
18. Murphy, T. P. Tin and Tinplate. In *Uhlig's Corrosion Handbook: Third Edition*; **2011**. <https://doi.org/10.1002/9780470872864.ch60>.
19. Lyon, S. B.; Bingham, R.; Mills, D. J. Advances in Corrosion Protection by Organic Coatings: What We Know and What We Would like to Know. *Progress in Organic Coatings*. **2017**. <https://doi.org/10.1016/j.porgcoat.2016.04.030>.
20. Sørensen, P. A.; Dam-Johansen, K.; Weinell, C. E.; Kiil, S. Cathodic Delamination of Seawater-Immersed Anticorrosive Coatings: Mapping of Parameters Affecting the Rate. *Prog. Org. Coatings* **2010**. <https://doi.org/10.1016/j.porgcoat.2010.03.012>.
21. Bautista, A. Filiform Corrosion in Polymer-Coated Metals. *Progress in Organic Coatings*. **1996**. [https://doi.org/10.1016/0300-9440\(95\)00555-2](https://doi.org/10.1016/0300-9440(95)00555-2).
22. Sangaj, N. S.; Malshe, V. C. Permeability of Polymers in Protective Organic Coatings. *Progress in Organic Coatings*. **2004**. <https://doi.org/10.1016/j.porgcoat.2003.09.015>.
23. Miszczyk, A.; Darowicki, K. Water Uptake in Protective Organic Coatings and Its Reflection in Measured Coating Impedance. *Prog. Org. Coatings* **2018**, *124*, 296–302.
24. Hirschorn, B.; Orazem, M. E.; Tribollet, B.; Vivier, V.; Frateur, I.; Musiani, M. Determination of Effective Capacitance and Film Thickness from Constant-Phase-Element Parameters. *Electrochim. Acta* **2010**. <https://doi.org/10.1016/j.electacta.2009.10.065>.
25. Deflorian, F.; Rossi, S. An EIS Study of Ion Diffusion through Organic Coatings. In *Electrochimica Acta*; **2006**. <https://doi.org/10.1016/j.electacta.2005.02.145>.
26. Gamry, I. I. Introduction to Electrochemical Impedance Spectroscopy. **2015**.

27. Bonora, P. L.; Deflorian, F.; Fedrizzi, L. Electrochemical Impedance Spectroscopy as a Tool for Investigating Underpaint Corrosion. *Electrochim. Acta* **1996**, *41* (7–8), 1073–1082. [https://doi.org/10.1016/0013-4686\(95\)00440-8](https://doi.org/10.1016/0013-4686(95)00440-8).
28. Murtomaki, L.; Kallio, T.; Lahtinen, R. Electrochemistry <https://mycourses.aalto.fi/mod/book/tool/print/index.php?id=388663> (accessed Nov 1, **2019**).
29. Gamry. Basics of Electrochemical Impedance Spectroscopy. *Application Note AC*. **2010**. <https://doi.org/10.1152/ajpregu.00432.2003>.
30. Tait, W. S. Using Electrochemical Measurements to Estimate Coating and Polymer Film Durability. *J. Coatings Technol.* **2003**, *75* (942), 45–50.
31. Deflorian, F.; Rossi, S.; Fedel, M. Organic Coatings Degradation: Comparison between Natural and Artificial Weathering. *Corros. Sci.* **2008**. <https://doi.org/10.1016/j.corsci.2008.06.009>.
32. Charbonneau, J. E. Recent Case Histories of Food Product - Metal Container Interactions Using Scanning Electron Microscopy-X-Ray Microanalysis. *Scanning* **1997**, *19* (7), 512–518.
33. Charbonneau, J. E. Investigation of Corrosion and Container Integrity in Metal Food Containers Using Scanning Electron Microscopy-x-ray Microanalysis. *Scanning* **2001**, *23* (3), 198–203.
34. Barella, S.; Cincera, S.; Boniardi, M.; Bellogini, M.; Gelati, S.; Montanari, A. Failure Analysis of Tuna Cans. *J. Fail. Anal. Prev.* **2011**, *11* (4), 446–451.
35. Badilla, G. L.; Salas, B. V.; Wiener, M. S. Analysis of Corrosion in Steel Cans in the Seafood Industry on the Gulf of California. *Mater. Perform.* **2012**, *51* (4), 52–57.
36. Nascimento, G. G. D.; Santos, J. L. C. D.; Margarit, I. C. P.; Mattos, O. R. Lacquered Tinplate: Corrosion Resistance in the Function of Lacquering Conditions. *Electrochim. Acta* **1996**. [https://doi.org/10.1016/0013-4686\(95\)00443-2](https://doi.org/10.1016/0013-4686(95)00443-2).
37. Kern, P.; Baner, A. L.; Lange, J. Electrochemical Impedance Spectroscopy as a Tool for Investigating the Quality and Performance of Coated Food Cans. *J. Coatings Technol.* **1999**, *71* (899), 67–74. <https://doi.org/10.1007/bf02697980>.
38. Almeida, E.; Costa, M. R.; De Cristofaro, N.; Mora, N.; Bastidas, J. M.; Puente, J. M. Environmentally Friendly Coatings for Tinplate Cans in Contact with Synthetic Food Media. *J. Coatings Technol. Res.* **2004**. <https://doi.org/10.1007/s11998-004-0004-4>.
39. Buttrey, F. E.; McAlister, J. A.; McMurray, H. N. Advanced Electrochemical Methods for Food Can Evaluation. *Ironmak. Steelmak.* **1999**, *26* (4), 291–296.

40. Catalá, R.; Cabañes, J. M.; Bastidas, J. M. An Impedance Study on the Corrosion Properties of Lacquered Tinfoil Cans in Contact with Tuna and Mussels in Pickled Sauce. *Corros. Sci.* **1998**. [https://doi.org/10.1016/S0010-938X\(98\)00050-X](https://doi.org/10.1016/S0010-938X(98)00050-X).
41. Bovard, F. S.; Burleigh, T. D.; Smith, A. T. Electrochemical Impedance Spectroscopy of Electrocoated Aluminium Food Cans. *Electrochim. Acta* **1995**, *40* (2), 201–207.
42. Hack, H. P.; Scully, J. R. Defect Area Determination of Organic Coated Steels in Seawater Using the Breakpoint Frequency Method. *J. Electrochem. Soc.* **1991**, *138* (1), 33–40.
43. Tait, W. S. Using Electrochemical Impedance Spectroscopy to Study Corrosion Behavior of Internally Coated Metal Containers. *J. Coatings Technol.* **1989**.
44. Zumelzu, E.; Cabezas, C.; Alvarado, R. Evaluation of the Degradation of Traditional and ECCS Canning Tinfoils in Acetic-Acetate Medium. *Sci. Eng. Compos. Mater.* **2006**, *13* (1), 13–20.
45. Zumelzu, E.; Silva, E.; Rull, F.; Muñoz, O.; Ugarte, R. Effect of Lactic Acid on Polyethylene Terephthalate (PET) and Polypropylene (PP) Coatings of Food Containers. *J. Polym. Environ.* **2018**, *26* (6), 2476–2488.
46. Zhou, C.; Wang, J.; Song, S.; Xia, D.; Wang, K.; Shen, C.; Luo, B.; Shi, J. Degradation Mechanism of Lacquered Tinfoil in Energy Drink by In-Situ EIS and EN. *J. Wuhan Univ. Technol. Sci. Ed.* **2013**, *28* (2), 367–372.
47. Wang, K.; Wang, J.; Wang, H.; Fu, C.; Xia, D.; Zheng, X.; Dang, L.; Shi, J. Corrosion Detection of Tinfoil Cans Containing Coffee Using EIS/EN Sensor. *J. Cent. South Univ.* **2014**, *21* (1), 76–82.
48. Doherty, M.; Sykes, J. M. Micro-Cells beneath Organic Lacquers: A Study Using Scanning Kelvin Probe and Scanning Acoustic Microscopy. *Corros. Sci.* **2004**, *46* (5), 1265–1289.
49. Study of Topography and Distribution State of the Nanoscale Passivation Film on a Rough Tinfoil Surface. *Coatings* **2018**. <https://doi.org/10.3390/coatings8030094>.
50. Melvin, C.; Jewell, E.; Miedema, J.; Lammers, K.; Vooy, A.; Allman, A.; McMurray, N. Identifying Interlayer Surface Adhesion Failure Mechanisms in Tinfoil Packaging Steels. *Packag. Technol. Sci.* **2019**. <https://doi.org/10.1002/pts.2443>.
51. Cova Caiazza, F.; Brambilla, L.; Montanari, A.; Mischler, S. Chemical and Morphological Characterization of Commercial Tinfoil for Food Packaging. *Surf. Interface Anal.* **2018**. <https://doi.org/10.1002/sia.6386>.
52. Mora, N.; Cano, E.; Bastidas, J. M.; Almeida, E.; Puente, J. M. Characterization of Passivated Tinfoil for Food Can Applications. *J. Coatings Technol.* **2002**. <https://doi.org/10.1007/bf02697957>.



53. Wu, F. J.; Liu, X. J.; Xiao, X. Surface Characterisation of Electroplated Tinplate with Different Coating Mass. *Surf. Eng.* **2018**. <https://doi.org/10.1080/02670844.2017.1288343>.
54. Chen, S.; Xie, L.; Xue, F. X-Ray Photoelectron Spectroscopy Investigation of Commercial Passivated Tinplate Surface Layer. *Appl. Surf. Sci.* **2013**. <https://doi.org/10.1016/j.apsusc.2013.03.115>.
55. Benitez, G. J.; Cirillo, P. A.; Gines, M. J. L.; Egli, W. A. INTERNAL CORROSION IN TINPLATE CANS. In *16 th Rolling Conference*; **2006**; pp 583–590.
56. Morsch, S.; Lyon, S.; Greensmith, P.; Smith, S. D.; Gibbon, S. R. Water Transport in an Epoxy-Phenolic Coating. *Prog. Org. Coatings* **2015**. <https://doi.org/10.1016/j.porgcoat.2014.08.006>.
57. Morsch, S.; Lyon, S.; Gibbon, S. R. The Degradation Mechanism of an Epoxy-Phenolic Can Coating. *Prog. Org. Coatings* **2017**, *102*, 37–43.
58. Kefallinou, Z.; Lyon, S. B.; Gibbon, S. R. A Bulk and Localised Electrochemical Assessment of Epoxy-Phenolic Coating Degradation. *Prog. Org. Coatings* **2017**. <https://doi.org/10.1016/j.porgcoat.2016.04.042>.
59. Swapp, S. Scanning Electron Microscopy [https://serc.carleton.edu/research\\_education/geochemsheets/techniques/SEM.html](https://serc.carleton.edu/research_education/geochemsheets/techniques/SEM.html) (accessed Nov 1, **2019**).
60. Nanosurf. How does AFM work? <https://www.nanosurf.com/en/how-afm-works/afm-operating-principle> (accessed Nov 1, **2019**).
61. Melvin, C.; Jewell, E.; de Voys, A.; Lammers, K.; Murray, N. M. Surface and Adhesion Characteristics of Current and Next Generation Steel Packaging Materials. *J. Packag. Technol. Res.* **2018**. <https://doi.org/10.1007/s41783-018-0031-8>.
62. Álvarez, D.; Collazo, A.; Nóvoa, X. R.; Pérez, C. Electrochemical Behavior of Organic/Inorganic Films Applied on Tinplate in Different Aggressive Media. *Prog. Org. Coatings* **2014**. <https://doi.org/10.1016/j.porgcoat.2014.02.004>.
63. Abd El Rehim, S. S.; Zaky, A. M.; Mohamed, N. F. Electrochemical Behaviour of a Tin Electrode in Tartaric Acid Solutions. *J. Alloys Compd.* **2006**. <https://doi.org/10.1016/j.jallcom.2005.12.080>.
64. Lyon, S. B. Corrosion of Tin and Its Alloys. In *Shreir's Corrosion*; **2010**. <https://doi.org/10.1016/B978-044452787-5.00099-8>.
65. Montgomery, D. C.; Runger, G. C. Applied Statistics and Probability for Engineers. *Eur. J. Eng. Educ.* **1994**. <https://doi.org/10.1080/03043799408928333>.

# APPENDIX A

## AFTER PULL-OFF SEM IMAGES OF COATED SAMPLES

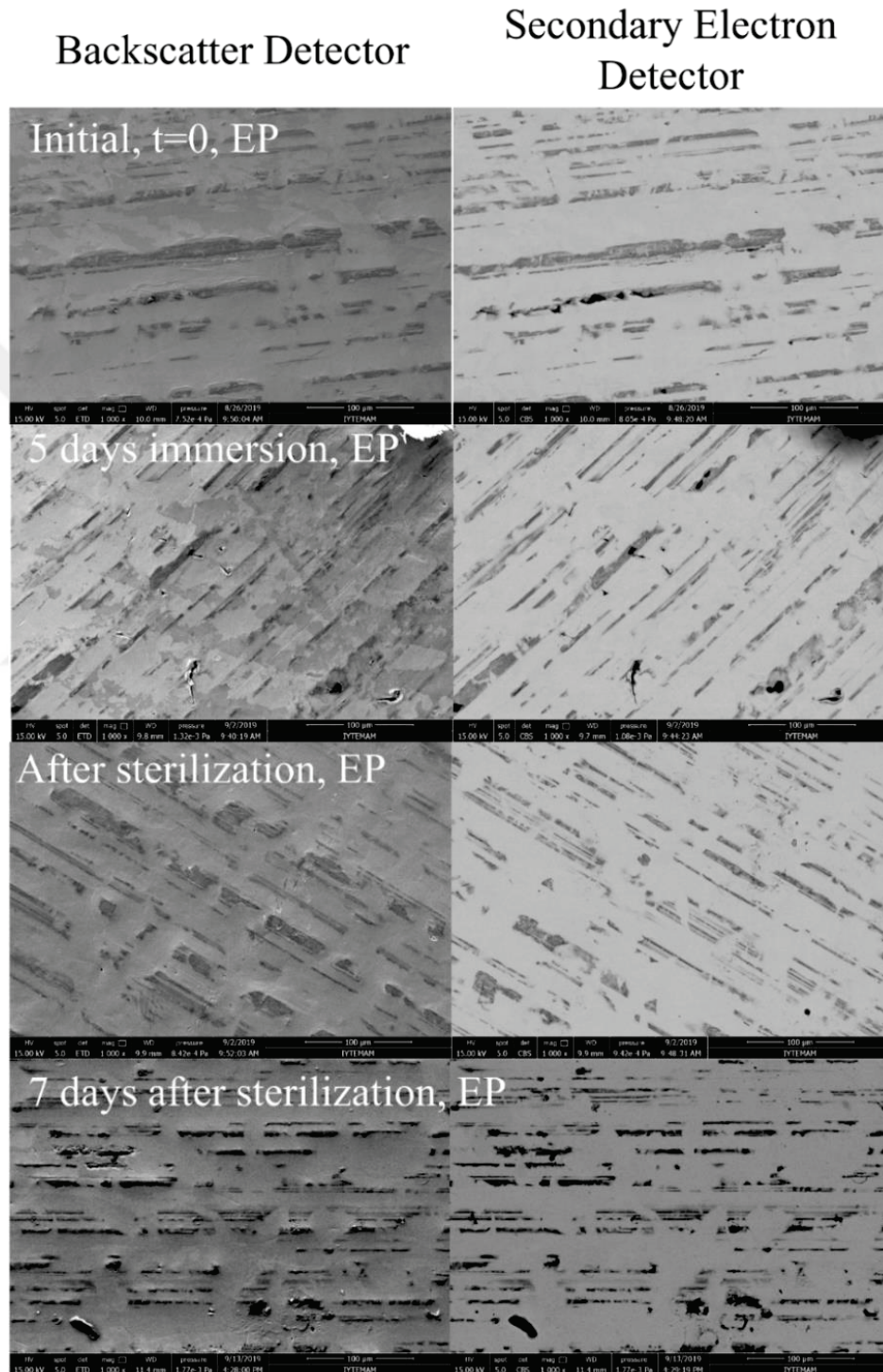


Figure A.1. SEM images of pulled-off epoxy coated tinplates

Backscatter Detector

Secondary Electron Detector

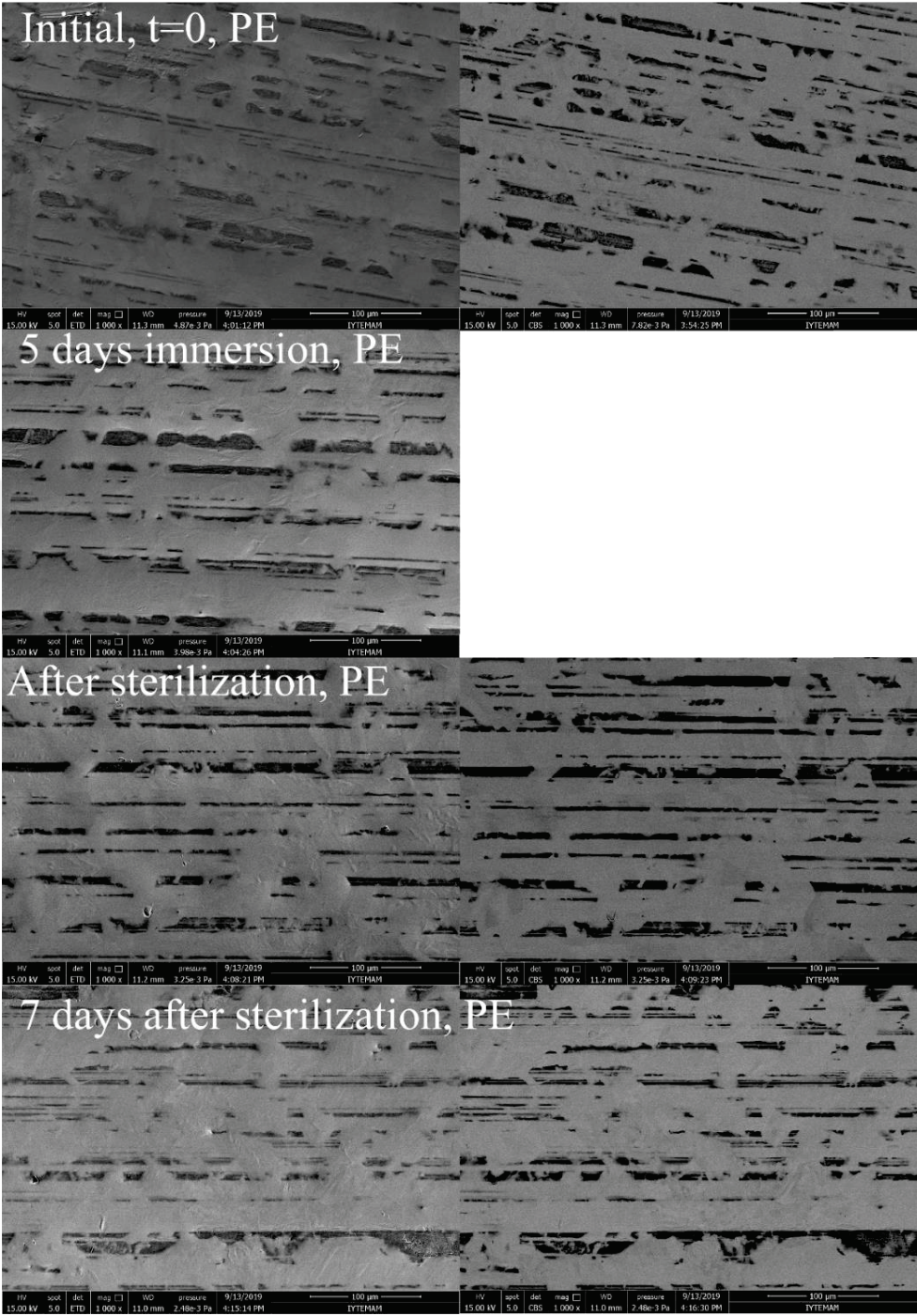


Figure A.2. SEM images of pulled-off polyester coated tinplate

## APPENDIX B

### MAGNITUDES OF FITTED PHYSICAL ELEMENTS

Table B.1. Equivalent electrical circuit fitted elements for bare samples.

	time	Rsol	Rox	Cox	a(ox)	Rct	Cdl	a(dl)	W	Goodness of Fit	Fitted model
	h	$\Omega\text{cm}^2$	$\Omega\text{cm}^2$	$\text{Ss}^a/\text{cm}^2$		$\Omega\text{cm}^2$	$\text{Ss}^a/\text{cm}^2$		$\text{Ss}^{0.5}/\text{cm}^2$		
3 % Acetic acid 1% NaCl	1	1,54E+02	1,02E+02	4,46E-04	5,95E-01	1,67E+03	2,56E-04	8,28E-01		1,16E-04	III
	±	2,78E+00	4,39E+01	1,27E-04	3,09E-02	6,20E+01	1,15E-04	9,23E-02			
	6	1,48E+02	9,27E+01	4,17E-04	6,16E-01	2,92E+03	8,15E-05	9,16E-01		3,39E-04	III
	±	2,86E+00	5,75E+01	6,03E-05	2,60E-02	1,12E+02	5,65E-05	1,06E-01			
	14	1,48E+02				7,99E+03	2,07E-04	7,09E-01		3,77E-04	I
	±	1,30E+00				1,43E+02	3,03E-06	4,68E-03			
	22	1,48E+02				1,04E+04	1,27E-04	7,01E-01		5,72E-05	I
	±	1,42E+00				1,71E+02	1,93E-06	4,28E-03			
	31	1,41E+02				8,51E+03	1,08E-04	6,99E-01		2,08E-04	I
±	1,42E+00				1,25E+02	1,82E-06	4,41E-03				
1% Citric acid 3% NaCl	1	5,93E+01				1,66E+02	2,12E-03	6,11E-01	1,95E-02	2,80E-04	II
	±	6,68E-01				1,14E+01	1,94E-04	2,37E-02	1,00E-03		
	6	5,77E+01	3,38E+02	9,79E-04	6,70E-01	1,13E+03	9,55E-03	6,46E-01		1,19E-04	III
	±	7,41E-01	4,40E+01	1,07E-04	2,42E-02	4,99E+02	2,49E-03	1,17E-01			
	14	5,73E+01	9,55E+02	4,17E-04	6,96E-01	4,29E+03	1,70E-03	4,99E-01		1,49E-04	III
	±	7,91E-01	2,69E+02	4,37E-05	2,00E-02	2,68E+03	5,75E-04	1,44E-01			
	22	6,02E+01	2,51E+03	2,49E-04	7,08E-01	7,25E+03	1,07E-03	4,77E-01		1,18E-04	III
	±	8,33E-01	7,21E+02	1,79E-05	1,38E-02	7,91E+03	6,71E-04	2,42E-01			
30	5,78E+01	2,22E+03	1,71E-04	7,41E-01	9,04E+03	5,94E-04	4,18E-01		6,82E-05	III	
±	8,24E-01	9,35E+02	1,54E-05	1,58E-02	7,47E+03	2,99E-04	1,89E-01				
0.1M NaCl 0.1M Acetic acid 0.01M Citric acid	1	2,51E+02	9,80E+01	5,91E-04	5,24E-01	1,25E+03	2,27E-04	8,43E-01		1,13E-03	III
	±	5,95E+00	5,34E+01	1,55E-04	4,11E-02	7,39E+01	1,39E-04	1,25E-01			
	5	2,47E+02				1,02E+03	2,13E-03	4,30E-01	5,96E-03	1,16E-04	II
	±	3,53E+00				3,38E+02	2,40E-04	3,32E-02	1,05E-03		
	12	2,46E+02	4,50E+02	1,32E-03	5,04E-01	1,93E+03	2,04E-03	5,14E-01		9,17E-05	III
	±	3,78E+00	0,00E+00	1,89E-04	4,20E-02	7,33E+02	8,24E-04	1,25E-01			
	27	2,47E+02	1,21E+03	4,51E-04	5,76E-01	2,19E+03	3,55E-04	7,08E-01		1,34E-04	III
	±	3,53E+00	1,85E+02	5,38E-05	2,73E-02	0,00E+00	1,33E-04	6,55E-02			
	41	2,45E+02	1,23E+03	2,08E-04	6,43E-01	2,31E+03	5,46E-04	7,26E-01		1,27E-04	III
	±	3,84E+00	3,91E+02	4,69E-05	4,09E-02	4,48E+02	9,48E-05	1,01E-01			
55	2,40E+02	1,23E+03	1,29E-04	7,14E-01	4,29E+03	6,01E-04	6,74E-01		1,44E-04	III	
±	3,29E+00	2,16E+02	2,09E-05	3,06E-02	4,83E+02	5,99E-05	5,79E-02				

Table B.2. Equivalent electrical circuit fitted elements for Epoxy coated samples.

Units		immersion time	Cc-1	a(c-1)	Re-1	Re-2	Cc-2	a(c-2)	Rct	Cdl	a(dl)	W Porous bound	B(W)	Goodness of Fit	Fitted model
		h	$S_s^3/\text{cm}^2$	$\Omega\text{cm}^2$	$\Omega\text{cm}^2$	$\Omega\text{cm}^2$	$S_s^3/\text{cm}^2$		$\Omega\text{cm}^2$	$S_s^3/\text{cm}^2$		$S_s^{0.5}/\text{cm}^2$	$s^{0.5}$		
		2	7,07E-09	5,89E-01	6,81E+06	1,10E+08	1,06E-09	9,80E-01						7,69E-04	I
		±	2,95E-10	1,82E-02	1,25E+06	2,96E+06	7,38E-11	7,63E-03							
		7	6,98E-09	6,25E-01	7,19E+06	7,95E+07	1,08E-09	9,78E-01	3,97E+07	5,60E-08	1,00E+00			1,17E-04	II
		±	2,38E-09	8,35E-02	2,11E+06	2,64E+07	9,33E-11	9,34E-03	2,29E+07	4,10E-08	2,79E-01				
		9	8,23E-09	5,87E-01	6,06E+06	8,35E+07	1,05E-09	9,81E-01	3,64E+07	7,23E-08	1,00E+00			1,04E-04	II
		±	2,57E-09	7,90E-02	2,03E+06	2,89E+07	1,00E-10	1,02E-02	2,42E+07	6,58E-08	3,24E-01				
		20	1,18E-08	5,42E-01	5,29E+06	8,45E+07	1,08E-09	9,79E-01	6,04E+07	7,78E-08	6,49E-01			1,00E-04	II
		±	2,21E-09	5,42E-02	1,49E+06	2,20E+07	9,90E-11	9,88E-03	0,00E+00	4,60E-08	1,26E-01				
		35	1,62E-08	5,48E-01	4,38E+06	8,83E+07	1,23E-09	9,66E-01	4,35E+07	8,42E-07	1,00E+00			2,52E-04	II
		±	1,30E-09	3,06E-02	7,80E+05	1,04E+07	1,05E-10	9,26E-03	0,00E+00	8,33E-07	2,59E-01				
		96	1,03E-08	7,98E-01	1,28E+06	6,32E+06	1,02E-09	9,83E-01	4,05E+07	5,16E-08	8,53E-01			1,55E-04	II
		±	3,94E-09	6,42E-02	1,72E+05	1,10E+06	1,29E-10	1,32E-02	1,97E+06	3,37E-09	3,71E-02				
		Sameday after sterilization	2,63E-06	4,50E-01	1,90E+05	8,77E+04	4,69E-09	8,88E-01				4,31E-07	3,16E+00	4,19E-04	III
		±	8,21E-07	6,14E-02	4,30E+04	4,12E+04	2,30E-09	4,76E-02				1,93E-07	1,43E+00		
		1 week after sterilization	3,35E-06	5,23E-01	3,24E+05	1,20E+05	5,56E-09	8,71E-01				5,89E-07	3,10E+00	2,17E-04	III
		±	5,28E-07	8,63E-02	6,62E+04	3,99E+04	1,62E-09	2,77E-02				3,39E-07	2,60E+00		
		1 month after sterilization				9,11E+04	6,51E-09	8,54E-01		3,02E-06	2,07E-01			1,05E-03	IV
		±				1,53E+04	2,16E-09	2,42E-02		1,05E-06	6,60E-02				

Table B.3. Equivalent electrical circuit fitted elements for Polyester coated samples.

immersion time	Cc-1	a(c-1)	Re-1	Re-2	Cc-2	a(c-2)	Rct	Cdl	a(dl)	W Porous bound	B(W)	Goodness of Fit	Fitted model
Units	Ss <sup>3</sup> /cm <sup>2</sup>		Ωcm <sup>2</sup>	Ωcm <sup>2</sup>	Ss <sup>3</sup> /cm <sup>2</sup>		Ωcm <sup>2</sup>	Ss <sup>3</sup> /cm <sup>2</sup>		Ss <sup>0.5</sup> /cm <sup>2</sup>	S <sup>0.5</sup>		
2	1,77E-08	6,44E-01	1,38E+06	6,47E+07	7,74E-10	9,85E-01						4,92E-04	I
±	4,57E-10	8,64E-03	1,03E+05	1,49E+06	8,04E-11	1,09E-02							
9	3,00E-08	6,97E-01	1,49E+06	2,96E+07	8,96E-10	9,72E-01	1,93E+07	1,03E-07	1,00E+00			8,71E-05	II
±	4,85E-09	3,62E-02	1,10E+05	9,03E+06	9,24E-11	1,10E-02	8,56E+06	5,97E-08	2,22E-01				
20	4,80E-08	6,46E-01	1,49E+06	1,59E+07	1,03E-09	9,58E-01	2,50E+07	1,09E-07	6,78E-01			4,86E-04	II
±	2,08E-08	7,09E-02	2,28E+05	1,43E+07	1,14E-10	1,17E-02	1,73E+07	8,98E-08	2,50E-01				
48	1,51E-08	7,40E-01	8,10E+05	1,60E+07	8,18E-10	9,80E-01	1,02E+07	1,56E-07	4,36E-01			3,06E-05	II
±	1,01E-09	1,59E-02	6,06E+04	0,00E+00	1,20E-10	1,51E-02	0,00E+00	2,95E-08	7,93E-02				
72	2,46E-08	7,37E-01	8,03E+05	1,69E+07	8,35E-10	9,78E-01	2,27E+06	7,68E-06	8,99E-01			3,57E-05	II
±	8,09E-10	9,73E-03	3,72E+04	0,00E+00	1,01E-10	1,27E-02	0,00E+00	6,59E-06	3,09E-01				
96	2,85E-08	7,55E-01	8,25E+05	1,41E+07	8,72E-10	9,74E-01	1,47E+06	2,45E-05	1,00E+00			8,80E-05	II
±	1,16E-09	1,20E-02	3,36E+04	2,50E+05	9,95E-11	1,20E-02	0,00E+00	0,00E+00	2,77E-01				
Sameday after sterilization	2,17E-06	5,07E-01	3,40E+05	7,63E+04	4,54E-09	8,56E-01				5,19E-07	1,18E+00	5,71E-04	III
±	2,21E-07	7,26E-02	1,58E+05	1,66E+04	2,24E-09	4,64E-02				1,16E-07	1,07E-01		
1 week after sterilization	3,17E-06	3,97E-01	1,38E+05	1,05E+05	6,53E-09	8,33E-01				2,85E-07	3,92E-01	3,49E-04	III
±	1,00E-06	3,69E-02	1,17E+05	4,42E+04	2,79E-09	4,70E-02				1,35E-07	1,21E-01		
1 month after sterilization				6,84E+04	3,16E-08	7,40E-01	8,84E+05	1,92E-06	4,12E-01			2,53E-03	V
±				3,10E+04	1,09E-08	3,96E-02	2,12E+05	2,38E-07	2,52E-02				

Polyester

## APPENDIX C

### FITTING PROCEDURE AND CALCULATION OF STANDARD ERRORS

Gamry Echem Analyst program was used to fit EIS data to proposed models. After completing a successful fit, the program gives the magnitude of the physical elements with the calculated errors. These are fitting errors and should not be confused with measurement errors. Standard error was calculated using following formula<sup>65</sup>,

$$\text{Standard error} = \text{Standard deviation} / (\text{number of measurements})^{0.5}$$

While calculating the average of fitted physical elements, both fitting and measurement errors were included. However, fitted magnitudes should be considered as average values and taking average of average values can mislead the error values. To include fitting and measurement errors, virtual data were created by adding and subtracting error value ( $\pm e$ ) from the fitted value ( $x$ ). As an example of fitted values of 2 numbers,  $x_1$  and  $x_2$ ;

$$(x_1 + e_1), (x_1 - e_1), (x_2 + e_2), (x_2 - e_2)$$

numbers were created. By doing so, the data are doubled with included errors. Standard deviation of these 4 numbers were divided by square root of 4. Fitting errors can also be discarded with low error values however due to the overlapped time constants, most of the relative errors are higher than 10%. Therefore, fitting errors were included to the overall error calculations.